APPLICATION OF THE EQUIVALENT MECHANICAL FLAP CONCEPT TO JET FLAPPED WING-BODY COMBINATIONS

A. E. Holmes, et al

Lockheed-Georgia Company

Prepared for:

Aerospace Research Laboratory

November 1974

UNCLASSIFIED

SECURITY CLASSIFICATION OF THIS PAGE (When Data Entered)

REPORT DOCUMENTATION PAGE		READ INSTRUCTIONS BEFORE COMPLETING FORM
1. REPORT NUMBER ARL 74-0136	2. GOVT ACCESSION NO.	3. RECIPIENT'S CATALOG NUMBER AD/A-000 431
4. TITLE (and Subtitle) APPLICATION OF THE EQUIVALENT MECHANICAL FLAP CONCEPT TO JET FLAPPED WING-BODY COMBINATIONS		5. TYPE OF REPORT & PERIOD COVERED Technical - Final May - December 1973 6. PERFORMING ORG. REPORT NUMBER LG74BR0115
7. AUTHOR(s) A. E. Holmes Lane Barnett Willi F. Jacobs (Consultant)		8. CONTRACT OR GRANT NUMBER(s) F33615-73-C-4142
9. PERFORMING ORGANIZATION NAME AND ADDRESS Lockheed-Georgia Company 86 South Cobb Drive Marietta, Georgia 30060		10. PROGRAM ELEMENT, PROJECT, TASK AREA & WORK UNIT NUMBERS DoD Element 61102F 70710120
11. CONTROLLING OFFICE NAME AND ADDRESS Applied Mathematics Research Laboratory/LB Aerospace Research Laboratories (AFSC) Wright-Patterson AFB, Ohio 45433		12. REPORT DATE Novembe. 1974 13. NUMBER OF PAGES
14. MONITORING AGENCY NAME & ADDRESS(if different from Controlling Office)		15. SECURITY CLASS. (of this report) Unclassified 15a. DECLASSIFICATION/DOWNGRADING SCHEDULE

16. DISTRIBUTION STATEMENT (of this Report)

Approved for public release; distribution unlimited.

17. DISTRIBUTION STATEMENT (of the abstract entered in Block 20, if different from Report)

18. SUPPLEMENTARY NOTES

19. KEY WORDS (Continue on reverse side if necessary and identify by block number)

jet flap
powered high lift

20. ABSTRACT (Continue on reverse side if necessary and identify by block number)

A method is given for calculating span load distribution for swept jet flapped wings in pitch and in sideslip, from which lift, axial force, rolling moments, sidewash, and downwash are calculated. The method is based on a swept lifting line in sideslip and on simple sweep theory. Section circulation properties in the simple sweep plane are those for the basic flapped airfoil plus a flat mechanical flap extension. The circulation lift on the flap extension approximates the circulation lift of a suitable portion of the jet sheet. The extended

DD FORM 1 JAN 73 1473 EDITION OF 1 NOV 65 IS OBSOLETE

UNCLASSIFIED

SECURITY CLASSIFICATION OF THIS PAGE (When Data Entered)

20.

flap is called the Equivalent Mechanical Flap (EMF). The length of the EMF chord extension is dependent on momentum coefficient, momentum injection angle, the geometry of the real airfoil, and local flow inclination due to fuselage interference. Its size is also dependent on the effectiye angle of attack, and therefore upon the three dimensional induced angle. The simultaneous equations for span loading are therefore nonlinear and must be solved by iteration. Comparisons of calculated lift and axial force coefficients with experimental data are generally good over a wide range of variables. Rolling moments due to sideslip also compare well for wing-body combinations but suffer somewhat due to the effects of large pylon-nacelle arrangements. A computer program with utilization instructions is included.

NOTICES

When Government drawings, specifications, or other data are used for any purpose other than in connection with a definitely related Government procurement operation, the United States Government thereby incurs no responsibility nor any obligation whatsoever; and the fact that the Government may have formulated, furnished, or in any way supplied the said drawings, specifications, or other data, is not to be regarded by implication or otherwise as in any manner licensing the holder or any other person or corporation, or conveying any rights or permission to manufacture, use, or sell any patented invention that may in any way be related thereto.

Organizations or individuals receiving reports via Aerospace Research Laboratories automatic mailing lists should refer to the ARL number of the report received when corresponding about change of address or cancellation. Such changes should be directed to the specific laboratory orginating the report. Do not return this copy; retain or destroy.

Reports are not stocked by the Aerospace Research Laboratories. Copies may be obtained from:

National Technical Information Services
Clearinghouse
Springfield, VA 22151

This technical report has been reviewed and is approved for publication.

This report has been reviewed and cleared for open publication and public release by the appropriate Office of Information in accordance with AFR 190-12 and DODD 5230.0. There is no objection to unlimited distribution of this report to the public at large, or by DDC to the National Technical Information Service.

PREFACE

This report was prepared by Mr. A. E. Holmes and Mr. Lane Barnett (principal investigator) of the Advanced Flight Sciences Department, Lockheed-Georgia Company, Marietta, Georgia 30063, and by Dr. Willi F. Jacobs, Consultant. The study was sponsored by the USAF Aerospace Research Laboratories (Applied Mathematics Research Laboratory). The program monitor was Dr. Karl Guderley, ARL/LB, Wright-Patterson Air Force Base, Dayton, Ohio, who worked in coordination with Mr. Henry Woolard of the Flight Dynamics Laboratory. The project was conducted over the period 1 May to 30 December 1973, under Contract F33615-73-C-4142, entitled "Study of the Applicability of Simplifying Concepts, in particular, that of a Flat Mechanical Flap Equivalent to a Jet Flap", Project Number 7071.

The authors are grateful to Mrs. Barbara Reagan for her efforts in manuscript preparation.

This report is also known as Lockheed-Georgia Report LG74ER0115.

TABLE OF CONTENTS

TABLE OF CONTENTS (Cont'd)

LIST OF TABLES

LIST OF ILLUSTRATIONS

LIST OF ILLUSTRATIONS (Cont'd)

LIST OF ILLUSTRATIONS (Cont'd)

LIST OF SYMBOLS

In certain instances a specific symbol has more than one meaning in order to maintain familiar notation. In addition, certain parameters such as force and momentum coefficients, chords, dynamic pressure, and angles of attack, deflection, and injection can be taken in both streamwise and normal planes. For all such cases the particular meanings are clear in context.

ENGLISH

a	parameter used in elliptic to circular transformation
a_1	width of elliptic body cross section
A	matrix of error differentials
A_1	spacing parameter for rolled up vortex system, distance between vortices = $\pi/4\ bA_1$
AR	aspect ratio of wing in clean configuration
b	wing span
b_1	depth of elliptic body cross section
B	(1) error matrix (2) ratio of vortex drag to that for elliptic loading at same circulation parameter $\Gamma_o/2bV$
c	chord of wing, mechanical flaps extended
c'	chord of wing plus Equivalent Mechanical Flap, mechanical flaps extended
c_f	chord of trailing edge mechanical flap in extended position
c_n	chord of nose flap in extended position
c_{avg}	average wing chord, mechanical flaps extended
c_μ	section momentum coefficient based on extended mechanical chord
c_{ℓ_j}	lift component of injected thrust based on extended mechanical chord
c_{ℓ_γ}	circulation lift for 2-D section plus equivalent mechanical flap, based on extended mechanical chord

c_ℓ	section total lift coefficient based on extended mechanical chord
C_L	wing total lift coefficient based on clean wing reference area and freestream q, L/qS_{ref}
C_{L_α}	slope of lift curve $dC_L/d\alpha_{ref}$
C_X	axial force coefficient based on clean wing reference area and freestream q, positive for forward acceleration, acc. force/qS_{ref}
C_μ	wing momentum coefficient based on total injected momentum, clean wing reference area and freestream q, J/qS_{ref}
C_ℓ	rolling moment coefficient, (moment)/qsb
C_{D_p}	profile drag coefficient for vehicle, $D_{profile}/qS_{ref}$
$C_{D_{RAM}}$	total ram drag coefficient for all inlets, including that for AW flap inlet, D_{RAM}/qS_{ref}
D	body diameter
e_Γ	span efficiency of total vortex system (wing plus vortex sheet)
G	circulation parameter Γ/bV
H	EMF sizing function
j	flux of momentum injected per unit of span
J	total flux of injected momentum
K	wake factor, $\beta = K\alpha_i$
L	total wing lift force
m	number of control points across wing semispan
m_j	mass flux for 2-D jet
q	dynamic pressure
Q	function denoting inverse relationship between α_e and current iteration error, $\alpha_e = Q(\varepsilon)$
R	radius of curvature for 2-D jet sheet
S_{ref}	wing reference area
u,v,w	velocities in x,y,z directions, respectively

u,v	integration variables
v_j	jet velocity, fully expanded flow
v',w'	velocities in η, ξ directions, respectively
V	freestream velocity
x,y,z	vehicle coordinates, positive downstream, to pilot's right, and vertically, respectively
Z	complex variable $y + iz$

GREEK

α	angle of attack, usually implies local section geometric angle of attack
α_{ref}	reference angle of attack, angle between freestream and reference longitudinal axis
α_i	induced angle of attack at lifting line
α_e	effective section angle of attack, $\alpha_e = \alpha - \alpha_i$
α_δ	flap effectiveness parameter $\frac{\partial C_\ell}{\partial \delta} \Big/ \frac{\partial C_\ell}{\partial \alpha}$ (unpowered section)
β	(1) sideslip angle, position for crosswind from pilots right hand side (2) inclination of trailing vortex system to freestream, positive downward
γ	local intensity of transverse vorticity on airfoil and jet sheet
Γ	(1) lifting line bound vortex strength, for airfoil and EMF Γ_o = centerline value, $\bar{\Gamma}$ = spanwise average (2) wing dihedral angle, positive for tips above wing centerline
δ_f	main flap deflection
δ_n	nose flap deflection, positive for leading edge down
δ_j	jet injection angle, measured positive downward from main flap reference line

δ_{ail}	aileron deflection
δ_{f_a}	IBF auxiliary control flap deflection
ε	(1) error in α_e, ε = calculated α_e minus guessed α_e
	(2) downwash angle
η	(1) normalized span station, 2y/b
	(2) turning/spreading efficiency for jet, fraction of injected thrust projected into pitch plane
θ_j	injection angle of jet relative to stream direction
λ	wing taper ratio
ξ, η	body coordinates in ζ plane
Λ	wing sweep angle, usually at quarter-chord
ϕ	span station, $\eta = \cos\phi$
ψ	airfoil coordinate, see text and figures for subscripted and superscripted meanings
σ	sidewash angle

SUBSCRIPTS

ν, n	control point indices
∞	indicates conditions far downstream
s	indicates streamwise plane
n	indicates normal or simple sweep plane
p	indicates pitch plane
$\perp$	indicates perpendicular to simple sweep plane

ABBREVIATIONS

AW	Augmentator Wing
BLC	Boundary Layer Control
EBF	Externally Blown Flap
EMF	Equivalent Mechanical Flap
HL	Hinge Line
IBF	Internally Blown Flap
RMS	Root Mean Square
USB	Upper Surface Blowing

SECTION I

INTRODUCTION

1. OVERVIEW

The analysis of powered lifting systems of the jet flap type requires an accounting of the mutual aerodynamic interference between the airframe (hard boundary) and the jet efflux (soft boundary). This differs from the classical interference problem in that boundary conditions of tangential flow must additionally be satisfied over a surface whose unknown geometry is self-adaptive in terms of both jet properties and hard surface loading conditions, where such loading is partially defined by the jet interference.

The development of a very generalized analysis technique is hardly feasible. However, the Externally Blown Flap (EBF), Upper Surface Blowing (USB), Internally Blown Flap (IBF), and the Augmentor Wing (AW) constitute a family of powered lifting systems which are reducible to a common overall aerodynamic concept, but which differ primarily in their mechanical implementation and secondarily in aerodynamic detail. This family is best thought of as analogous jet flapped wings differing primarily in the spanwise distribution of the efflux momenta at the trailing edge.

This report presents a relatively simple technique based on careful application of linearized theory. The method applies to the analogous systems mentioned above. The comparison of theoretical results with experimental data shows that the method is sufficiently accurate to be very useful in practice.

2. JET FLAP BACKGROUND

The basic concept of our treatment is the same as that of a number of other theoretical approaches. (Some of their features will be described subsequently.) The jet is considered as a thin sheet of fluid emerging from the trailing edge of the wing. The flows, both internal and external to this jet sheet, are considered as inviscid so that no mixing or diffusion takes place. Due to the pressure differences exerted by the outer flow on the jet sheet it is bent back. So far this shape is unknown. According to this model the effect of the jet sheet on the external field is solely given by its geometry; one could think of it as rigid. The pressure distribution, which determines its shape, is determined by the conditions of dynamic equilibrium with the outer field. Because of the pressure difference which exists between the two sides of the sheet, it can be represented by a vortex layer. All trailing vortices, those from the wing as well as those from the vortex distribution in the sheet, lie on this sheet.

One should remember that the forces exerted on this sheet from the outside are exactly balanced by the momentum change of the jet within. The forces exerted by the sheet on the outer flow do not act directly on the wing. A direct effect on the wing is given by the reaction of the jet as it exits from the wing, usually at its trailing edge. It is determined by the momentum

coefficient of the jet and its direction. The pressure forces (in other words the vortex distribution over the jet sheet) exerted by the jet sheet on the outer flow cause a change of the pressure distribution over the wing. The assessment of this effect is the crucial step in the treatment of jet flaps. It is obvious that the vortex distribution in the sheet at stations close to the wing is of primary importance. In practical computations, one frequently prefers to determine the combined lift of the wing and of a suitable part of the jet rather than the lift on the wing alone. In this case the redirected jet momentum as it emerges from the "truncated" sheet is taken into account. This merely amounts to a different kind of bookkeeping, which is made possible by the fact that the outer forces on the sheet are balanced by the momentum changes of the jet. Sometimes it may be desirable to go back to primary quantities, namely, the lift on the wing by itself and the momentum of the jet as it exits from the wing.

If one uses this model, then, for an infinite swept wing, the jet sheet will have the shape of a (general) cylinder generated by straight lines parallel to the line along which the jet emerges. Of course, for a wing of finite dimension this configuration will appear only locally. But this is the region in which the vortex distribution on the jet sheet is of most importance. Therefore, one can hope that by this idea the effect of the sheet vorticity on the wing is rather well approximated.

The classical mathematical treatment of the two dimensional jet flap problem is best typified by that of Spence[1], which was corroborated by Malvard's rheoelectric analogy[2]. The physical model consists of a wing with a simple-hinged mechanical flap from which a thin jet of fluid issues parallel to the flap at the trailing edge. Flows both external to and internal to the jet are inviscid, so that no mixing or diffusion takes place. The jet bends rearward due to a pressure differential across it which results from its interference with the external field. The loading over the jet is replaced by a distribution of vorticity. The jet then becomes a vortex layer over which the normal boundary conditions apply when the jet and external field are in dynamic equilibrium.

The condition for dynamic equilibrium is that pressure forces across the jet are balanced by centrifugal forces on each element of efflux, which relates local vorticity distribution to jet radius of curvature and thus to z'', where z is the distance from the jet to the wing reference plane (small slopes assumed). This condition, together with the normal thin airfoil formulation, leads to a pair of integro-differential equations having as unknowns (a) the vortex distribution of the airfoil and (b) the jet parameter z'' (and hence the jet vortex distribution). The calculated jet boundary is required to conform to the injection angle at the trailing edge, and to be aligned with the freestream infinity, and the usual boundary conditions of tangential flow apply over the airfoil and sheet.

Spence solved the problem for the specific case of a flat plate airfoil and simple hinged flap, with the jet injected parallel to the flap. These results have always been of great interest since they serve as a comparative baseline for assessing the utility of more approximate methods. Spence's results are fairly accurate for many cases, and in fact give good results well outside the normal bounds of linearized theory. At the same time, they are

difficult to extend to include real wing characteristics such as a camber, large leading edge devices, multi-hinged flap segments, and momentum injection which is nonplanar with the flap.

The extension of such concepts to three dimensional wings immediately leads to far greater complications. As in the two dimensional case the jet sheet vortex loading, with its interaction with the wing, is the critical driving function, so that the impact of three dimensionality on its shape requires careful assessment. The jet sheet loading, being three dimensional, also sheds its spanwise gradient of lateral vorticity, so that the accumulated trailing vorticity increases to its asymptotic value at downstream infinity.

This problem has been attacked in numerous ways. Maskell and Spence[3] developed first order trends by collapsing the chordwise dimension of both wing and jet sheet to an elliptically loaded lifting line, and by assuming a flat wake with the usual doubling of downwash from the loaded line to the far field. In applying Spence's previously developed section properties[1] an additional factor must be taken into account, namely, that at the lifting line the downwash is α_i, but that the jet sheet far downstream is subjected to a downwash angle $\beta_\infty = 2\alpha_i$. The total jet turning angle is therefore $(\theta_j - \alpha_i) - (\beta_\infty - \alpha_i)$, where θ_j is the injection angle measured from the freestream direction. The jet sheet loading, and therefore section properties, are adjusted to reflect a curve freastream. The section properties, in local flow coordinates, are therefore in part determined by three dimensional downwash. The basic elliptic loading results by Maskell and Spence can give good lift results for nonelliptic cases, provided that appropriate part span factors are used, but they are not suitable for calculating span load distribution and induced drag.

Other researchers have produced workable techniques while addressing fairly generalized planforms and distributions of flap chord, flap deflection, local momentum coefficients and injection angle. Some of the more notable works are due to Das[4], Lopez and Shen[5], Lissaman[6], Hackett and Lyman[7], and Davenport[8]. The approach reported in this document is in many ways a lifting line counterpart of the Hackett-Lyman approach, but with some modifications in the assumptions. Davenport's method, which became available to these authors fairly late in the study, is of considerable interest since it is also a lifting line technique, but which differs somewhat in approach, assumptions, and method of solution.

It is pointed out that the sheet vortex loading is highest in the vicinity of the wing, followed by a rapid decay. Generally, at some nominally "short" distance downstream, the substantially one-to-one conversion of jet momentum lift to sheet vortex lift is essentially complete, particularly insofar as its lift interference with the wing is concerned. Accordingly, the system may be suitably truncated for calculation of interference between the jet sheet and wing. Moreover, for most cases of present interest the sheet roll-up occurring between the wing and truncation point is ignored, although this can be significant when spanwise gradients are sufficiently large. Additionally, questions arise concerning the nonplanar character of the wake, since it is outside the wing reference plane and it may have considerable warp due to spanwise variations in both injection angle and downwash field. Even so, the analysis has shown that a completely planar, linearized approach is capable of giving good results although several factors neglected in the linearization are known to be individually significant.

3. APPROACH

The approach taken here is based on a completely planar system using linearized theory and linearized boundary conditions. Moreover, it is based on the assumption that, as far as its influence on the total lift of the wing is concerned, the jet sheet can be approximated by a flat plate which possesses, at the spanwise station considered, the inclination of the injected jet momentum and a (unknown) length in the streamwise direction which is determined by properties of the jet sheet. Details will be discussed later. The solution involves iteration of the spanwise-varying *length* of a flat sheet whose inclination is that of the injected momenta, in contrast to the classical problem of shape calculation.

The primary objective of this program was the calculation of rolling moments and sidewash in sideslip. However, such calculations necessarily require accuracy in span loadings and a clear distinction between vortex forces and "residual" efflux momentum forces, thereby providing the information essential to an accurate assessment of $C_L - \alpha$ and $C_L - C_X$ relationships.

SECTION II

THEORY

The analysis procedure given in this report consists of a swept lifting line approach to the analysis of jet flap type systems in sideslip. The method makes use of the Equivalent Mechanical Flap Concept (EMF) for calculation of powered section properties. First order fuselage interference is taken into account. There are certain elements and special considerations which require explanation. The following text is confined primarily to these areas and to the manner in which they fit into the total picture.

This section considers the two dimensional EMF in both uniform and curved streams, the particular boundary conditions used, fuselage interference, the nonlinear system of equations and method of iteration, the circulation and residual jet lifts, the assessment of axial force (partly as a point of validation for span load distributions), and sidewash and downwash. These areas are summarized in Figure 1.

1. THE TWO DIMENSIONAL EQUIVALENT MECHANICAL FLAP IN A UNIFORM FREESTREAM

a. Physical Considerations.

A typical 2-D jet flap arrangement is illustrated in Figure 2. The condition for dynamic equilibrium of the sheet is that the pressure differential across the jet locally balances the centrifugal force of the jet efflux. For small perturbations this leads directly to

$$\gamma_j = \frac{m_j V_j}{\rho V R} = \frac{m_j V_j}{\rho V} z''$$

so that the jet sheet lift exerted over the region between the trailing edge and some arbitrary location downstream, say $x = x'$, is

$$\Delta \ell_j = \int_{x = x_{TE}}^{x'} \rho V \gamma_j dx = m_j v_j z' \Big|_{x=x_{TE}}^{x'} = -J\left(\theta_j - \beta(x')\right) = -J\theta_j \left(1 - \frac{\beta(x')}{\theta_j}\right)$$

where θ is the total injection angle relative to the freestream direction. Thus, the accumulated vortex lift equals the difference in the lift component of the jet between the two stations. Typically the curvature z'' is large near the trailing edge, followed by a rapid downstream decay, so that β/θ typically becomes very small a short distance downstream. This is especially true for nominal momentum coefficients. The distance in chords required for β/θ to

degenerate to a specified level increases with increasing momentum, C_μ. It also increases with increasing levels of the power-off lift of the mechanical system, since a pre-existing local flow inclination of the trailing edge reduces the effective jet disturbance for a specified injection angle. Thus the sheet geometry is sensitive to C_μ, angle of attack, flap chord, flap deflection, airfoil camber, and injection angle.

In 1958 Jacobs and Paterson[9] proposed that the two dimensional analysis be simplified by replacing the sheet by a finite-length curved hard surface flap characterized by semi-empirical logarithmic-type shape functions, and establishing by iteration a chordwise extent of flap sufficient to carry the total vortex lift on the sheet. The results of their study compared very well with experimental data.

Parallel studies considered a simpler case in which the sheet was replaced by a straight mechanical flap which was deflected parallel to the jet injection angle. The procedure is basically simple, since it is only required to establish with thin airfoil theory an extended length Δc which carries a lift $c_\mu \sin\theta$ in the presence of the actual airfoil. The calculated lift results were also quite good. This is the approach used in this report.

b. Derivation.

For completeness, the discussion which follows reiterates the original derivation of Jacobs and Paterson[9] and the closed form solution given more recently by Hackett[7].

It is presumed that a flat mechanical flap extension, henceforth referred to as the Equivalent Mechanical Flap (EMF), can be used to represent the lift aspects of the jet sheet. The direct jet lift and accordingly the sheet vortex lift, is $c_\mu \sin\theta$, and an EMF length will be established so that $c_\mu \sin\theta = \Delta c \ell_{EMF}$.

In order to do this, reference is made to Munk's integral theorems for thin airfoils (see Ref. 10, Section E.11, Equations 9.14, 9.20). These are written

$$\gamma(\psi') = \frac{V}{\pi \sin\psi'} \int_0^{2\pi} \left(-\frac{dz}{dx}\right) \cot\frac{\psi' - \psi}{2} \sin\psi d\psi + \frac{\Gamma}{2\pi\ c/4\ \sin\psi'}$$

$$\Gamma = 2\left(\frac{c}{4}\right) V \int_0^{2\pi} \left(-\frac{dz}{dx}\right) (1 + \cos\psi)\ d\psi$$

where the notation is adapted to that shown in Figure 3. These equations combine to give

$$\gamma(\psi') = \frac{V}{\pi \sin\psi'} \int_0^{2\pi} \left(-\frac{dz}{dx}\right) \left(\cot \frac{\psi' - \psi}{2} \sin\psi + 1 + \cos\psi\right) d\psi$$

Consider the special case shown in Figure 3 where dz/dx is constant over an element of airfoil defined by $0 \leq \psi \leq \bar{\psi}$. The γ distribution due to that element is, based on the preceding expression,

$$\frac{\pi\gamma(\psi')}{2V\left(-\frac{dz}{dx}\right)} = \frac{1}{2\sin\psi'} \int_{-\bar{\psi}}^{+\bar{\psi}} \left(\cot \frac{\psi' - \psi}{2} \sin\psi + 1 + \cos\psi\right) d\psi \qquad (1)$$

The identity

$$\cot \frac{\psi' - \psi}{2} \sin\psi \equiv \cot \frac{\psi' - \psi}{2} \sin\psi' - \cos\psi - \cos\psi'$$

allows Eq (1) to be written

$$\frac{\pi\gamma(\psi')}{2V\left(-\frac{dz}{dx}\right)} = \int_{-\bar{\psi}}^{+\bar{\psi}} \left(\frac{1}{2} \cot \frac{\psi' - \psi}{2} + \frac{1 - \cos\psi'}{2 \sin\psi'}\right) d\psi$$

which is directly integrable to

$$\frac{\pi\gamma(\psi')}{2V\left(-\frac{dz}{dx}\right)} = \bar{\psi} \tan\frac{\psi'}{2} + \ln\left|\frac{\sin\frac{\bar{\psi} + \psi'}{2}}{\sin\frac{\bar{\psi} - \psi'}{2}}\right| \qquad (2)$$

Now consider the region $0 \leq \psi \leq \psi_1$, which will subsequently become the equivalent mechanical flap. The lift induced on this region is

$$\Delta C_\ell = \int_{\frac{x_1}{c}}^{1} \frac{\rho V \gamma(\psi')}{q} \, d\left(\frac{x'}{c}\right)$$

which, with Eq (2), gives

$$\Delta C_\ell = \frac{2\left(-\frac{dz}{dx}\right)}{\pi} \int_0^{\psi_1} \left[\bar{\psi} \tan\frac{\psi'}{2} + \ln\left| \frac{\sin\frac{\bar{\psi}+\psi'}{2}}{\sin\frac{\bar{\psi}-\psi'}{2}} \right| \right] \sin\psi' \, d\psi' \qquad (3)$$

By rearranging Eq (3) one writes

$$\frac{\pi \Delta C_\ell}{2\left(-\frac{dz}{dx}\right)} = I_1 + I_2 \qquad (4)$$

where

$$I_1 = \int_0^{\psi_1} \left[\bar{\psi}\,(1 - \cos\psi') + \sin\bar{\psi}\right] d\psi'$$

$$= \bar{\psi}\ \psi_1 - \bar{\psi} \sin\psi_1 + \psi_1 \sin\bar{\psi} \qquad (5)$$

$$I_2 = \int_0^{\psi_1} \left[\sin\psi' \ln\left| \frac{\sin\frac{\bar{\psi}+\psi'}{2}}{\sin\frac{\bar{\psi}-\psi'}{2}} \right| - \sin\bar{\psi}\right] d\psi'$$

By incorporating the identities

$$\sin\psi' \equiv \sin\frac{\bar{\psi}+\psi'}{2}\cos\frac{\bar{\psi}-\psi'}{2} - \cos\frac{\bar{\psi}+\psi'}{2}\sin\frac{\bar{\psi}-\psi'}{2}$$

$$\sin\bar{\psi} \equiv \sin\frac{\bar{\psi}+\psi'}{2}\cos\frac{\bar{\psi}-\psi'}{2} + \cos\frac{\bar{\psi}+\psi'}{2}\sin\frac{\bar{\psi}-\psi'}{2}$$

The integral I_2 becomes

$$I_2 = 2\int_0^{\psi_1}\left[\ln\frac{v}{u}\left(-v\frac{du}{d\psi'}-u\frac{dv}{d\psi'}\right)+v\frac{du}{d\psi'}-u\frac{dv}{d\psi'}\right]d\psi' \qquad (6)$$

$$= 2uv\ln\left|\frac{u}{v}\right|\Bigg|_0^{\psi_1}$$

where

$$u = \sin\frac{\bar{\psi}-\psi'}{2}, \quad v = \sin\frac{\bar{\psi}+\psi'}{2}$$

The final expression for Δc_ℓ, from Eqs (4), (5) and (6), is

$$\Delta c_\ell = \frac{2}{\pi}\left(-\frac{dz}{dx}\right)\left[\bar{\psi}\psi_1 - \bar{\psi}\sin\psi_1 + \psi_1\sin\bar{\psi}\right.$$

$$\left. + 2\sin\frac{\bar{\psi}-\psi_1}{2}\sin\frac{\bar{\psi}+\psi_1}{2}\ln\left|\frac{\sin\frac{\bar{\psi}-\psi_1}{2}}{\sin\frac{\bar{\psi}+\psi_1}{2}}\right|\right] \qquad (7)$$

which is the total lift in the range $0 \le \psi \le \psi_1$, due to a constant deflection $-dz/dx$ over the range $0 \le \psi \le \bar{\psi}$. The corresponding total airfoil lift is obtained from Eq (7) with $\psi_1 = \pi$ (load integrated over the entire chord). That is, with $-dz/dx = \delta$

$$c_\ell = 2(\bar{\psi} + \sin\bar{\psi})\delta$$

For a section lift curve slope $\partial c_\ell/\partial\alpha = 2\pi$, this reduces to the familiar α_δ relationship

$$c_\ell = 2\pi\ \alpha_\delta\ \delta \tag{8}$$

where

$$\alpha_\delta(\bar{\psi}) = \frac{\bar{\psi} + \sin\bar{\psi}}{\pi} \tag{9}$$

The preceding result may be generalized to a Δc_ℓ consisting of the total contributions of N airfoil components (see Hackett and Lyman (7)). However, the present case is restricted to a plane airfoil with nose flap, a single main flap, and the EMF as shown in Figure 4.

The elements are as follows:

Element	Flap Size Parameter, $\bar{\psi}$	Deflection (-dz/dx)
$0 \le \psi \le \pi$	π	$\alpha - \delta_n$
$0 \le \psi \le \psi_n$	ψ_n	δ_n
$0 \le \psi \le \psi_o$	ψ_o	δ_f
$0 \le \psi \le \psi_1$	ψ_1	δ_j

The elements are superimposed to give the airfoil geometry shown. The following geometric relations apply

$$\frac{c}{c'} = \frac{1}{2}(1 + \cos\psi_1) \tag{10}$$

$$\cos\frac{\psi_o}{2} = \sqrt{1 - \frac{c_f}{c}}\ \cos\frac{\psi_1}{2} \tag{11}$$

$$\cos\frac{\psi_n}{2} = \sqrt{\frac{c_n}{c}}\ \cos\frac{\psi_1}{2} \tag{12}$$

The length of the equivalent flap (or equivalent ψ_1) is now determined by the requirement that the vortex lift exerted on it equals the total vortex lift of the jet sheet. The total vortex lift on the EMF is obtained by applying Eq (7) to all wing elements listed above and adding the results. The total vortex lift of the jet sheet (referred to chord length c') is given by the change of the vertical momentum in the jet sheet, that is, by

$$c_\mu \, \mathrm{Sin}(\alpha + \delta_f + \delta_j) \, \frac{c}{c'}$$

where c_μ is referred to the geometric chord c. One thus obtains the final equivalence relation

$$\frac{\pi}{4} c_\mu \sin(\alpha + \delta_f + \delta_j) = H(\alpha, \psi_1) \tag{13}$$

where

$$H(\alpha, \psi_1) =$$

$$\frac{1}{1+\cos\psi_1}\left\{[\alpha - \delta_n]\left[\pi(\psi_1 - \sin\psi_1) + 2\sin\frac{\pi-\psi_1}{2}\sin\frac{\pi+\psi_1}{2}\ln\frac{\sin\frac{\pi-\psi_1}{2}}{\sin\frac{\pi+\psi_1}{2}}\right]\right.$$

$$+ [\delta_n]\left[\psi_n\psi_1 + \psi_1\sin\psi_n - \psi_n\sin\psi_1 + 2\sin\frac{\psi_n-\psi_1}{2}\sin\frac{\psi_n+\psi_1}{2}\ln\frac{\sin\frac{\psi_n-\psi_1}{2}}{\sin\frac{\psi_n+\psi_1}{2}}\right]$$

$$+ [\delta_f]\left[\psi_o\psi_1 + \psi_1\sin\psi_o - \psi_o\sin\psi_1 + 2\sin\frac{\psi_o-\psi_1}{2}\sin\frac{\psi_o+\psi_1}{2}\ln\frac{\sin\frac{\psi_o-\psi_1}{2}}{\sin\frac{\psi_o+\psi_1}{2}}\right]$$

$$\left. + [\delta_j]\left[\psi_1^2\right]\right\} \tag{14}$$

In a similar manner the total airfoil lift is obtained by superimposing the contributions of the four elements (see Eqs (8), (9)). The resulting lift coefficient based on physical chord c, is then

$$c_{L_\gamma} = 2\pi \frac{2}{1+\cos\psi_1}\left[(\alpha - \delta_n) + a_\delta(\psi_n)\,\delta_n + a_\delta(\psi_o)\,\delta_f + a_\delta(\psi_1)\,\delta_j\right] \tag{15}$$

Since the jet is ultimately turned back to the direction of the free-stream, and the aerodynamic drag of the combined wing and jet sheet is zero, the axial force is given by

$$C_X = C_\mu \tag{16}$$

as stated by the classical thrust recovery arguments.

Calculation of ψ_1 in (14) to match the value of H specified in Eq (13) required use of the relations (11) and (12). The quantity H is single valued in ψ_1 over the range $0 \leq \psi_1 \leq \pi(dH/d\psi_1 \geq 0)$, so that the initial guess $\psi_1 = \pi/2$ establishes, by comparing left and right sides, which quadrant ψ_1 falls within. The second guess is the mid-range of the appropriate quadrant ($\psi_1 = \pi/4$ or $\psi_1 = 3\pi/4$), so that the second sector containing ψ_1 is reduced in size to $\pi/2^n$ in n steps.

The iterated value of ψ_1, with the corresponding ψ_o and ψ_n, are used in (15) for calculation of the lift.

It is reiterated that ψ_1, while sensitive to the direct jet lift $c_\ell \sin(\alpha + \delta_f + \delta_j)$, is also sensitive to the size and deflection of each airfoil element. This is of course reflected as a sensitivity of jet induced super-circulation lift to the geometry of the mechanical system.

2. EFFECT OF LONGITUDINAL VARIATION IN THE INDUCED ANGLE

A longitudinal variation of the downwash angle, relative to its value α_i at the wing, will change the total sheet vortex load and its longitudinal distribution. This will be taken into account only to the extent that it changes the loading induced by the jet on the physical wing. Only the forward portion of the jet sheet need be taken into account for determination of the lift. The portion of the sheet taken into account is subjected to the induced angle α_i at its upstream edge and to the induced angle β at its downstream edge (see Figure 5). The change of jet momentum in the direction normal to the local flow at the wing is

$$c_\mu \left[\sin(\alpha - \alpha_i + \delta_f + \delta_j) - \sin(\beta - \alpha_i)\right]$$

which is the revised vortex lift to be carried by the EMF.

The appropriate lift equations are

$$\frac{\pi}{4} c_\mu \left[\sin(\alpha - \alpha_i + \delta_f + \delta_j) - \sin(\beta - \alpha_i)\right] = H(\alpha - \alpha_i, \psi_1) \tag{17}$$

where $H(\alpha - \alpha_i, \psi_1)$ is obtained from Eq (15) with α replaced by $\alpha - \alpha_i$. Correspondingly, section circulation lift is obtained from Eq (15).

$$c_{\ell_\gamma} = 2\pi \frac{2}{1+\cos\psi_1} \left[(\alpha - \alpha_i - \delta_n) + \alpha_\delta(\psi_n)\delta_n + \alpha_\delta(\psi_o)\delta_f + \alpha_\delta(\psi_1)\delta_j \right] \quad (18)$$

$$c_\ell = c_{\ell_\gamma} \cos\alpha_i + c_\mu \sin\beta \quad (19)$$

$$\approx c_{\ell_\gamma} + c_\mu \sin\beta$$

It is emphasized that $\beta - \alpha_i$ is the variation in downwash angle across that portion of the jet sheet which is presumed to determine the super-circulation or jet interference lift on the wing.

It is pointed out that $\beta = \alpha_i$ at the wing. If the entire sheet is taken into account, then $\beta = \beta_\infty$, where, for an elliptically loaded system, $\beta = 2\alpha_i$ (flat wake) and $\beta = (4/\pi^2)\alpha_i$ (rolled wake). Thus, $\beta - \alpha_i$ is at most of order α_i (flat wake) or $-(1 - 4/\pi^2)\,\alpha_i$ (rolled wake).

Since the variation $\beta - \alpha_i$ is proportional to α_i it is significant only when α_i itself is large. This condition is best typified by large C_μ and concentrated part span blowing (high lift, low effective aspect ratio). For such extreme cases consistently good lift results have been obtained simply by assuming that $\beta = \alpha_i$ and neglecting the downwash variation entirely. In the computer programs included in this report β is set equal to α_i.

3. THE LIFTING LINE METHOD FOR SPAN LOAD CALCULATION

a. The Boundary Condition

The method reported here uses the strip approach and simple sweep theory. Most methods based on this approach impose the boundary condition of tangential flow at the three-quarter chord location. A strict interpretation required the section lift curve slopes to be 2π; otherwise, a chordwise adjustment in control point location is required. In the present case the lift curve slope of the airfoil plus EMF is taken to be 2π, based on the effective chord c'. However, the effective chord length c' is itself initially unknown in the 3-D field since it is dependent on the induced angle, α_i. Thus, enforcement of boundary conditions at the 3/4 chord point requires that the physical locations of all control points be simultaneously iterated along with α_i. This would further require that influence coefficients be recalculated in each iteration step. (See Figure 6a.)

In order to minimize both computer time and potential convergence problems the following approach is used. It is assumed that section properties are merely the response to an effective angle of attack $\alpha_e = \alpha - \alpha_i$, where α_i is evaluated at the lifting line itself, normally taken as the 1/4 chord line. The boundary condition to be met at specified control points is then $\alpha_e = \alpha - \alpha_i$. The vortex or circulation lift due to the combined

mechanical airfoil and EMF (c_{ℓ_γ} for the equivalent airfoil) is represented as a bound vortex on the quarter chord. The gradient of the distribution of bound vorticity establishes the strength of the trailing vortices in the usual manner. The induced angle consists of that induced by the trailing vortices, and, when the wing is swept, by the contribution of the bound vortex representing the opposite wing panel. (See Figure 6b.) This is in contrast to the 3/4 chord boundary condition which requires the downwash contribution from all vortex elements.

The computational procedure developed in this study is based on a straight lifting line from wing root to tip, onto which all section properties are lumped. In practice the location of a constant percent chord line is shifted due to either mechanical flap extension or the EMF extension. This shift depends upon the spanwise location. For a *constant* longitudinal shift of the lifting line, all equations remain the same since all properties are lumped onto the line itself. In this sense the procedure has a limited self-adaptive capability. The user may elect to use *any* constant sweep line which is believed to most effectively represent the wing and EMF by a straight bound vortex. Good results have been obtained by using the quarter chord of the basic wing planform, which indicates that this selection is not critical.

b. Influence Coefficients of Lifting System

The loaded line and its associated trailing vortex system is identical to the Weissinger approach given in Ref. 11 with the exception that influence coefficients for downwash are calculated at the lifting line itself rather than at the 3/4 chord location.

The calculation of downwash influence coefficients is a straightforward modification of those in Ref. (11), and only summary comments follow. The method considers a distribution of bound vortex strength, Γ which is continuous along the lifting line and which vanishes at each wing tip. The Γ distribution is allowed to be unsymmetrical. The downwash integrals include both Γ (bound vortex) and $d\Gamma/dy$ (trailing sheet) in the integrand. Integration by parts allows the complete downwash integral to be written as a function of geometry and $d\Gamma/dy$ only. By writing Γ in terms of ϕ ($y = b/2 \cos \phi$) and using Multhopp's quadrature formula, the final influence coefficients a_{ν_n} are obtained, giving

$$\alpha_{I_\nu} = \sum_{n=1}^{m} a_{\nu n} G_n, \quad \nu = 1, 2 \text{ --- } m \tag{20}$$

where α_{I_ν} is the angle induced in the streamwise plane at span station ϕ_ν and $G_n = \Gamma(\phi_n)/bV$ represents the bound vortex strength at span station ϕ_n. Stations ϕ_ν and ϕ_n are standard for each specified m number of control points, that is, $\phi_\nu = \nu\pi/(m+1)$.

For a given geometry the influence coefficients a_{ν_n} can be computed once and for all. They do not depend upon the sizing of the EMF, which changes in each iteration step. The iteration is described later.

c. Fuselage Interference on the Wing

The first order effect of the fuselage on the wing is generation of a local flow inclination due to both pitch and sideslip, which is treated here by superimposing onto the wing an equivalent change in local geometric angle of attack. The method used is extremely simple, in that the wing is assumed to be submerged in the field generated by the isolated body. Additionally, the body is represented by a cylinder which extends to infinity in both directions, and whose constant cross section is chosen as that of the body in the vicinity of the inboard wing, where the effects are significant. For simplicity, the body cross section is approximated by an ellipse, of arbitrary axis ratio, whose center is arbitrarily located in the vertical direction. The calculation of the fuselage cross flow is nonlifting about the fuselage itself, so that its impact is confined to wing interference. Therefore, in the calculation program the interference angle of attack on the wing is treated as an equivalent geometric wash-in or wash-out which is constant during the span load iteration. In all subsequent discussion the geometric angle of attack of each airfoil section is understood to consist of

$$\alpha_{Geom} = \alpha_{Body} + \alpha_{Incidence} + \alpha_{Twist} + \frac{\Delta\alpha}{\alpha_{Body}}\,\alpha_{Body} + \frac{\Delta\alpha}{\beta}\,\beta + \frac{d\alpha_\Gamma}{d\beta}\,\beta \qquad (21)$$

where the last term is the result of geometric dihedral in sideslip. The calculation of $\Delta\alpha/\alpha_{Body}$ and $\Delta\alpha/\beta$ is given in Appendix A.

d. The Nonlinear System and Method of Iteration

(1) Simple Sweep Considerations. In keeping with simple sweep theory the boundary condition ($\alpha_e = \alpha - \alpha_i$) is imposed in the simple sweep plane. However, the equation is unchanged in streamwise coordinates since the transformation is the same for all α's. The system of equations in streamwise coordinates is therefore

$$\alpha_{e_\nu} = \alpha_\nu - \sum_{n=1}^{m} a_{\nu n}\, G_n \qquad \nu = 1, 2, \cdots m \qquad (22)$$

where

$$G = \frac{\Gamma}{bV} . \qquad (23)$$

Equation (22) represents a system of m equations for m unknown values of α_{e_ν}, since α_ν and a_{ν_n} are specified by the geometry and since G_n is ultimately expressible in terms of α_{e_n}. The circulation function $G_n(\alpha_{e_n})$ is expressible in terms of the section circulation lift coefficient given by Eq (18), with $\alpha - \alpha_i$ replaced by α_e (note that sweep must be taken into account). The quantity ψ_1 which occurs in Eq (18) is expressed by Eq (17) in terms of geometric quantities, momentum coefficient, and α_e. Thus, one can write

$$G_n = G_n(\alpha_{e_n}) \tag{24}$$

where this relation encompasses a rather lengthy algorithm involving Eqs (18) and (17), and the simple sweep conversions given in Figures 7 and 8.

(2) Iteration. For the special case of zero momentum coefficient the quantity ψ_1 is zero so that Eq (22) is linear in the unknowns α_{e_ν}. In the general case the system is nonlinear and iteration is required.

Equation (22) may be written

$$\alpha_{e_\nu} - \alpha_\nu + \sum_{n=1}^{m} a_{\nu_n} G_n(\alpha_{e_n}) = \varepsilon_\nu \qquad \nu = 1,2 \ldots m \tag{25}$$

$$\varepsilon_\nu = 0$$

or, in vector form

$$\vec{\varepsilon}(\vec{\alpha}_e^*) = 0 \tag{26}$$

where the star superscript indicates the actual solution.

In the vicinity of the solution $\alpha_{e_\nu} = \alpha_{e_\nu}^*$, $\varepsilon_\nu = 0$, one may make the linear approximation

$$\varepsilon_\nu = \sum_{n=1}^{m} \frac{\partial \varepsilon_\nu}{\partial \alpha_{e_n}} (\alpha_{e_n} - \alpha_{e_n}^*) \qquad \nu = 1,2 \ldots m \tag{27}$$

or alternatively

$$\alpha_{e_\nu} = \alpha_{e_\nu}{}^* + \sum_{n=1}^{m} \frac{\partial \alpha_{e_\nu}}{\partial \varepsilon_n} \varepsilon_n \qquad \nu = 1,2 \ldots m \tag{28}$$

Now make a guess for the m values of α_{e_ν}. These are used in (25) to calculate the error ε_ν. The root mean square error is calculated for future reference. The guessed α_e and the calculated error ε are substituted into Eq (28). The result is m number of equations which are linear in the m values of $\alpha_{e_\nu}^*$ and linear in the m^2 number of partial derivatives $\partial\alpha_{e_\nu}/\partial\varepsilon_n$. The m equations involve a total of m (m+1) unknowns. By making a total of m+1 linearly independent guesses one has m (m+1) equations and m (m+1) unknowns.

The equations are solved for $\alpha_{e_\nu}^*$ which are then used in (25) to obtain corresponding errors and the RMS error. The guess whose RMS error is greatest is replaced by the "improved guess" $\alpha_{e_\nu}^*$. The approximately linear relationship[28] is thus updated and a new value of $\alpha_{e_\nu}^*$ is calculated. The iteration is terminated when the RMS value of α_e^* is within a prescribed tolerance.

e. Three Dimensional Residual and Total Lift

With the iterated effective angle of attack known at m points across the span, the corresponding section circulation lift is calculated and numerically integrated to give total circulation lift for the wing and EMF combined. There is, in addition, a residual momentum lift, which must be taken into account. Within the framework of simple sweep theory (infinite yawed wing), there are no pressure or area gradients in the spanwise direction, so that loads and momentum changes are due only to the velocities and geometry which project onto the simple sweep plane. Although particles of fluid move along a nonplanar path, the pressure distribution is defined by the propagation of that motion onto the simple sweep plane. The classical arguments are readily extended to include the momentum injection when the momentum vector lies in the simple sweep plane.

In the general case the jet has a component of momentum normal to the simple sweep plane, and the skew angle between the jet and the simple sweep plane is denoted by ε as shown in Figure 8. The component of momentum $j_n = j \cos\varepsilon$ which lies in the simple sweep plane, is turned back parallel to the projection of the incident stream onto the simple sweep plane. The component which is injected perpendicular to the simple sweep plane, $j_\perp = j \sin\varepsilon$, is unaffected and it must be transported intact during the turning process. Thus, the simple sweep theory still applies to this case without modification. Therefore, the projections of all relevant quantities, including the injected momentum vector, onto the simple sweep plane have been used as the basis for calculation of section circulation properties.

Consider now the corresponding residual lift. This lift term consists of the projection of two vectors onto the airplane lift axis. The two vectors are (a) the component which is injected normal to the simple sweep plane and transported intact during the turning in the simple sweep plane and (b) the airplane component which has been turned parallel to the incident stream in the simple sweep plane. The geometry is shown in Figure 9 The components perpendicular to, and contained by the simple sweep plane are denoted by $j_\perp$ and j_n, respectively. The residual lift is then

$$\ell_{residual} = [j_n \cos(\Lambda \pm \beta) + j_\perp \sin(\Lambda \pm \beta)] \sin \alpha_{i_s} \qquad (29)$$

where the upper and lower signs correspond to the left and right hand panels, respectively. In terms of the injection skew angle, ε, one has

$$j_n = j \cos\varepsilon$$

$$j_\perp = j \sin\varepsilon$$

from which the residual lift, Eq (29), becomes

$$\ell_{residual} = j \cos(\Lambda \pm \beta - \varepsilon) \sin \alpha_{i_s} \qquad (30)$$

This expression is integrated across the span to give the total residual lift.

It is noted that the residual lift in Eq (30) is not defined exclusively by conditions in the simple sweep plane. At $\delta_f + \delta_j = 0$ the preceding term corresponds exactly to the momentum component which is injected onto the plane containing the freestream velocity vector and the airplane lift axis (pitch plane when $\beta = 0$). In general, for $\delta_f + \delta_j \neq 0$, the component injected within the aforementioned plane is

$$j_p = j(\cos^2(\Lambda \pm \beta - \varepsilon) + \sin^2(\delta_f + \delta_j)\,(\cos^2\varepsilon \sin^2(\Lambda \pm \beta))$$

$$-2\,[(1 - \cos(\delta_f + \delta_j))\sin\varepsilon \cos\varepsilon \sin(\Lambda \pm \beta) \cos(\Lambda \pm \beta)]^{\frac{1}{2}}$$

If $\delta_f + \delta_j$ is not too large, this may be approximated by

$$j_p = j\cos(\Lambda \pm \beta - \varepsilon)\left[1 + \frac{\delta_f + \delta_j}{2} \frac{\cos\varepsilon \sin(\Lambda \pm \beta) \tan(\Lambda \pm \beta - \varepsilon)}{\cos(\Lambda \pm \beta - \varepsilon)}\right] \qquad (31)$$

In the ranges of $\Lambda \pm \beta$ and $\delta_f + \delta_j$ for which linearized theory is expected to apply, this expression is not seriously different from the term $j \cos(\Lambda \pm \beta - \varepsilon)$ used in the calculation of the residual lift.

f. Rolling Moments in Sideslip

Rolling moments in sideslip are obtained by integrating the moment of the total lift distribution, regardless of how direct jet thrust lift is split between residual and vortex lift. This is given by

$$C_{\ell_{(Roll)}} = \frac{1}{4} \int_{-1}^{1} \left(c_{\ell_{total}} \, c/c_{avg.}\right) \eta d\eta$$

The present computer program is restricted to symmetrical geometry and momentum injection at arbitrary sideslip. The extension to cover the more general case of engine-failed rolling moments and aileron/flap lateral trim and control is straightforward since only a c_μ and aileron/flap input generalization is required.

g. Axial Force

This portion of the study was originally conducted as a check on the total span load distribution, its split between residual and vortex lift, and the entire concept. The program modifications to do this are negligible. The C_X calculations to date give additional confirmation of both concept and computational accuracy and are of course extremely useful in themselves.

The following considerations are pertinent. First, lift is of first order in angle of attack, whereas axial force is of second order. Second, lift is obtained as the sum of circulation lift and jet efflux momentum lift, whereas axial force is obtained as a difference between jet efflux momentum (thrust) and a circulation (induced) drag.

Inasmuch as a redirection of the jet produces changes in the total level of circulation, it follows that axial force involves differences in terms which can individually involve terms of second order in angle of attack, where such second order thrust and drag terms become increasingly interactive for increasing levels of aeropropulsive integration.

Specifically, it has been assumed in earlier discussion that the character of the remote wake has negligible influence on the overall lift characteristics. It is also assumed that the local jet is bent back parallel to the local downwash angle and that additional jet bending further downstream is sufficiently remote that its effects on lift can be ignored. Such additional turning results in an additional conversion of thrust lift into sheet circulation lift. This conversion is on a one-to-one basis since it is assumed to produce no significant effect on the wing. The corresponding changes in residual thrust and in circulation or vortex drag do not compensate because of their second order nature.

The axial force coefficient is calculated from Trefftz plane considerations, for which a more precise breakdown of total circulation and thrust forces is required. The bookkeeping difference is illustrated in Figures 10(a) and 10(b). The wing circulation lift, labeled "A," is identical in both the

near and remote fields. The total jet efflux lift, consisting of a circulation lift "B" and a residual lift "C", is also identical. The particular breakdown of "B" and "C" corresponding to the near field calculation (Figure 10(a) is not proper for axial force calculation. The more correct far field breakdown is shown in Figure 10(b).

The method outlined in Appendix B takes into account this finer breakdown while making use of shape factors based on the spanwise distribution of circulation forces obtained from the near field lift calculation already described.

h. Sidewash and Downwash

In sideslip the planview of the trailing vortex system is skewed from the airplane centerline by the sideslip angle β (approximately). This lateral displacement is of course taken into account in sidewash and downwash calculation. However, the effects of the wake skew on the influence coefficients a_{ν_n} is small and therefore neglected in the lift calculation. The lift calculation establishes the vortex strengths from which sidewash and downwash are calculated according to the Biot-Savart law.

4. SUMMARY OF METHOD

The preceding discussion has dealt with the individual program elements, special considerations, and how they are used in the overall analysis.

In order to give a clearer overall view, the program with its more essential features is summarized in the functional flow diagram shown in Figure 11. The input-output details, with an example problem and print-outs, are given in Appendix D. Computational details are not shown, but can be obtained if required from the computer program listing given in Appendix E.

SECTION III

COMPARISON OF THEORY AND EXPERIMENT

The comparisons shown in this section illustrate the capabilities of the method. They are typical, are in no way selective, and are generally quite good where the theory is expected to apply. Poor lift comparison is generally confined to normal upper surface stall, to lower surface separation on leading edge devices at negative angles of attack, and to cases where C_μ is too small to maintain flow attachment over the flaps. Rolling moment comparisons are good except for cases involving large pylons and nacelles, which are not considered in this analysis

1. BASIC LIFT COMPARISONS

Most comparisons shown here were made early in the program development when unsymmetrical cases and axial forces were not yet treated, and are shown mainly to illustrate the overall accuracy of the method.

Figure 12 shows a basic lift comparison for a rectangular, AR = 2.75 wing without a mechanical flap. The data are from Reference 12 (Williams & Alexander). It is noted that Das tested a substantially identical model (Reference 13) for which the comparison is much better, as shown in Figure 13.

The lift curve slope at $\alpha = 0$ is shown as a function of C_μ in Figure 14 for an AR = 5 rectangular wing[14]. The three sets of data shown correspond to different freestream velocities, for which the differences are minor. The theoretical curve does not consider this since it is a function of C_μ only. The lift at $\alpha = 0$ is shown in Figure 15, as a function of C_μ, for both inboard and outboard half span blowing. The theory correctly shows the increased effectiveness of inboard blowing.

Figure 16 shows a comparison for a more realistic IBF system tested by Boeing[15]. The blown flap extends outboard to $\eta = 0.75$ and has a 40 degree deflection. An additional jet deflection angle of about 10° occurs because of the upper surface trailing edge angle. The comparison is extremely good.

Figure 17 illustrates the major features of a large scale IBF model tested in the NASA-Ames 40 x 80 foot wind tunnel as a joint AFFDL/NASA-Ames/Lockheed program[16]. The major features are segmented aileron-flap blowing, the Jacobs-Hurkamp expanding duct arrangement, and the trailing edge control flap. The control flap has the capability of modulating the jet injection angle at a fixed flap setting. Some lift comparisons are shown in Figures 18 through 23 as various flap deflections and blowing arrangements. Lift performance with full span 30° flaps and full span blowing (constant section C_μ is shown in Figure 18. The effect of increasing inboard flaps to 60 degrees is seen by comparing with Figure 19. The 60/30 flap arrangement of Figure 19 is shown in Figure 20, for which jet flap blowing is restricted to the 60 degree inboard flap with BLC levels only on the aileron. For these cases the

comparison is generally good. Figures 21 and 22 show C_{L_α} and C_L at $\alpha = 0$ as functions of C_μ for full span blowing with inboard/outboard deflections of 60/30 degrees and 60/60 degrees, respectively. It is clearly seen that excellent comparison is reached at high blowing levels typical of the design condition. It is noted that the blowing split between flap knee and trailing edge is 13 vs. 87 percent of the total flap C_μ.

Figure 23 compares theory and experiment for inboard/outboard flaps at 60/30 degrees, with inboard jet flap blowing, and with the control jet deflected 40 degrees. The jet is thus injected at 100 degrees relative to the wing plane, so that the optimistic theoretical result is to be expected.

2. LIFT AND AXIAL FORCE FOR ANALOGOUS JET FLAP SYSTEMS

This section compares calculated lift and axial force with experiment for four large scale models tested in the NASA-Ames 40 x 80 foot tunnel. The systems are the Internally Blown Flap discussed previously, the Augmentor Wing, Externally Blown Flap and Upper Surface Blowing (References 16, 17, 18, 19). The basic clean planforms and overall arrangements are similar for the four cases. System details are not shown; schematics are illustrated in Figures 17, 24 25 and 26. The EBF and USB calculations are based on estimated jet spreading. Augmentor wing calculations use ϕC_μ, rather than C_μ, where ϕ is the augmentation ratio under static conditions and C_μ is based on primary (ejector) thrust. The calculated augmentor wing C_X values shown have not been corrected for flap augmentor ram drag.

The compared results are summarized in Figures 27 through 30 for each of the four high lift concepts at typical takeoff and landing configurations. It is clearly seen that the present method accurately predicts the first order performance differences among these concepts. These calculations shown in Figures 27 through 30 are the first obtained by this method by persons other than the authors. They were obtained by Messrs. Y. T. Chin and Lee Brandt, of the Lockheed-Georgia Company, without prior experience in either program usage or "optimized" geometric interpretation of certain input parameters (e.g. optimum representation of USB Coanda flaps by a single flap element).

A typical span loading is shown in Figure 31 although no experimental data are available for comparison. This corresponds to the USB configuration cited in the preceding section at $C_\mu = 1.2$, $\alpha = 5°$, and with flaps in landing position (see Figure 31). The wing circulation lift, EMF circulation lift and residual momentum lift are indicated in the figure. The load gradients between successive flap panels are apparent. It is especially interesting that the fraction of direct lift converted to EMF vortex lift is about 25 percent. This is the direct result of the severe load gradients at the edges of the blown section, which in this case cause local downwash angles of 30 to 35 degrees. The effective injection angle (relative to the local flow) is thus reduced by about half.

3. ROLLING MOMENT DUE TO SIDESLIP

The majority of comparisons shown here are for the large scale IBF model shown earlier in Figure 26[20]. These tests were made tail-on. Calculated wing-body results have therefore been corrected for rolling moments due to the rather large vertical tail. Sidewash calculations were unavailable when the comparisons were made, so that the vertical tail correction was based on standard DATCOM techniques[21]. This in no way invalidates the comparisons since the expected differences in vertical tail rolling moment are small compared to the configuration total. Table 1 summarizes the range of variables covered in the sideslip runs. The variables covered are angle of attack, momentum coefficient, main flap deflection, and control flap deflection. All runs were at 30 degrees aileron deflection, with jet flap levels of blowing over the main flap and BLC blowing on the aileron.

Rolling moments for uniform 30 degree flap/aileron deflection are shown in Figures 32(a) through (c), for $\alpha = 4$ and 12 degrees and for $C_\mu = 0.51$, 1.01 and 1.52. The sensitivity of wing-body rolling moment to angle of attack is compensated by the shift in vertical tail contribution. It is surprising that the calculations are rather insensitive to variations in C_μ; nevertheless, this fact is supported by experimental data.

The effect of increasing the main flap deflection to 60 degrees is seen by comparing Figures 32(b) and 32(d). At both $\alpha = 4$ and 12 degrees this effect increases the rolling moment by about 35 percent.

Figures 32(e) through (g) cover the same α and C_μ range as Figures 32(a) through (c). The main flap/aileron/control jet deflections are 60/30/20/degrees, respectively. A general increase in rolling moment is apparent relative to the corresponding 30/30/0 degrees arrangement.

Figure 32(h) shows results at $C_\mu = 1.05$ only for the 60/30/40 arrangement. Comparisons of Figures 32(d), (f) and (h) show a sizeable increase in rolling moment due to increasing control flap deflection.

Rolling moment is shown in Figure 33 for the large scale USB model noted earlier[19]. The wing-body calculation corrected for vertical tail compares less favorably than did comparable IBF results, which is most likely due to the large over-the-wing nacelles. A coarse assessment of the nacelle contribution is made as follows. The effect of fuselage size scales approximately as $(\text{diameter})^2$ provides that the wing and body retain the same relative position; in this case the fuselage and nacelles are both approximately snugged to the wing. Thus,

$$\frac{\Delta C_{\ell_{2\,nac}}}{\Delta C_{\ell_{fus}}} = -2 \left(\frac{D_{nac}}{D_{fus}} \right)^2$$

for which it has been assumed that the fuselage effect and nacelle effects are pure couples. For $D_{nac}/D_{fus} \simeq 0.7$, the nacelles are expected to cancel the fuselage effect. The correction, $\Delta C_{\ell_\beta} \simeq +0.001$ per degree, gives considerable improvement, as seen in Figure 33.

The last comparison is given in Figure 34 for the Boeing IBF model noted previously (see Figure 16, Reference 15). The poor comparison is probably due primarily to pylon-nacelle crossflow blockage in sidewash. The assumption that fuselage crossflow is effectively blocked allows removal of about $\Delta C_{\ell_\beta} \simeq -0.001$ per degree. The cascade or flow straightening effect of the nacelles and pylons also reduces the effective wing sideslip. Moreover, the pylon sideloads due to sideslip shed vortices at each wing pylon juncture. The resulting four couples give an additional positive increment in C_ℓ. No attempt is made here to quantify the nacelle-pylon interference, which is an area requiring further work.

SECTION IV

EFFECTS STUDIES

This section presents a limited number of effects studies. The dependent variables are rolling moment and sidewash derivatives; independent variables are fuselage shape, size, and vertical location relative to the wing, wing sweep, goemetric dihedral, some planform effects, and distribution of trailing edge blowing and injection angle.

It is not intended to provide a wide range of working curves, but rather to illustrate the utility of the method and some first order trends. For this reason the effects are generated, in general, as perturbations to a baseline configuration, which is chosen as the large scale IBF model discussed earlier[20]. The total blowing coefficient (based on wing reference area) is $C_\mu = 1.01$, consisting of local blowing levels (based on extended chord) of 1.0294 for sections out to 70% span and 0.2628 for sections from 70% span to the wing tip. The wing has a full span leading edge device which contributes to a 14% chord extension. The leading edge device is 12.3% of the extended chord and is deflected 60 degrees. The main aft flap is 30.7% of the extended chord and is deflected 30 degrees. The control flap was at zero deflection; that is, the jet exited parallel to the main aft flap. All the effects shown are for a wing-body combination only. A common point of reference is in general given in all the parametric effects studies. This common baseline point is denoted by a circular symbol. Some effects studies are shown for off-baseline cases, for which the corresponding secondary variations are noted.

1. ROLLING MOMENT DUE TO SIDESLIP

Figure 35a presents the effect of body size and shape on the incremental rolling moment derivative, C_{ℓ_β}, due to the body. The effect of body size is shown for both a constant body height, b, and body width, a. The effect of body shape for a constant body frontal area, S_π, is also given. The prediction by Equation 5.2.2.1-c of DATCOM[21] is shown as the dashed line.

The effect of body shape and vertical wing location for bodies with frontal areas equal to the baseline body is presented in Figure 35b. As expected, the magnitude of C_{ℓ_β} increases with the high wing location. The incremental effect of the body increases as the wing becomes increasingly displaced from the center of the body.

The effects of sweep and vertical wing location are presented in Figures 35c and 35d for the extremes of body shapes considered. Note that the baseline configuration having a circular body appears slightly off the parametric line of Figure 35c. As expected, wing sweep angle is a very significant parameter.

Geometric dihedral angle is another significant parameter in the evaluation of wing-body rolling moment due to sideslip. The effect of geometric dihedral and vertical wing location is shown in Figures 35e and 35f for circular and vertical elliptic bodies, respectively. As can be seen, a few degrees of geometric dihedral can offset the effect of vertical location of the wing. Thus, for swept wing aircraft high wing configuration have negative dihedral or anhedral and low wing configurations have dihedral to maintain similar levels of C_{ℓ_β}.

The effect of momentum distribution is also a very significant parameter in predicting the wing-body C_{ℓ_β}. Previous difficulty in the analysis of this parameter is, of course, the primary reason for the development of the present method. In illustrating the effects of momentum distribution the fraction of blown span and momentum injection angle were considered. In all cases the total wing momentum coefficient was held constant at $C_\mu = 1.01$. Figure 35g illustrates these effects about the baseline configuration. Recall that the baseline had a low level (section $c_\mu = 0.263$) of blowing outboard of the 70% span station. In Figure 35g, the 50% inboard span blowing, as well as the baseline 70%, has an outboard section blowing level of $c_\mu = 0.263$. The jet angle, δ_{Jet}, is positive when the jet is injected downward relative to the flap reference plane. In this figure note that the injection angle is a strong parameter whereas the effect of the percent span of the main jet flap is small, and in general the magnitude of C_{ℓ_β} decreases as the jet flap span decreases. The cases illustrated in Figure 35h differ only in that there is no blowing on the outboard section (outboard potential flow assumed). Note that the effect of jet flap span is much greater and the trends are opposite of those shown in the previous figure. The magnitude of C_{ℓ_β} in this case shows significant increases as jet flap span is reduced. These two cases presented in Figures 35g and 35h graphically illustrate the sensitive nature of the rolling moment derivative to small changes in the distribution of blowing across the span. Contrasted to the high wing location data of Figure 35h, data for a low wing configuration are presented in Figure 35i. Note the vertical wing location effect is nearly a constant ($\Delta C_{\ell_\beta} \simeq + 0.0023$) for all combinations shown. This increment value is also approximately the same as shown in Figure 35b, which indicates that body effects can be superimposed and maintain a good degree of accuracy.

The final effects shown are for wing aspect ratio and taper ratio variations about the baseline planform. These effects are presented in Figure 35j. The momentum distribution for these cases differ from the baseline in that there is no blowing outboard of the 70% span station. The baseline point is denoted by the circular symbol for a point of reference. Note that the taper ratio has little effect on rolling moment derivative for this distribution of momentum. Aspect ratio has a relatively small effect as compared to other parameters examined.

2. SIDEWASH DUE TO SIDESLIP

The parametric effects of these variables on sidewash derivative at a typical field location are presented in Figure 36. The field point selected corresponded to the quarter chord of the vertical tail mean aerodynamic chord on the Ames IBF model described in Reference 16. This point was maintained constant with respect to the wing apex. Effect studies where wing vertical location is a parameter may therefore require special interpretation. The sidewash, as predicted by the computer program, is based on a flat wake trailing back streamwise from the one-quarter chord of the wing. This assumption is a first order approximation to the physical wake location and in general is sufficient for accurate downwash prediction in the vicinity of the horizontal tail. In the case of sidewash, however, the vertical location of the field point in question relative to the wake is a very strong parameter. Therefore, some judgment in the use of the sidewash prediction methods may be required.

The effects of body shape, holding body frontal area equal to the baseline value, and vertical location of the wing are presented in Figure 36a. Note that the high wing location shows a destabilizing effect of approximately 35 percent. The base case is again denoted by the circular symbol. The effects of wing sweep and vertical location are illustrated in Figure 36b. These cases differ from the baseline in that the body shape is that of a flat (b/a = 0.5) ellipse. The baseline point is, therefore, off the line of data presented but is given for reference. As before the high wing destabilizing effect is approximately the same, indicating that the effect of vertical wing location could be superimposed. As expected, increased wing sweep has a destabilizing effect.

The effect of wing dihedral and vertical location is presented in Figure 36c. Again, superposition of vertical location of the wing appears to be possible. Positive dihedral increments would tend to cause slight decreases in vertical tail stability contribution to restoring yawing moment.

The effect of momentum distribution via jet injection angle and percent span of the jet flap are shown in Figures 36d, 36e and 36f. Perturbations about the base case are given in Figure 36d. For this type of distribution the half span jet flap case shows a decrease in stability as injection angle is increased. When the small amount of outboard blowing present on the baseline is removed, the trend reverses, as seen in Figure 36c. The superposition of effect of vertical wing location is again verified between the high wing cases of Figure 36e and the low wing cases of Figure 36f.

The effect of planform on sidewash derivative is illustrated in Figure 36g. These cases differ from the baseline in that there is no blowing outboard of the 70% span station. The base case is denoted on the figure by the circular symbol for reference purposes. The figure indicates that increases in aspect ratio as well as taper ratio would reduce the vertical tail stabilizing effect.

SECTION V

CONCLUSIONS AND RECOMMENDATIONS

A simplified method has been devised for calculation of lift, axial force, rolling moment, sidewash, and downwash for jet flapped wing-body combinations in pitch and sideslip. A number of comparisons have been made with experimental data. From these comparisons the following general conclusions have been drawn.

(1) Lift coefficient, as a function of angle of attack, is predicted reasonably well over the range where linearized potential theory may be expected to apply. In many cases this is true well beyond the normal bounds of applicability. The exceptions are normal, such as upper surface stall, undersurface separation from large leading edge flaps, extremely high control flap deflections, and low C_μ insufficient to establish flow attachment. The preceding statements are true over a wide range of planform shape, leading and trailing edge mechanical flap geometry, deflection, and spanwise arrangement, and level and trailing edge distribution of the injected momentum vector.

(2) Conclusion (1) generally applies to axial force calculation, although it is noted that the planform variations in the data comparisons are more restrictive. The correct assessment of axial force requires consideration of the ultimate wake turning as well as the spanwise distribution of vortex loading. For the cases cited, good results are obtained without direct consideration of nonplanar effects in the near field.

(3) Rolling moments due to sideslip are adequately predicted for wing-body-vertical tail combinations when wing-body computer calculations are corrected for the vertical tail contribution. The rolling moment calculation does not include the effects of pylons and nacelles, which may have a significant contribution on some configurations.

(4) The entire EMF concept appears to provide a good preliminary design working tool. In view of the general levels of correspondence for lift, axial force, and rolling moment, it is believed that span load distributions are necessarily correct to about the same level.

Based on the preceding conclusions the following areas are recommended for follow-on studies.

(1) The input-output routines should be modified to include nonsymmetric momentum injection and flap-aileron deflection. This should provide insight into engine or duct failure and lateral trim against such failures. For such cases the yawing moments due to induced drag asymmetry can become important, and can perhaps be reasonably estimated by this method. Similarly, the imposition of an antisymmetric twist angle should give insight into the roll damping for jet flap type high lift systems.

(2) Pitching moment, not considered in the present study, is also a logical extension. The expected accuracy is not clear because of the simplifying assumptions; however, it is expected that at least first order effects can be calculated.

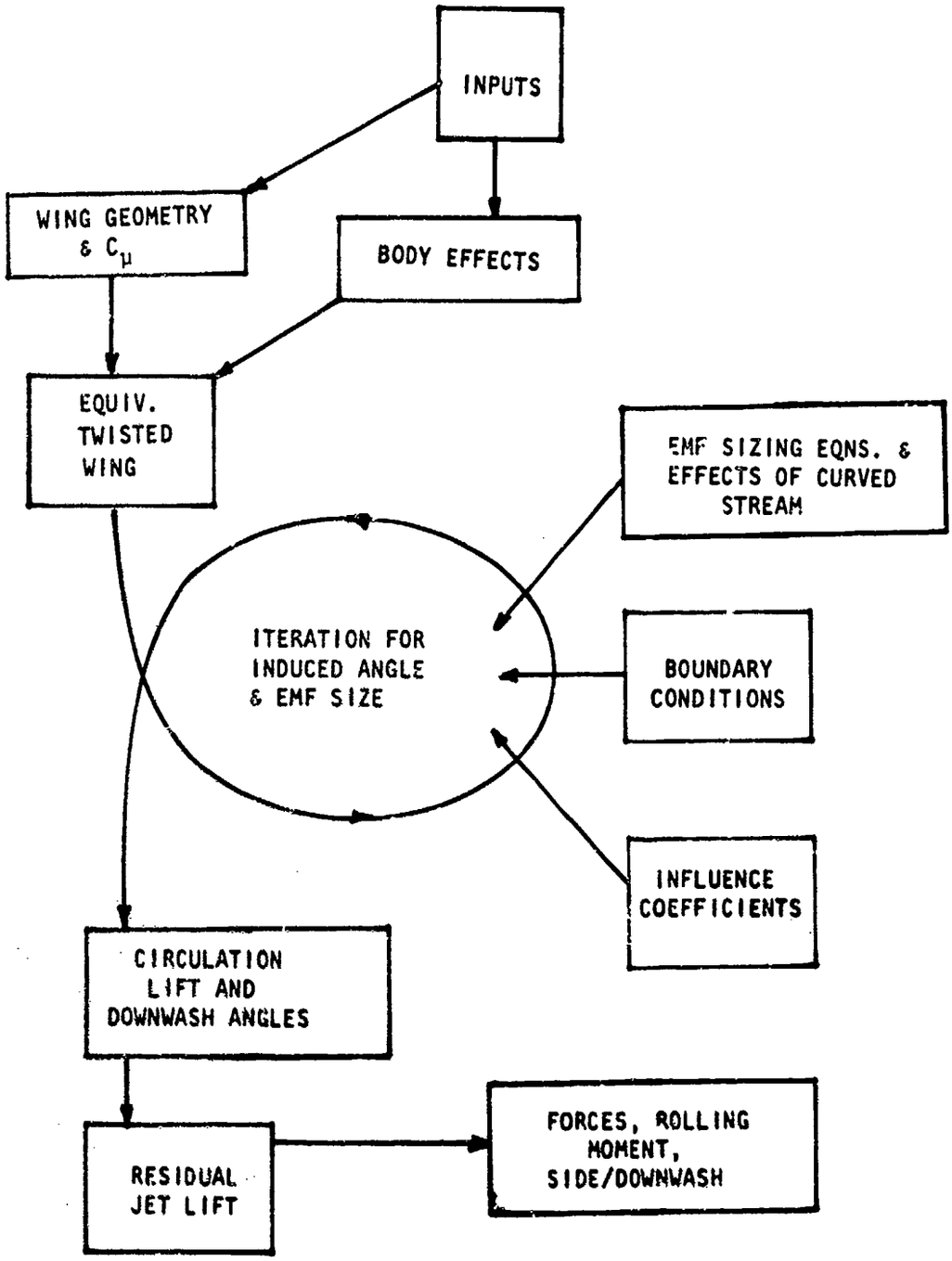

Figure 1. Essential Program Elements

$$\int_0^1 \frac{\gamma(x)}{V(x-x_o)}\,dx + \frac{c_\mu}{2}\int_1^\infty \frac{z''}{x-x_o}\,dx = 2\pi\alpha,\quad 0 < x_o < 1 - \frac{c_F}{c}$$

$$= 2\pi(\alpha + \delta_f),\quad 1 - \frac{c_F}{c} < x_o < 1$$

$$= 2\pi z'(x_o),\quad 1 < x_o < \infty$$

$$z'(1) = \alpha + \delta = \theta_j$$

$$z'(\infty) = 0$$

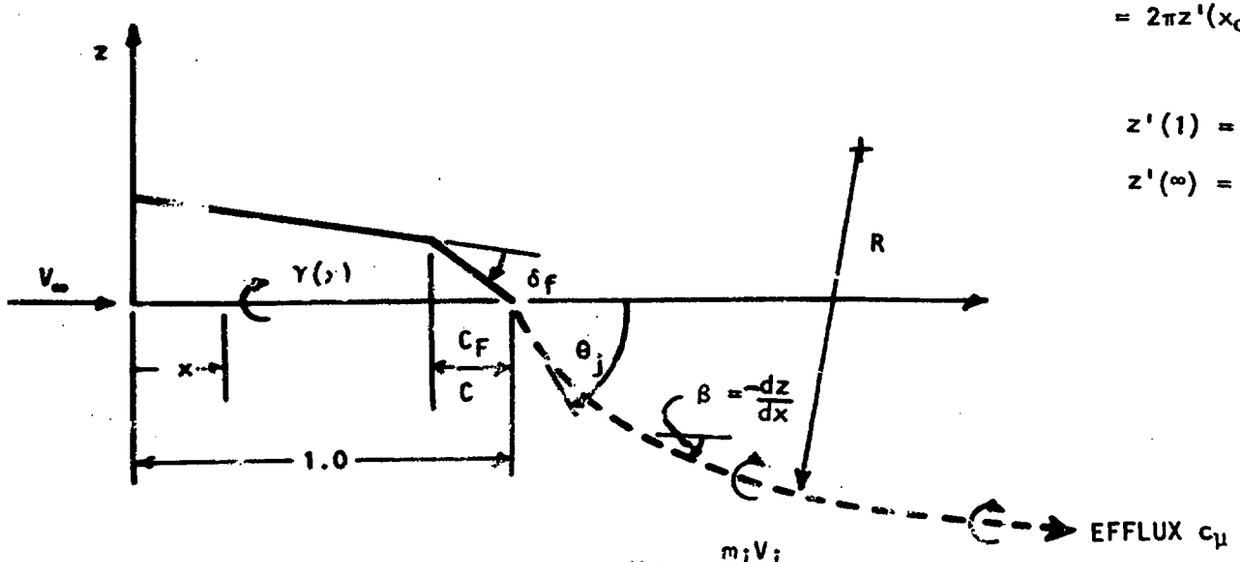

$$\rho V\gamma_j = \frac{m_j V_j}{R} \simeq m_j V_j z''$$

$$\frac{\gamma_j}{V} = \frac{c_\mu}{2} z''$$

Figure 2. Spence's 2-D Jet Flap Model

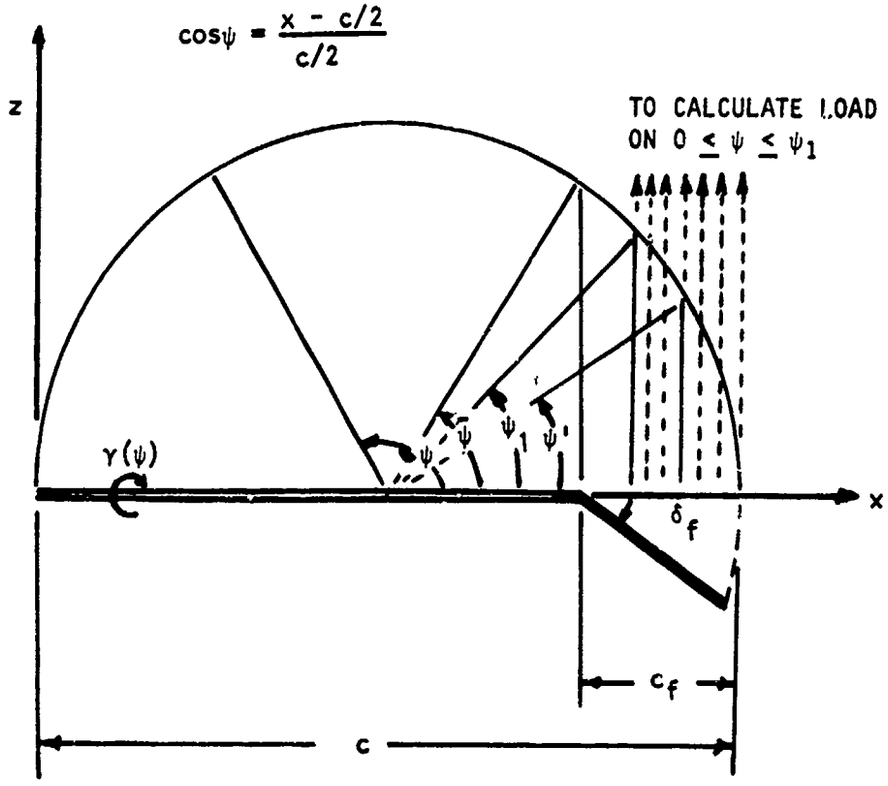

Figure 3. Coordinates for Airfoil with Simple Hinged Flap

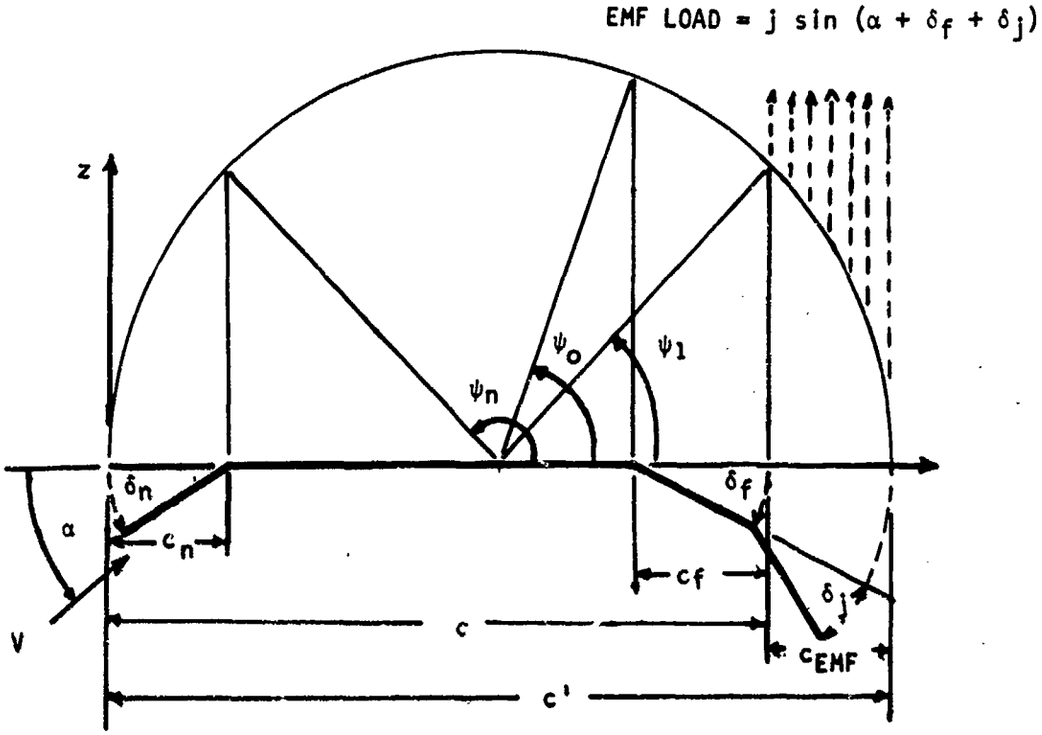

Figure 4. Schematic of 2-D Airfoil with Nose and Main Flap and Equivalent Mechanical Flap

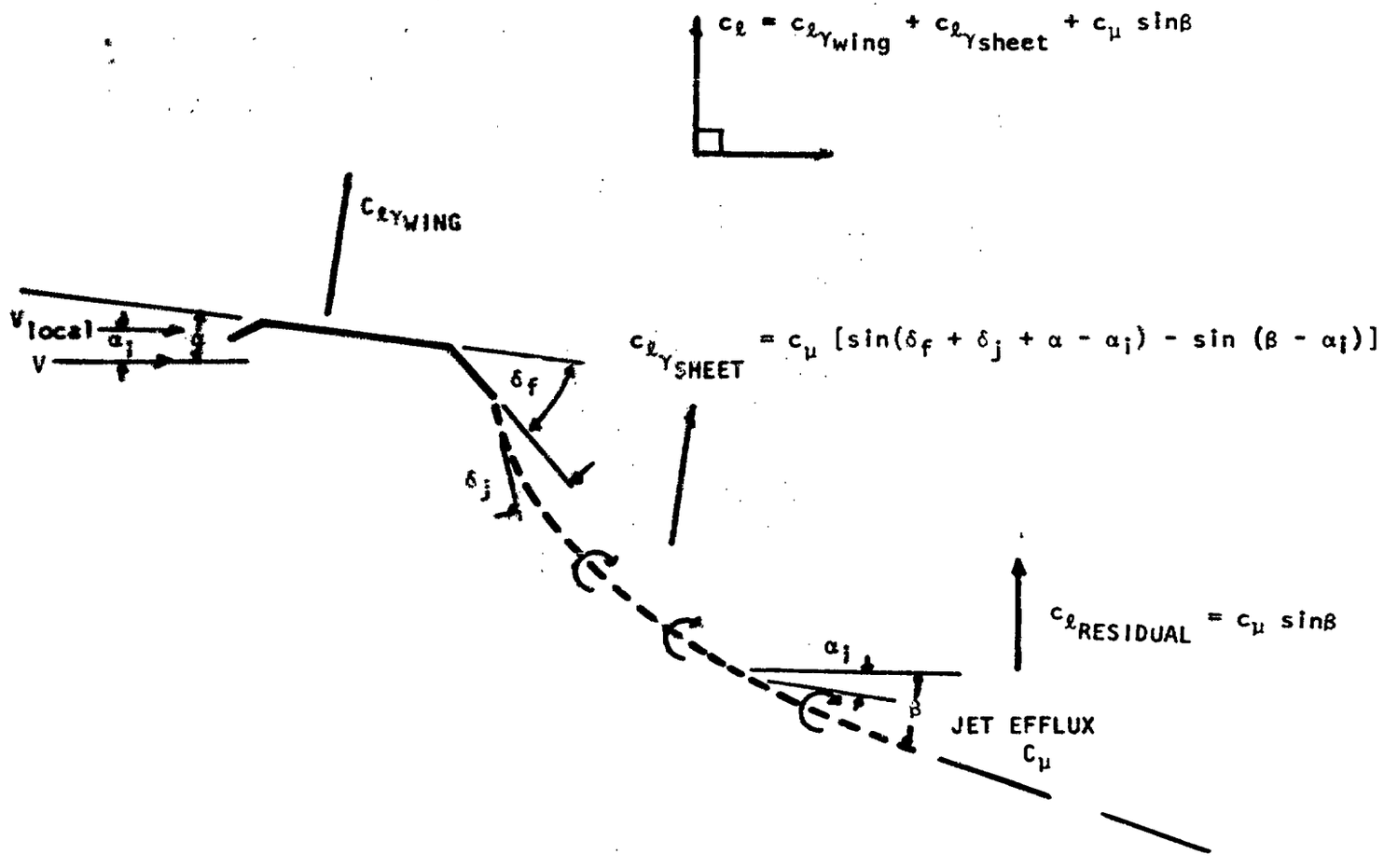

Figure 5. Two Dimensional Jet Flap in Curved Stream

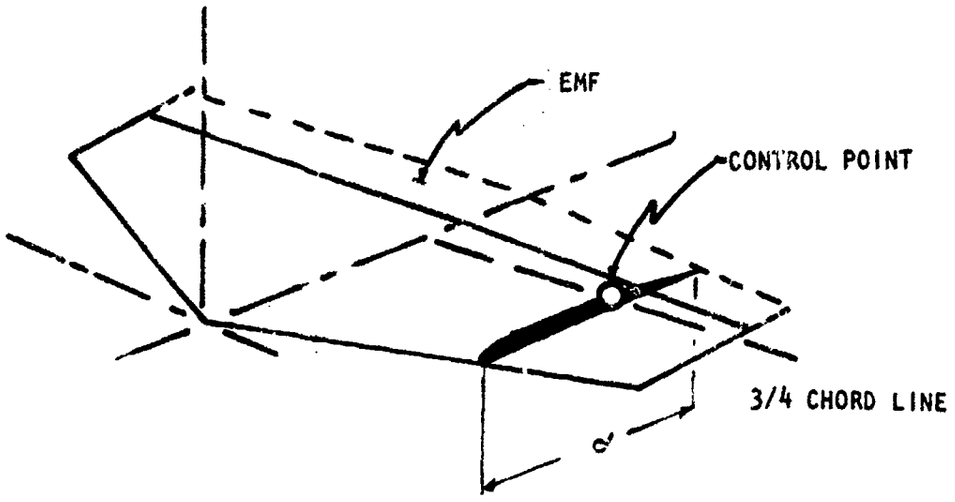

(a) c' is sensitive to effective α; location of 3/4 c' control point is variable during span load iteration.

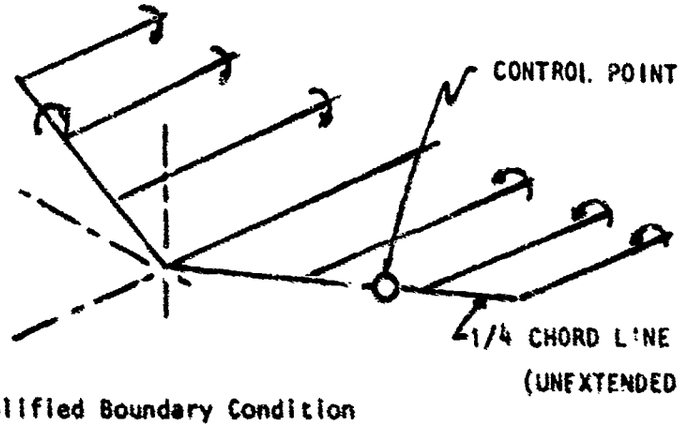

(b) Simplified Boundary Condition

$$\alpha_e = \alpha - \left(\frac{w}{V}\right)_{c/4}$$

Figure 6. Illustration of Boundary Conditions

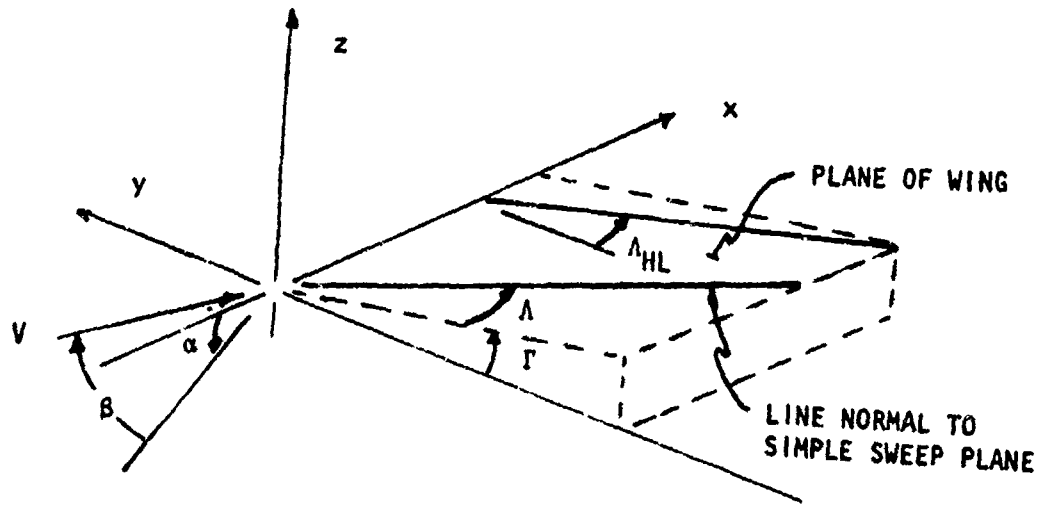

FOR SMALL α, Γ

$$\alpha_s = \alpha_{Body} + \alpha_{Incidence} + \alpha_{Twist} \mp \beta\Gamma - \frac{\omega}{V}$$

$$\alpha_n = \frac{\alpha_s}{\cos(\Lambda \pm \beta)}$$

$$\frac{q_n}{q_\infty} = \cos^2(\Lambda \pm \beta)$$

$$\tan \delta_n = \frac{\tan \delta_s}{\cos \Lambda_{HL}}$$

δ_s = ROTATION ABOUT y AXIS

δ_n = ROTATION ABOUT HL

δ_n IS USED IN NORMAL PLANE

NOTE: UPPER SIGN DENOTES
LEFT HAND PANEL

Figure 7. Pitch Plane and Simple Sweep Plane Resolution - α, q, δ

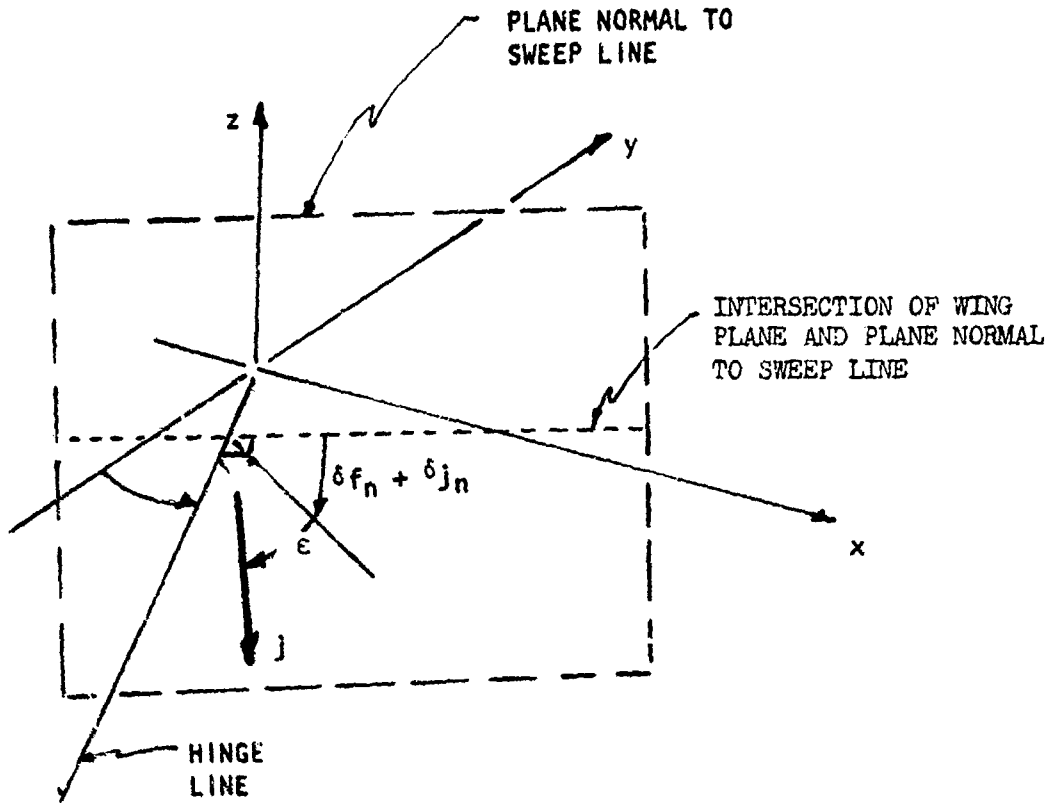

j = MOMENTUM EFFLUX PER UNIT OF SPAN (y) REGARDLESS OF DIRECTION

IN STREAMWISE COORDINATES:

$$c_{\mu_s} \equiv \frac{j}{q_s c_s}$$

$$c_{\mu_{s_{lat}}} = c_{\mu_s}(\text{cosec}\cos(\delta f_n + \delta j_n)\sin\Lambda_{HL} - \sin\text{ec}\cos\Lambda_{HL})$$

$$c_{\mu_p} = \sqrt{c_{\mu_s}^2 - c_{\mu_{lat}}^2}$$

NORMAL PLANE SECTION c_μ:

$$c_{\mu_n} = c_{\mu_s}\frac{\cos\varepsilon}{\cos^2(\Lambda \pm \beta)}$$

Figure 8. Pitch Plane and Simple Sweep Plane Resolution for Momentum

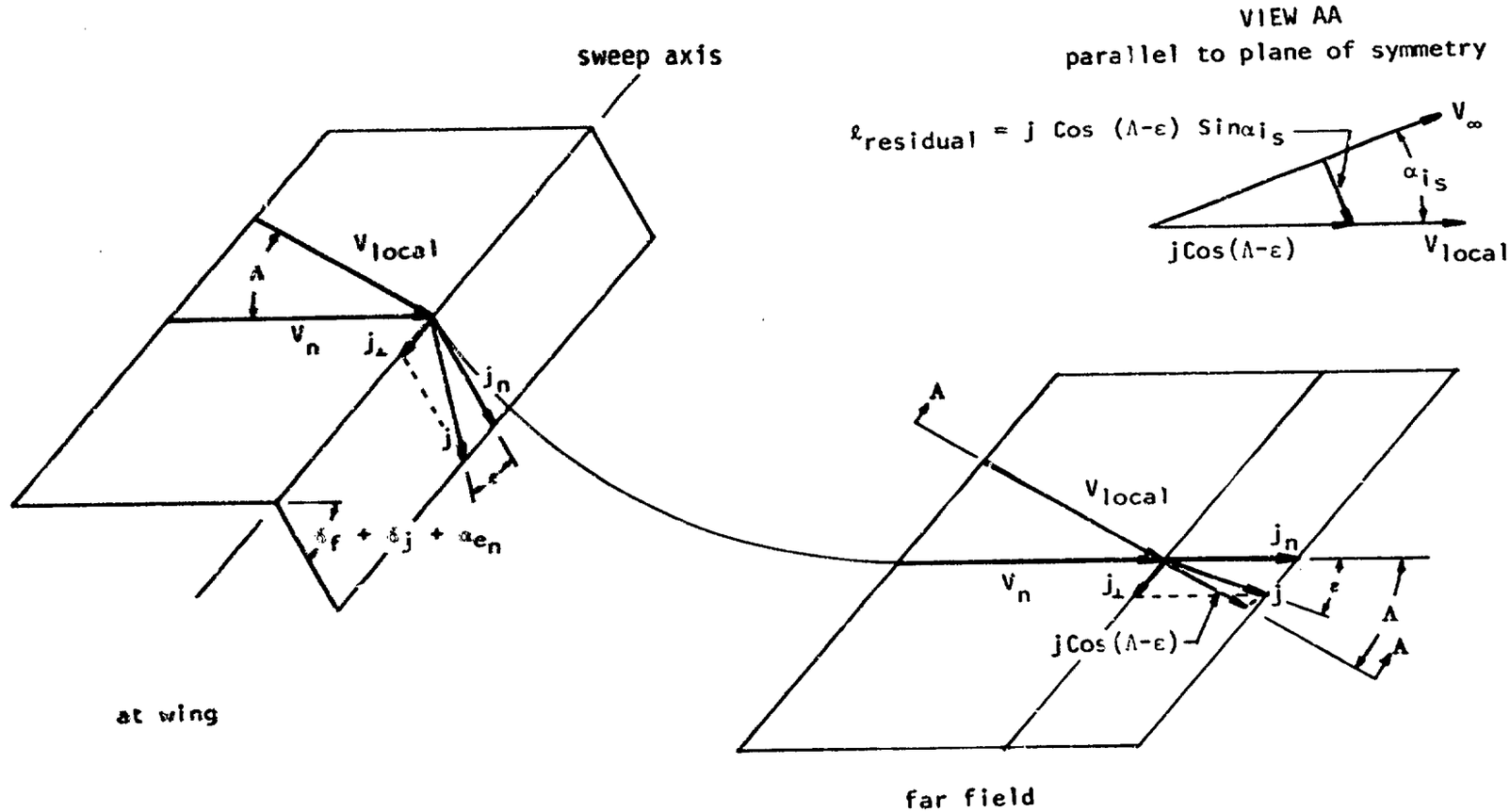

Figure 9. Calculation of Residual Lift Using Simple Sweep Theory

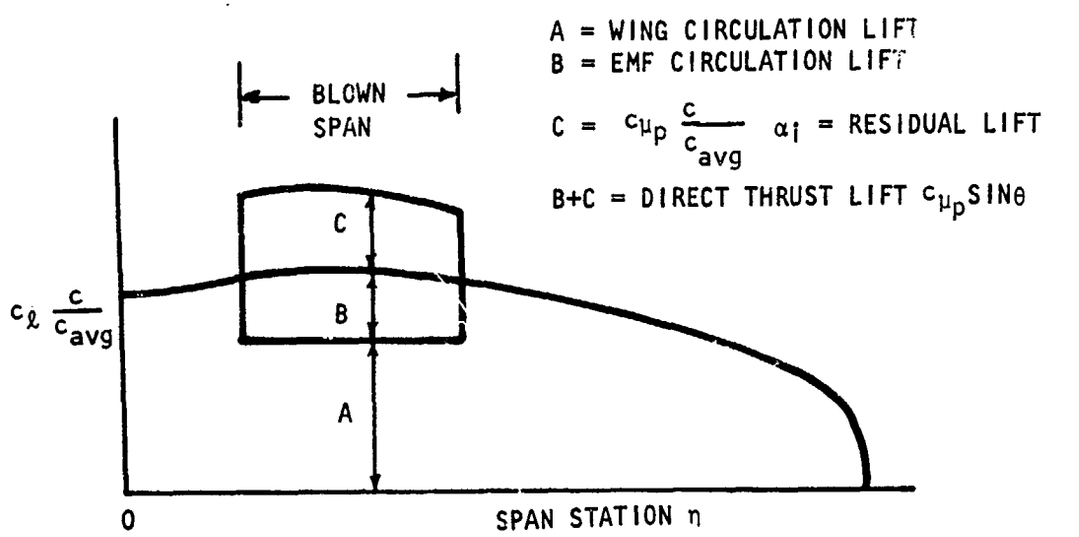

(a) Near Field Calculation, $\beta = \alpha_i$

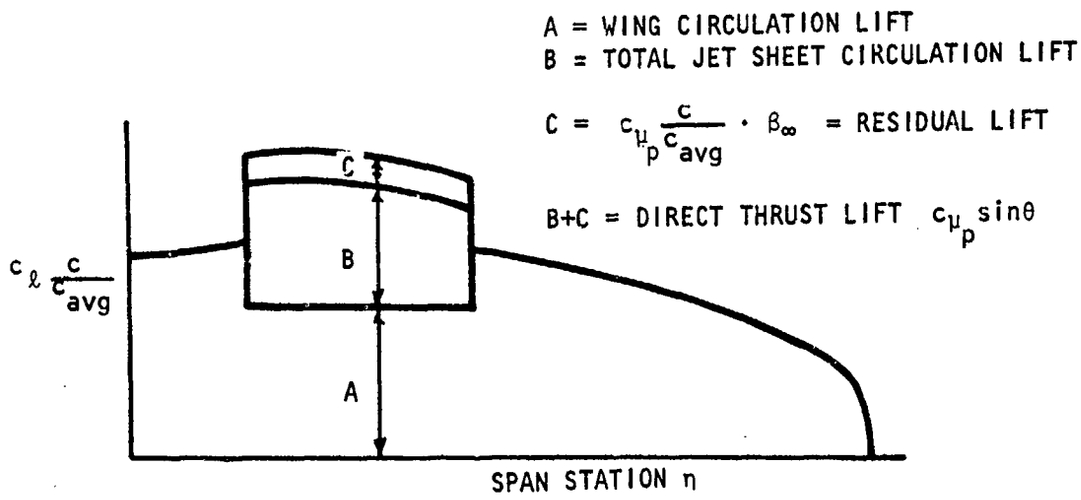

(b) Far Field, $\beta = \beta_\infty$

Figure 10. Continued Conversion of Jet Momentum to Vortex Forces Beyond Near Field Lift Calculation

(a) and (b) have equal lift, unequal drag

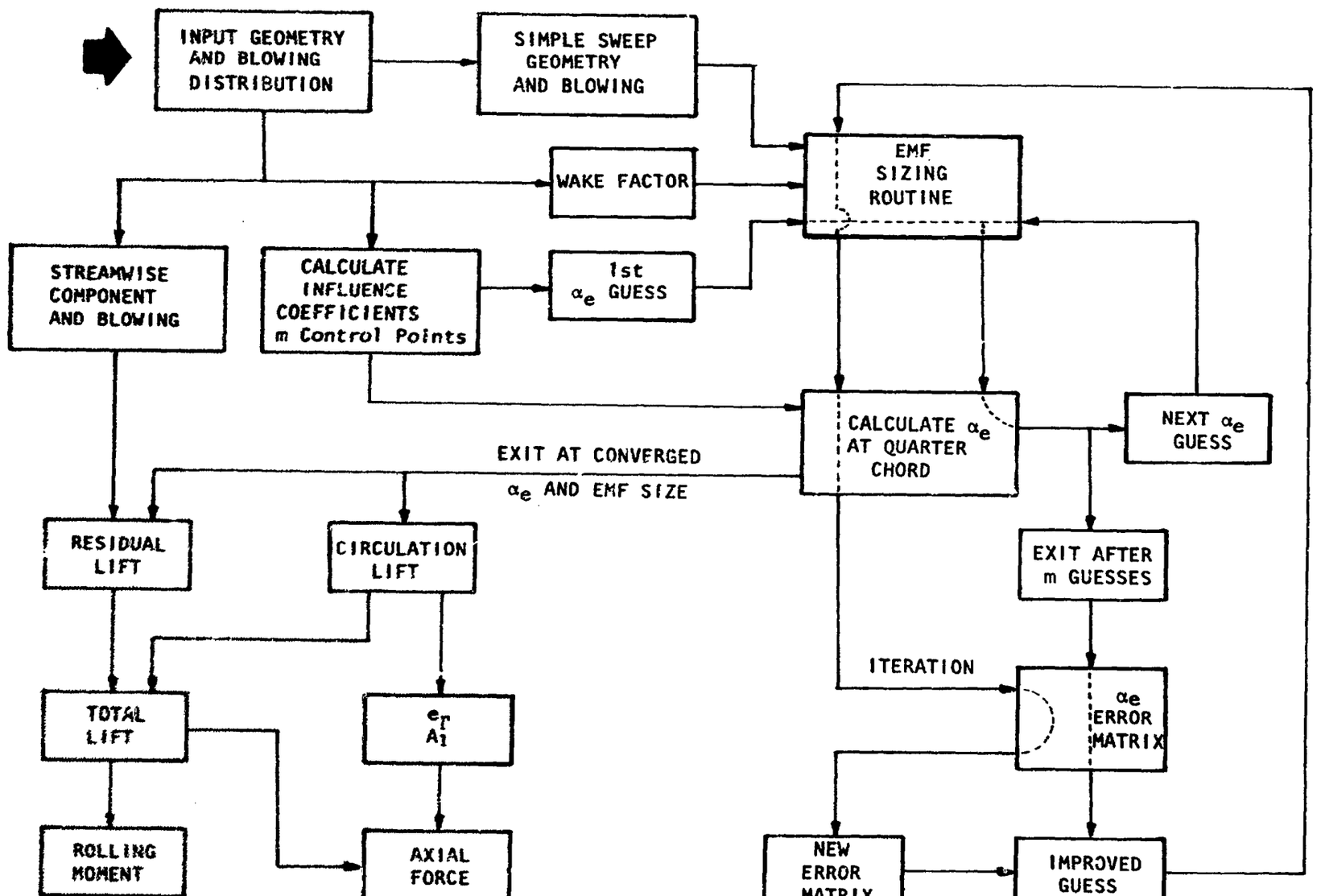

Figure 11. Functional Flow Chart

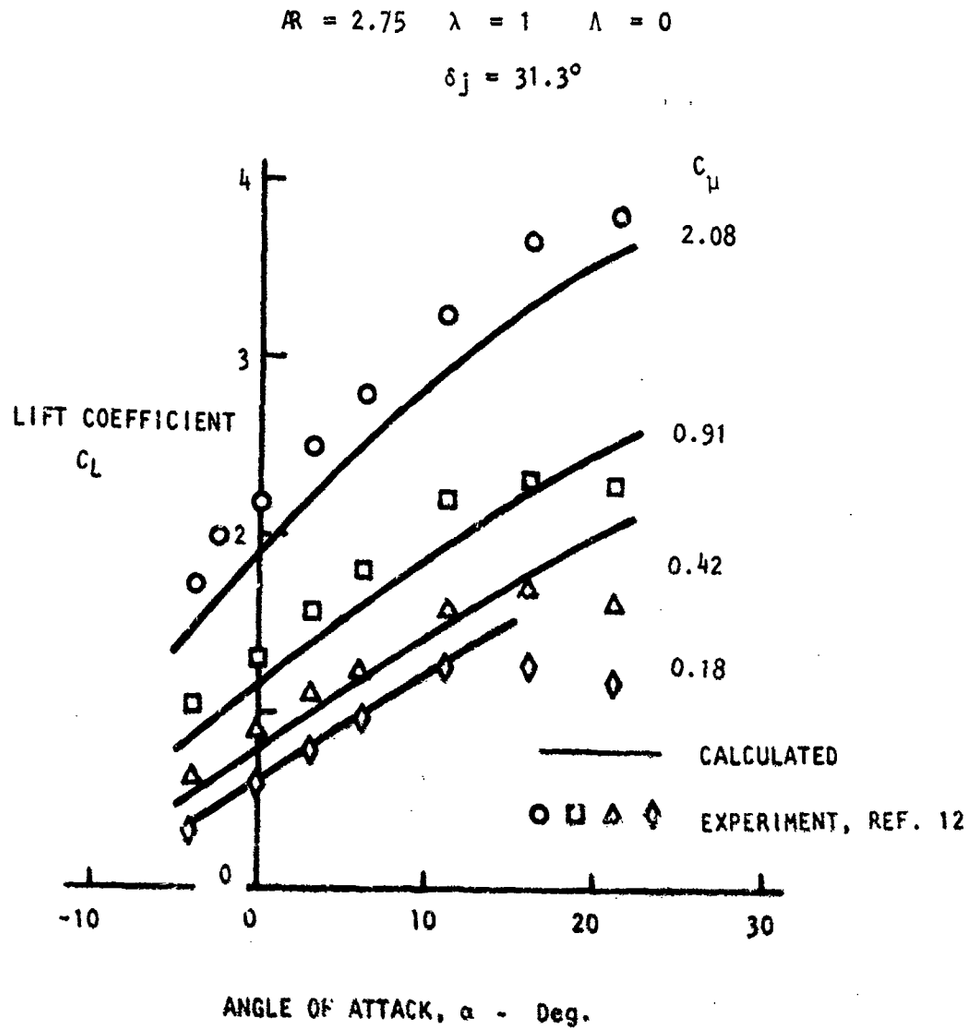

Figure 12. Lift Curve Comparison for Pure Jet Flap

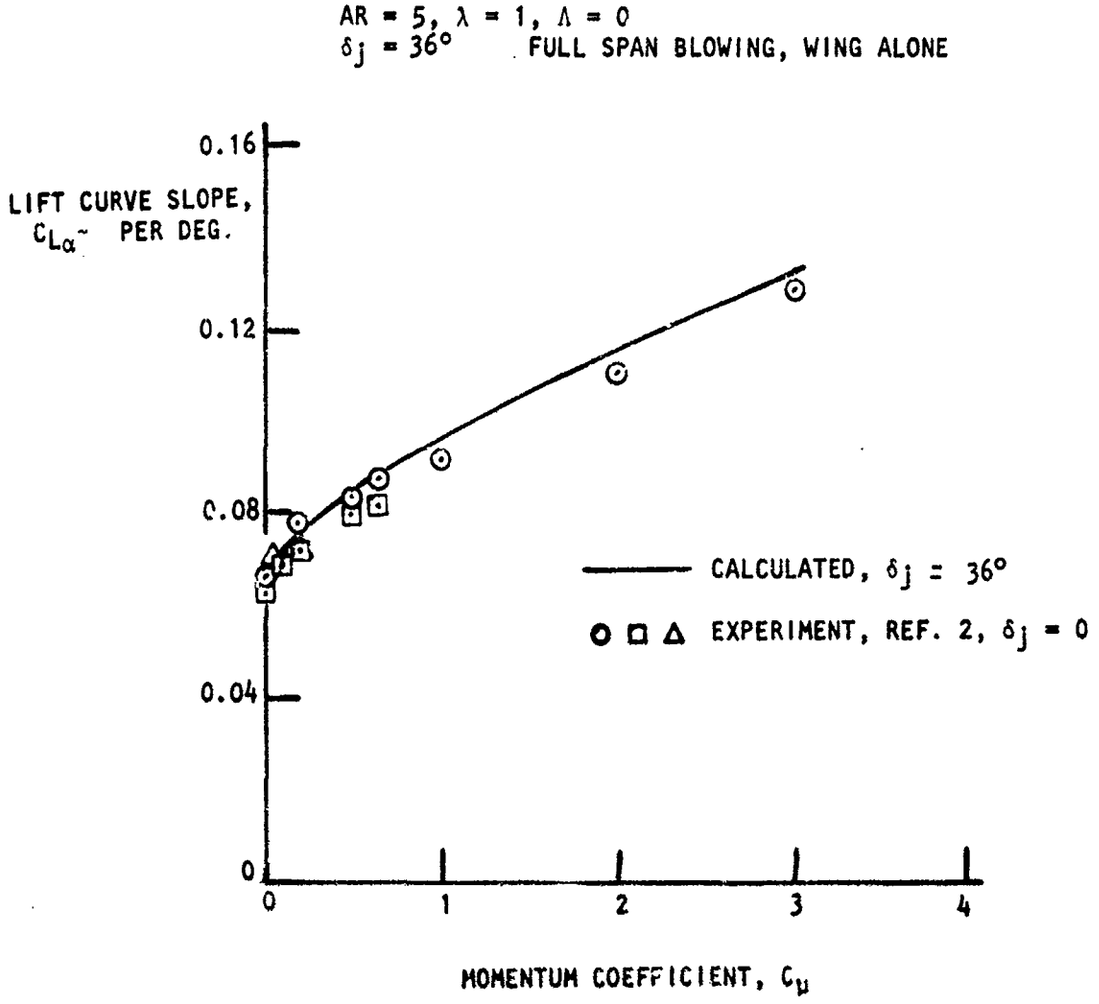

Figure 14. Comparison of Lift Curve Slope

AR = 5, λ = 1, Λ = 0
C_F/C = 0, α_j = 36°, α = 0

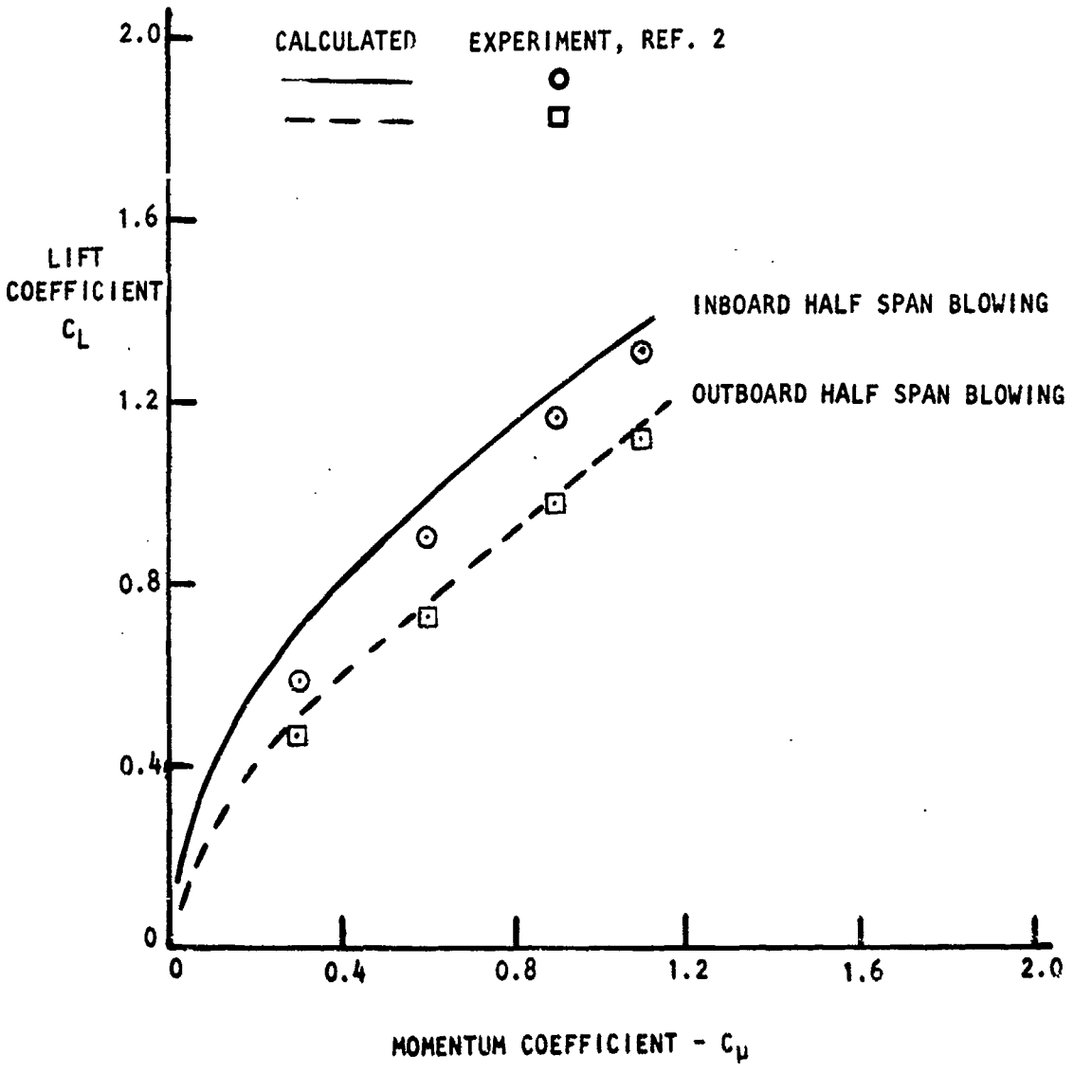

Figure 15. Lift at Zero Angle of Attack for Two Blowing Distributions

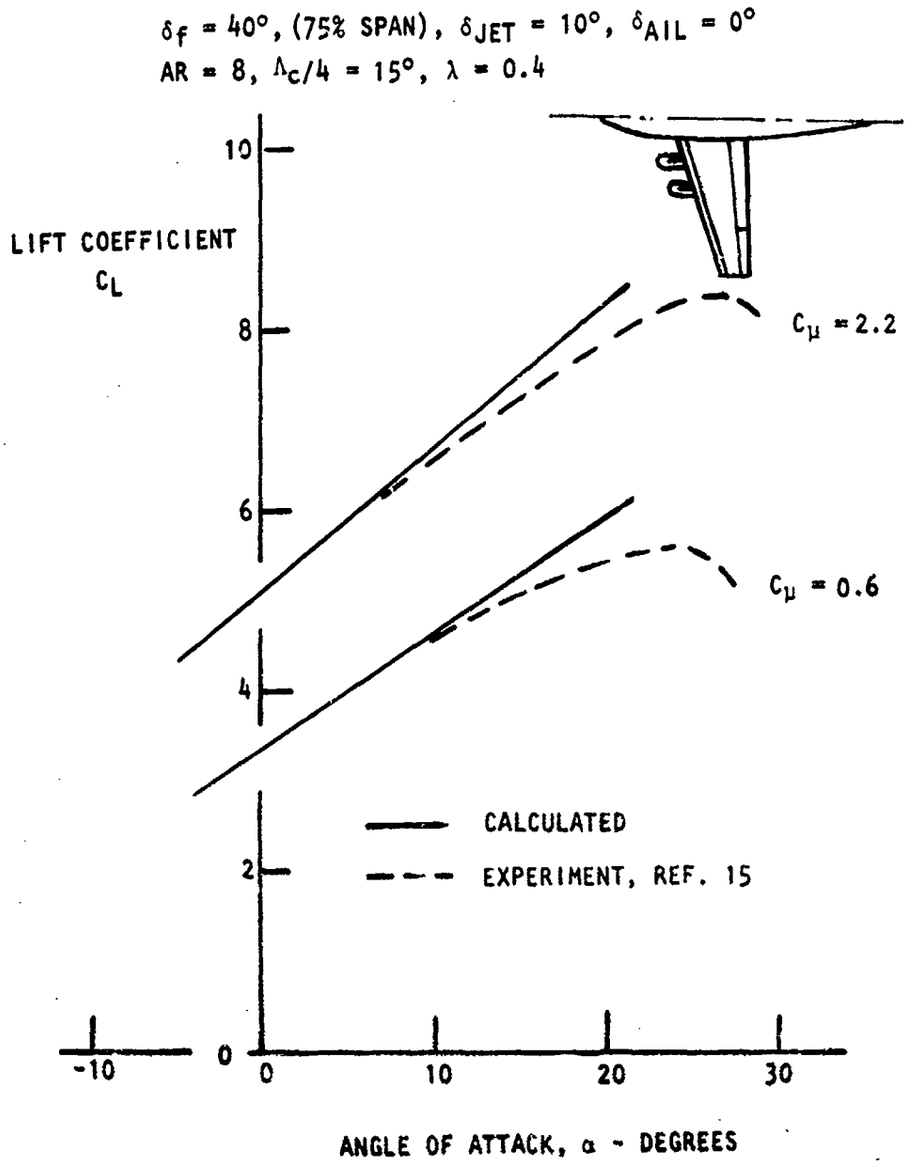

Figure 16. Lift Curve Comparison, IBF Configuration

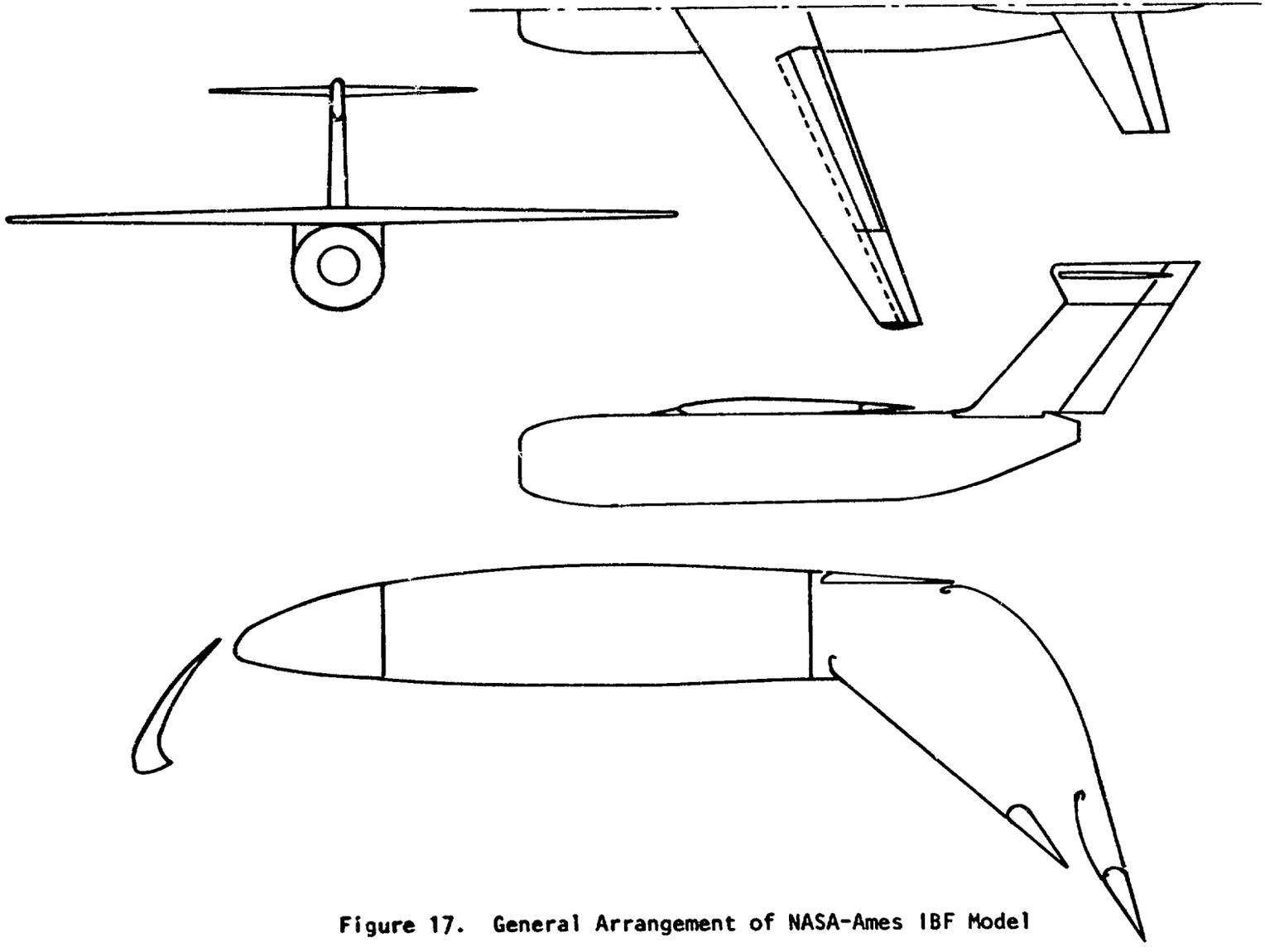

Figure 17. General Arrangement of NASA-Ames IBF Model

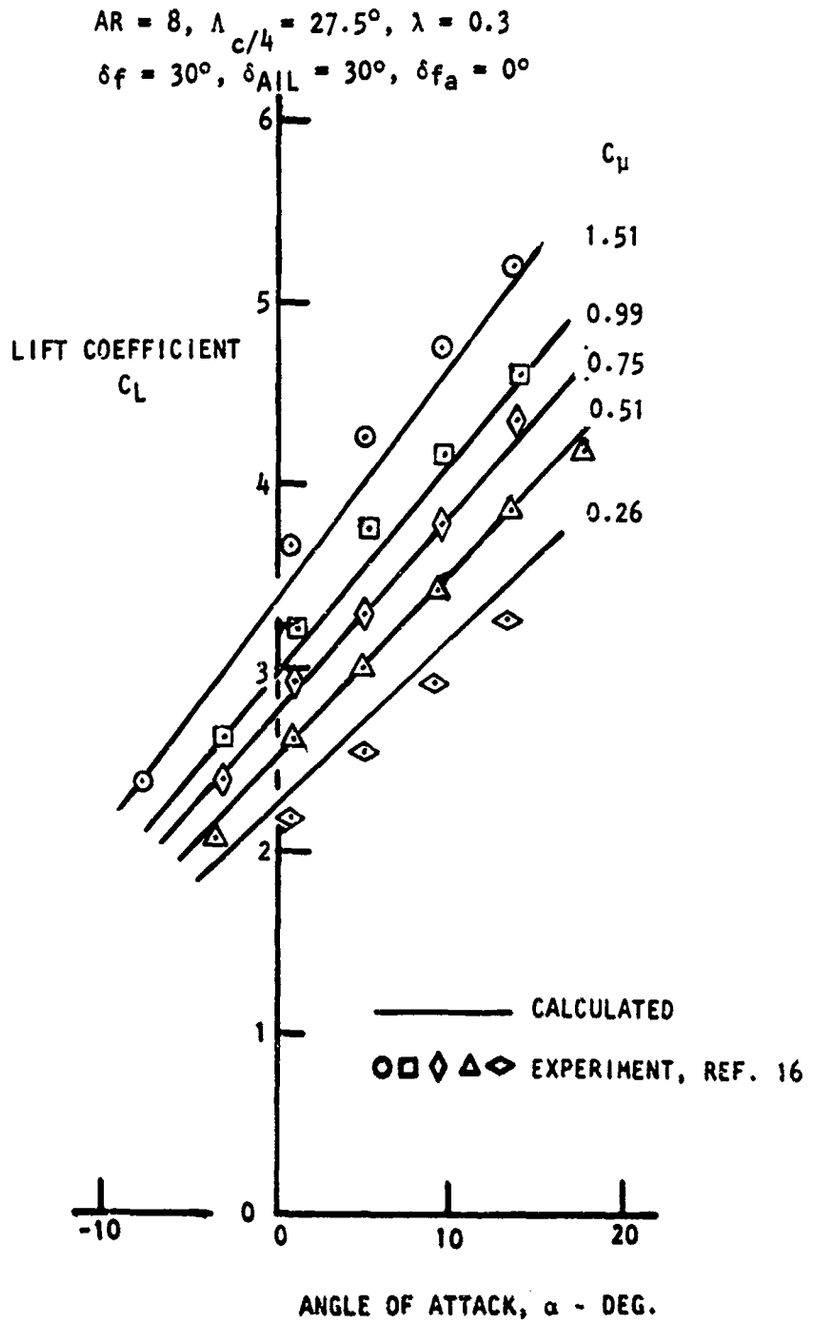

Figure 18. Lift Comparison, Large Scale 18F, Full Span Jet Flap Blowing, Take-off Flaps

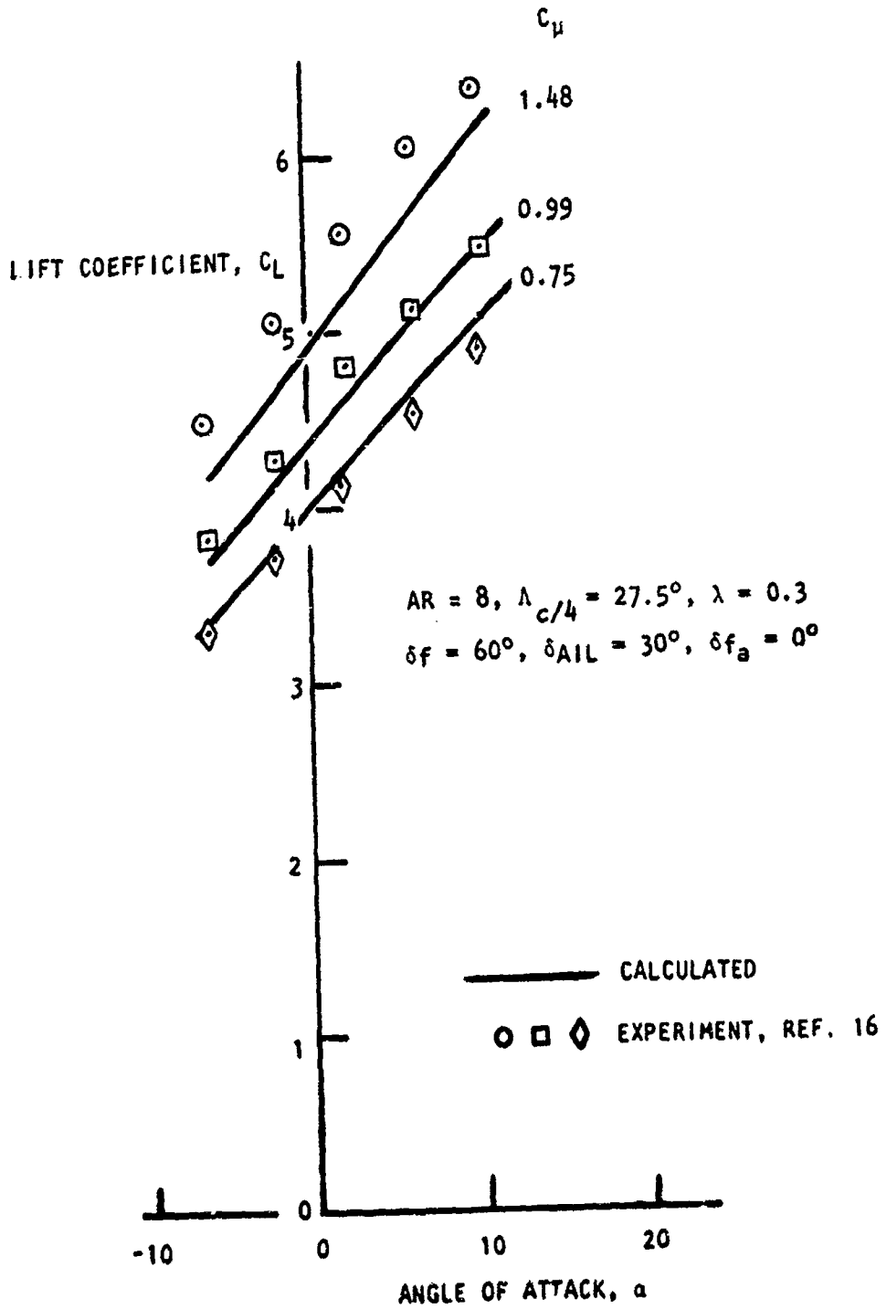

Figure 19. Lift Comparison, Large Scale IBF, Full Span Jet Flap Blowing, Landing Flaps

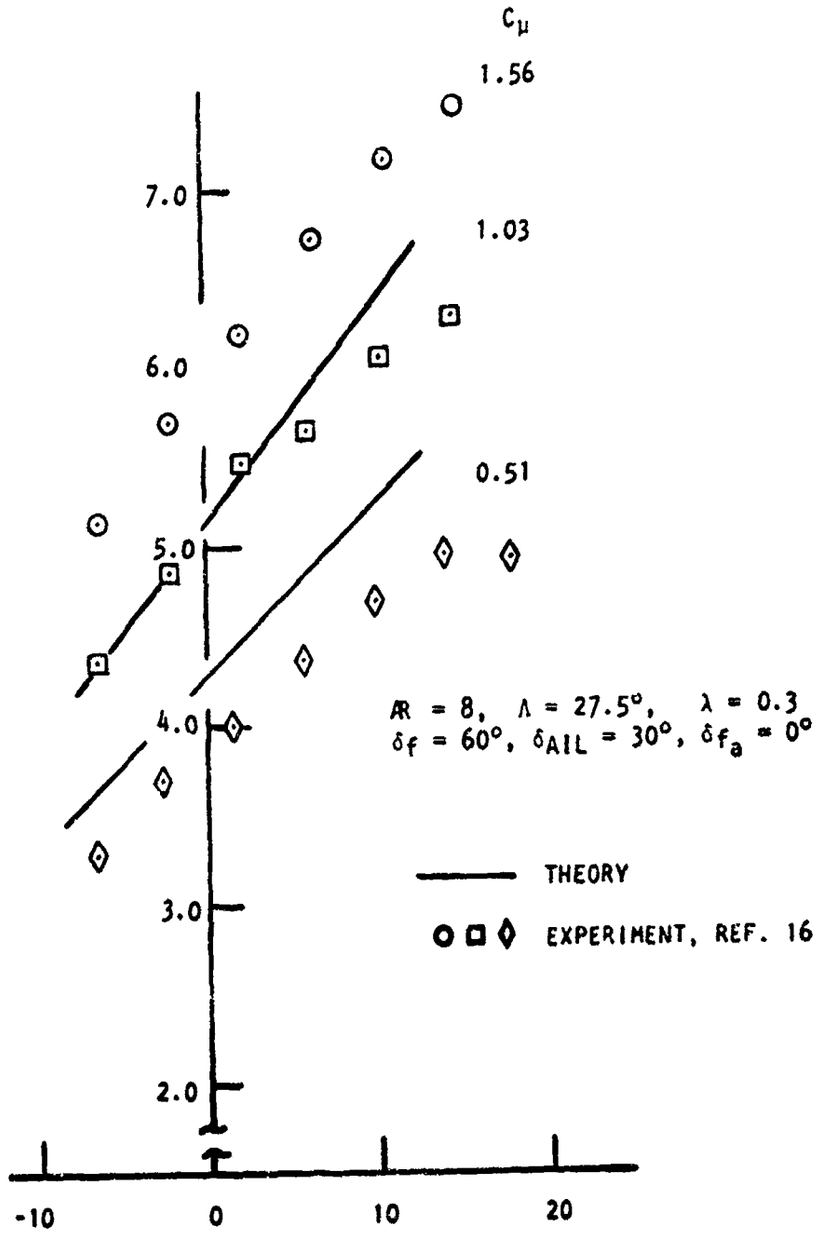

Figure 20. Lift Comparison, Large Scale IBF, Part Span Jet Flap Blowing, Landing Flaps

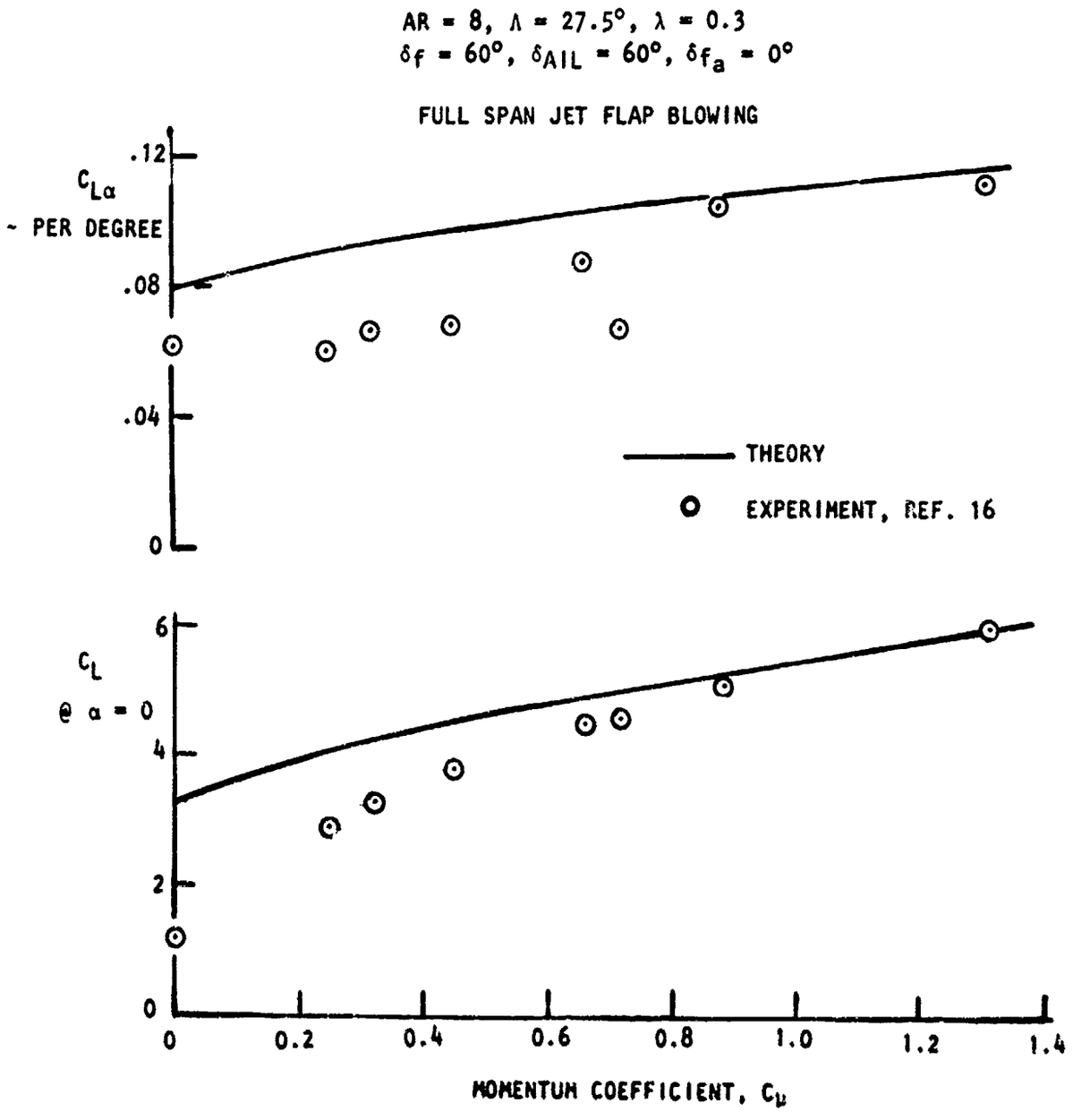

Figure 21. Lift Comparisons at α = 0, Large Scale IBF

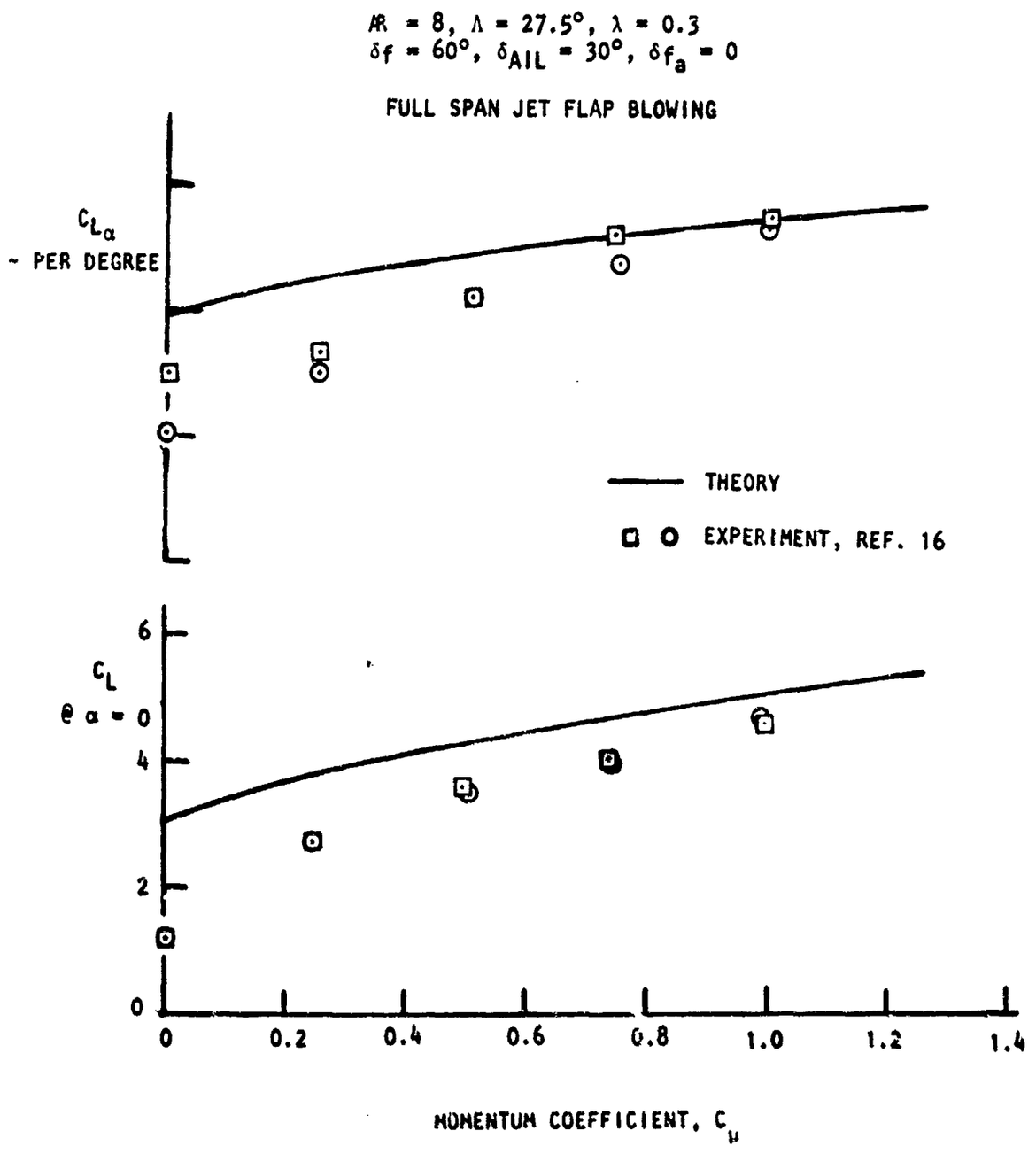

Figure 22. Lift Comparisons at α = 0, Large Scale IBF

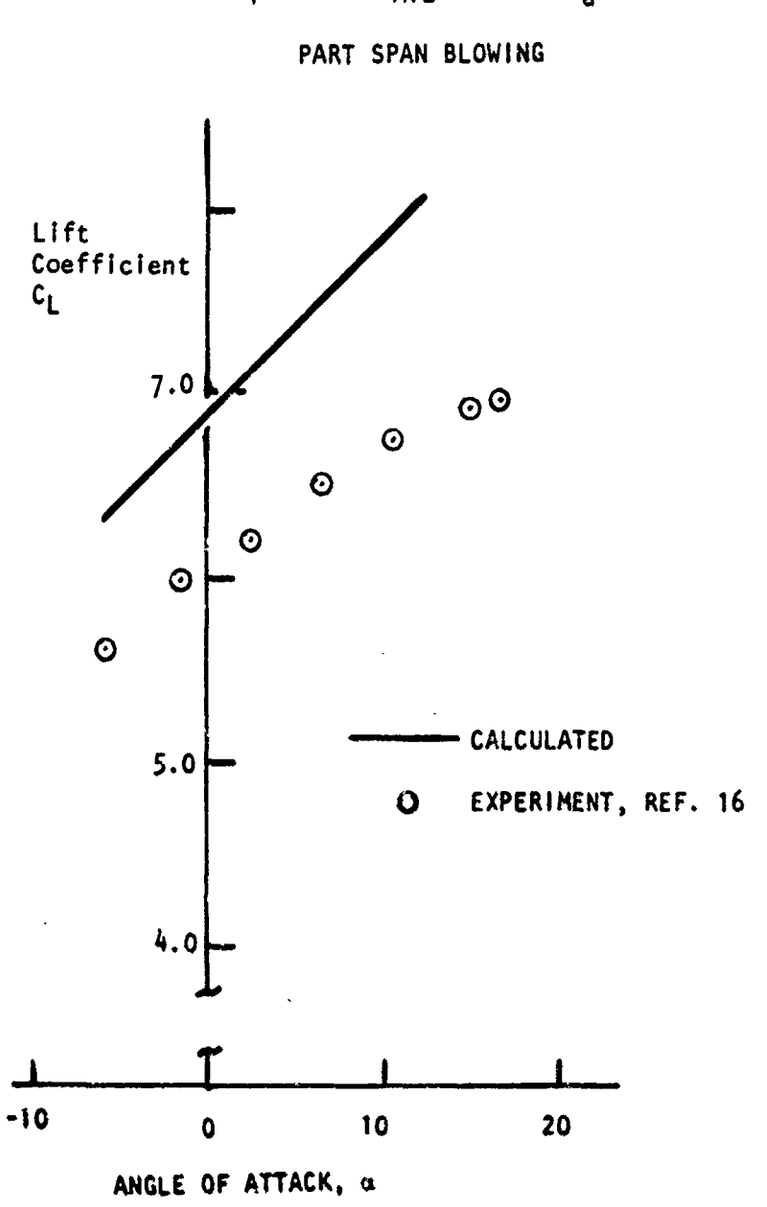

Figure 23. Lift Comparison, Large Scale IBF, Part Span Jet Flap Blowing, 60° Main Flap Auth. 40° Control Flap

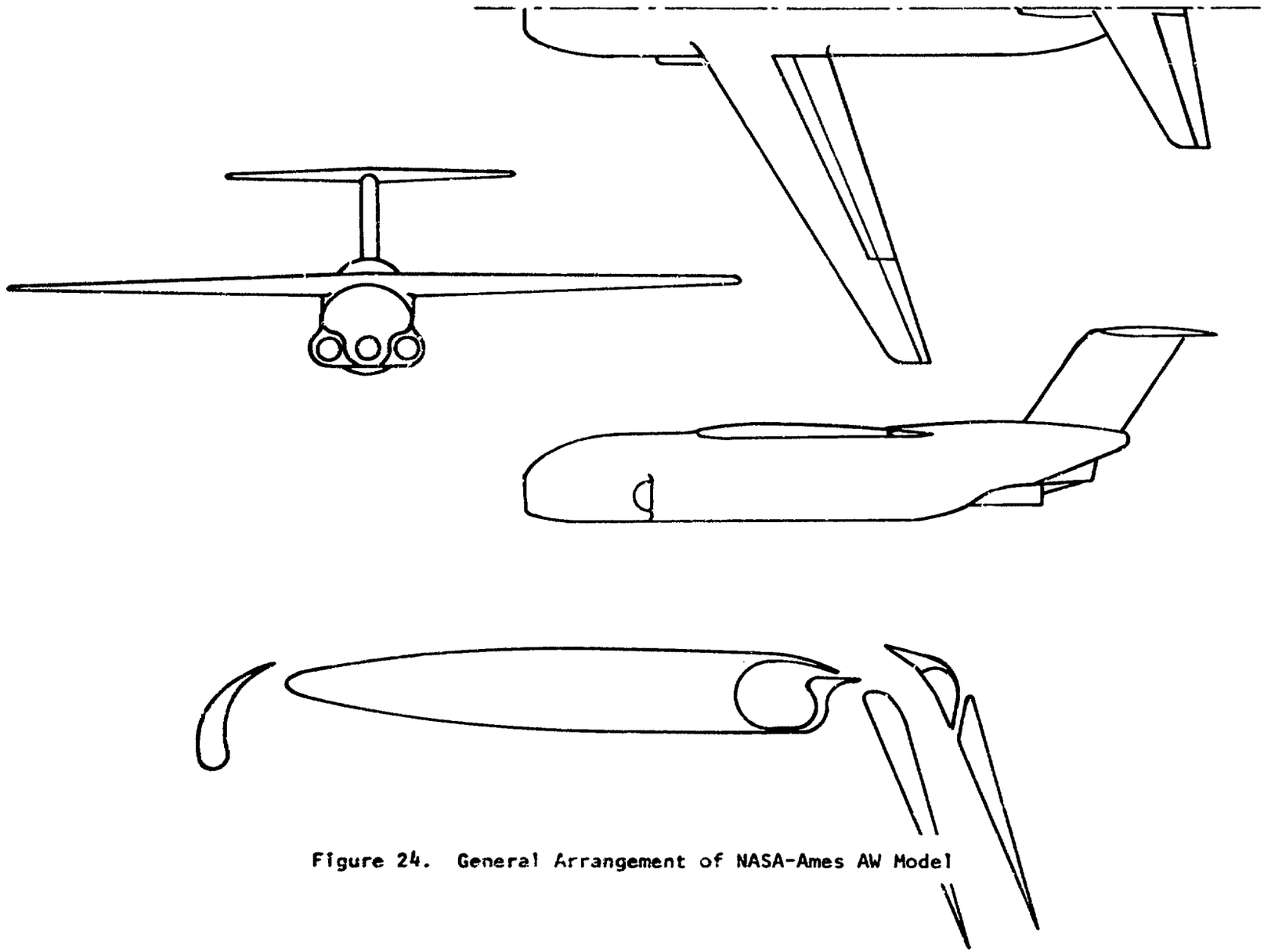

Figure 24. General Arrangement of NASA-Ames AW Model

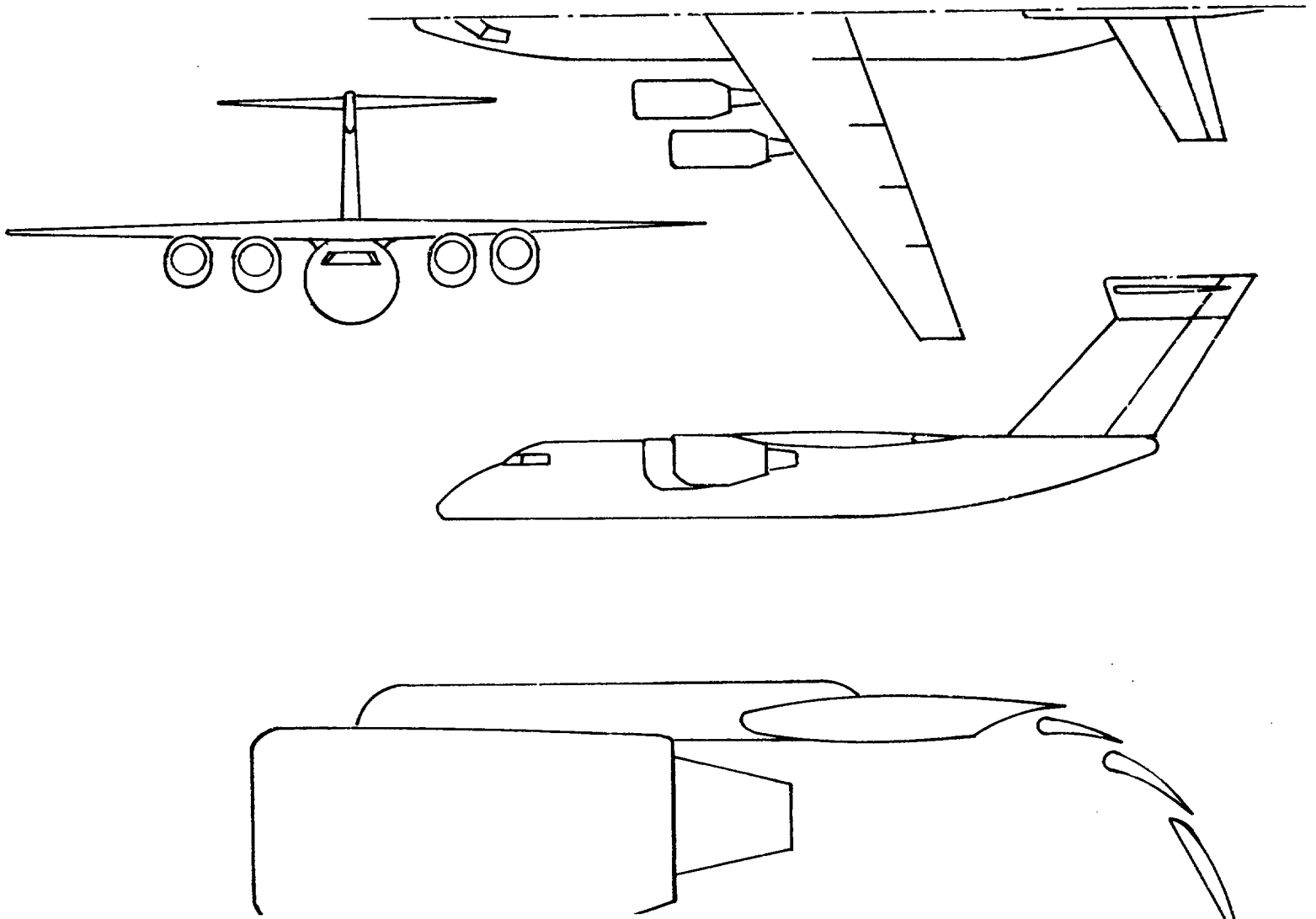

Figure 25. General Arrangement of NASA-Ames EBF Model

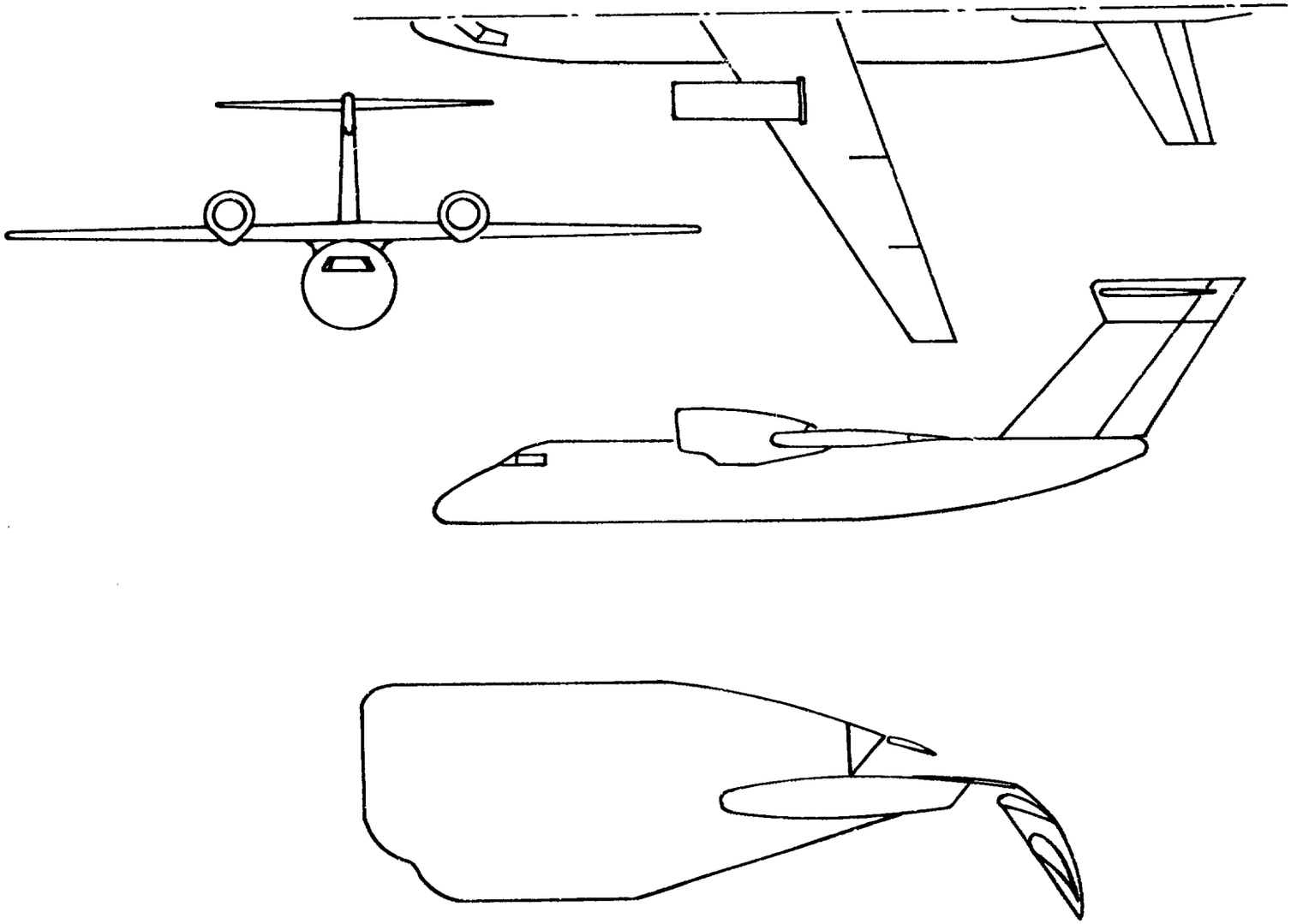

Figure 26. General Arrangement of NASA-Ames USB Model

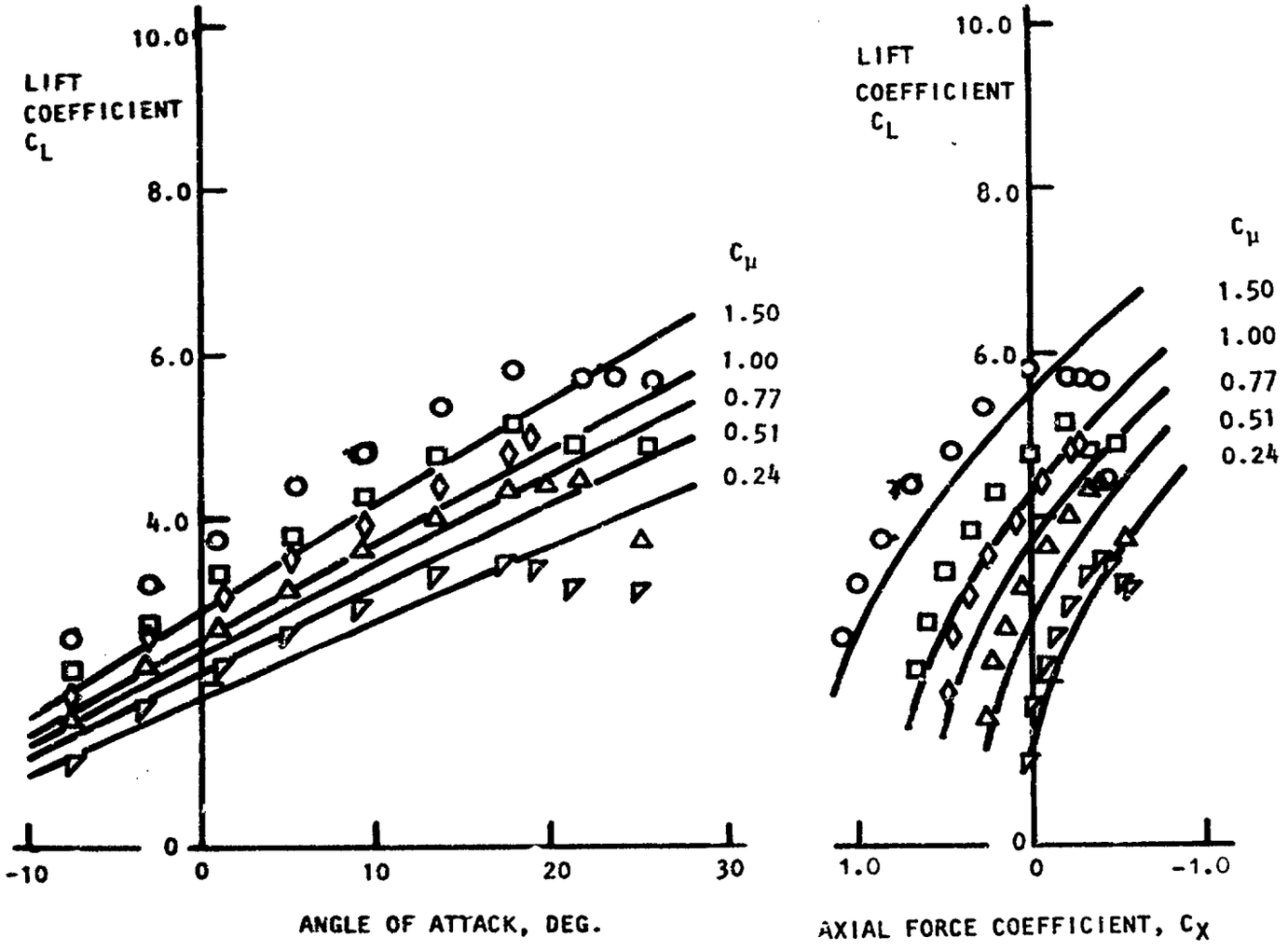

Figure 27. Lift and Axial Force Comparisons, Large Scale IBF

(a) Take-off Flaps

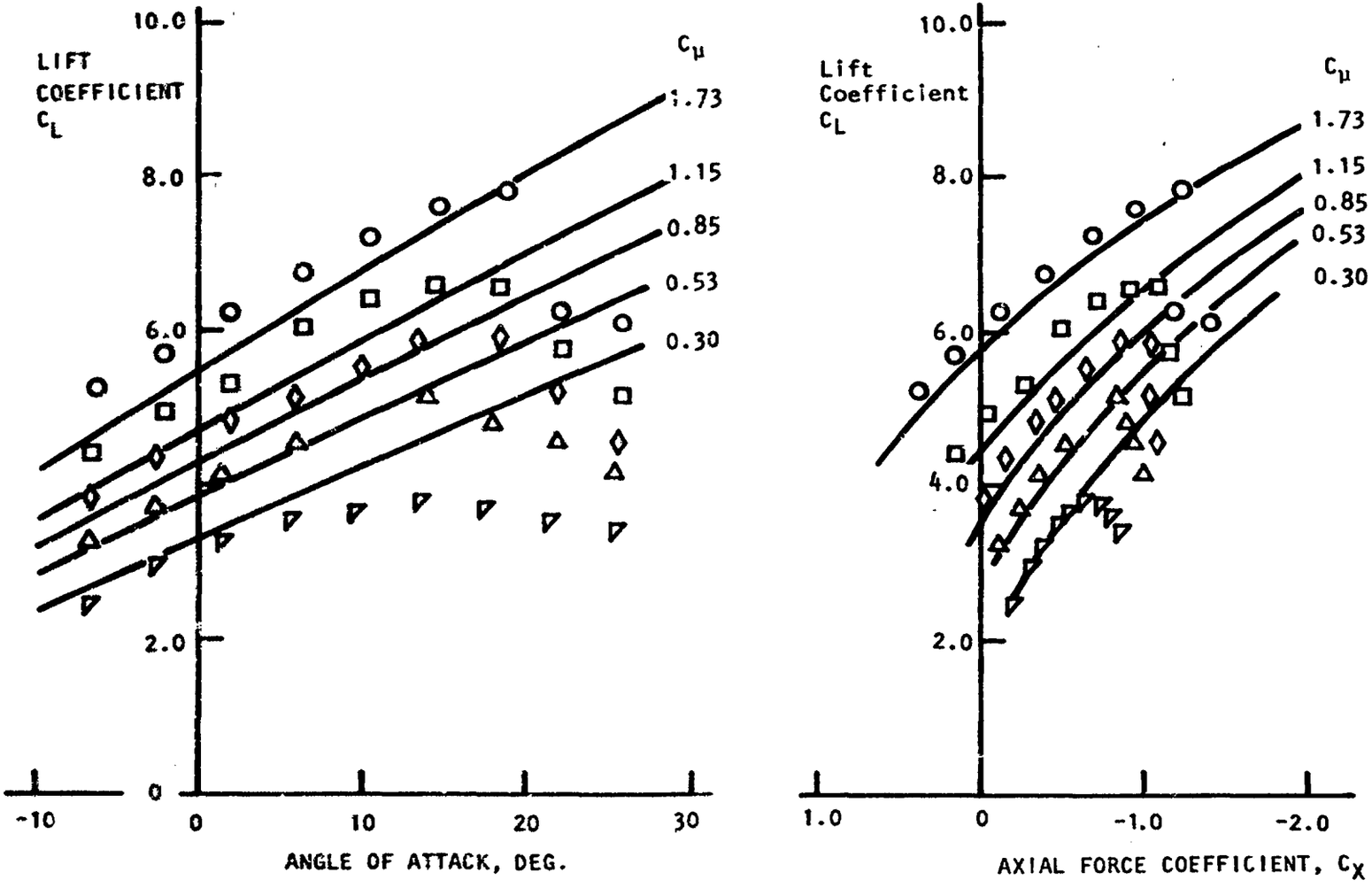

Figure 27. Concluded.

(b) Landing Flaps

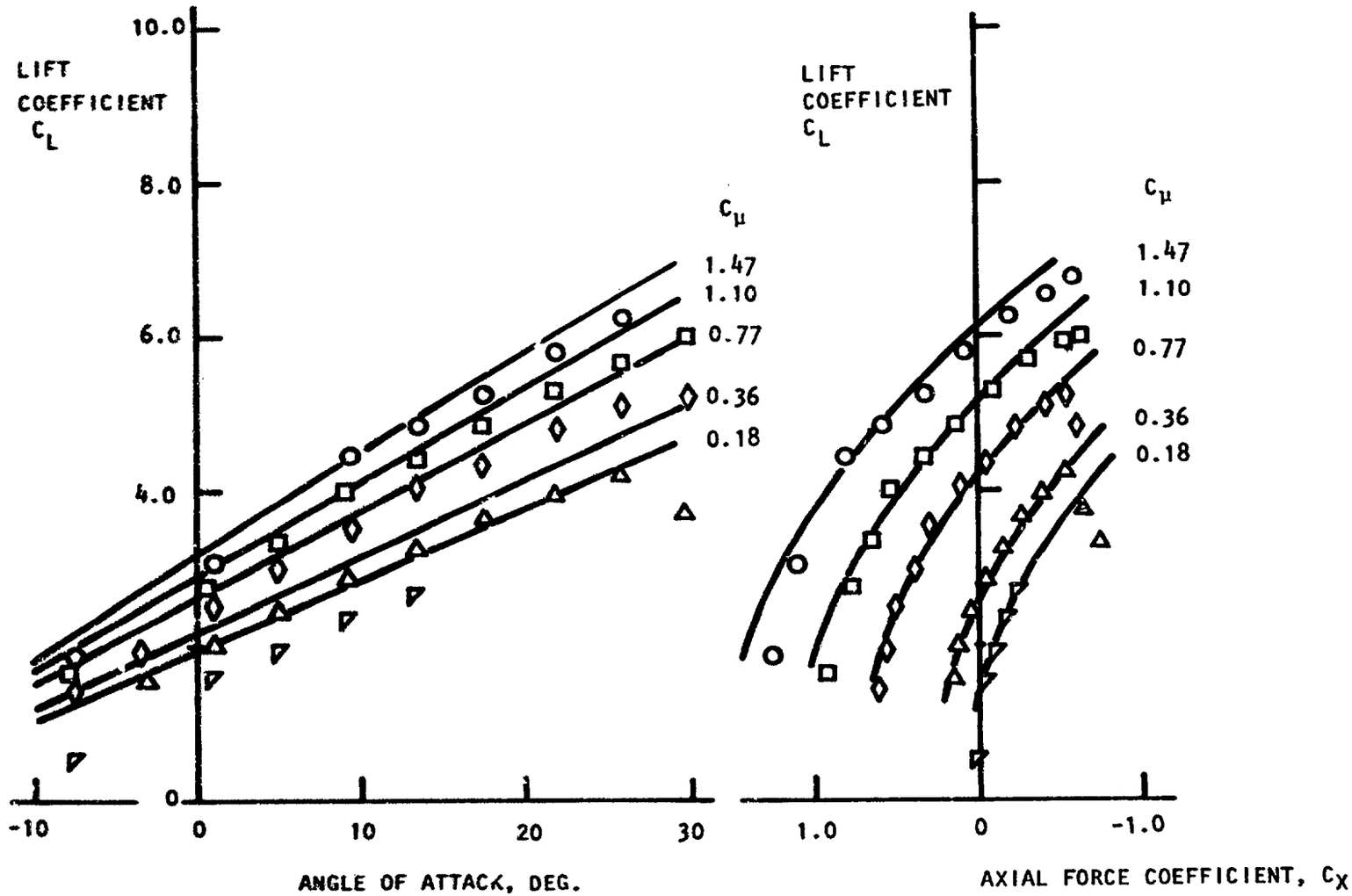

Figure 28. Lift and Axial Force Comparisons, Large Scale AW

(a) Take-off Flaps

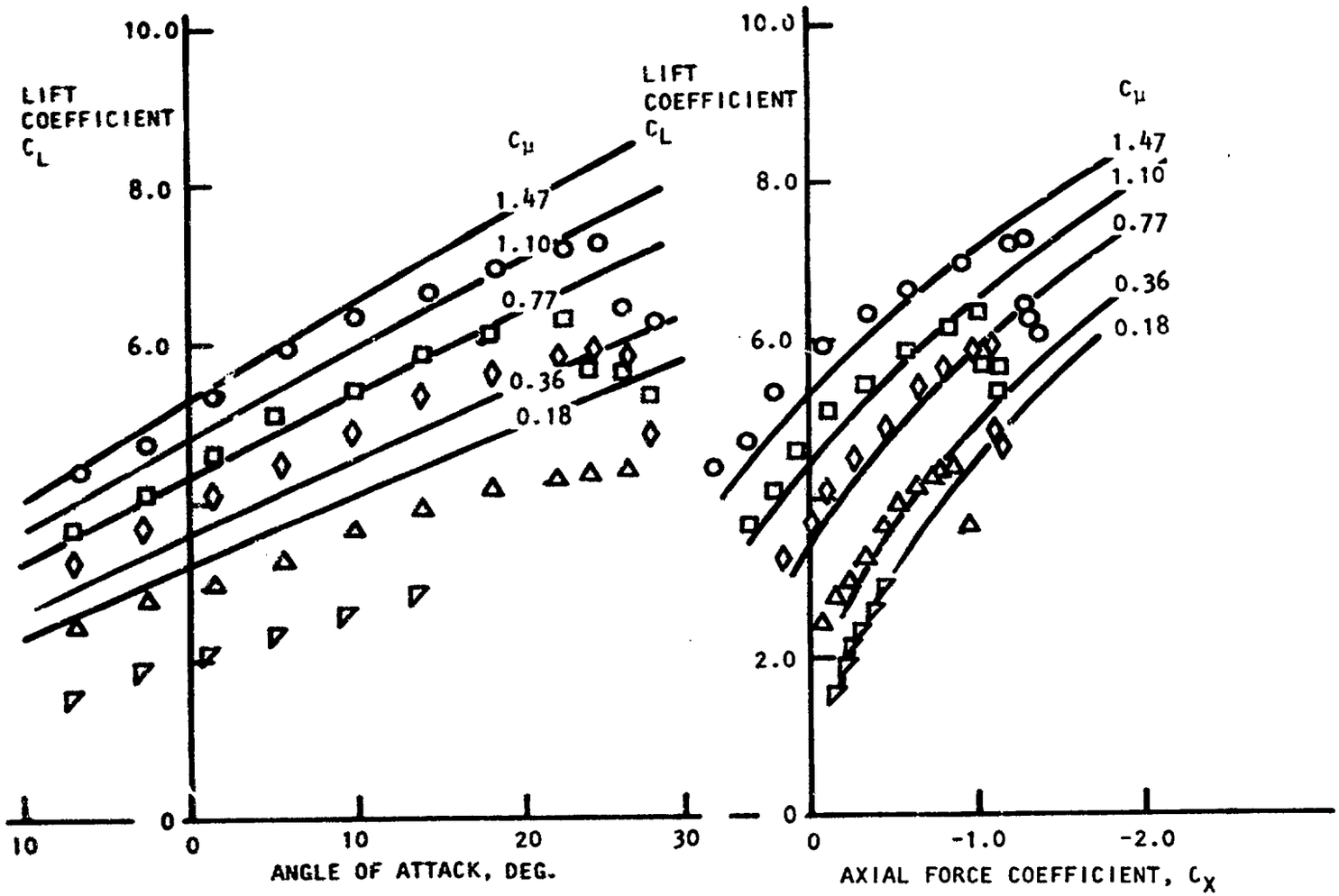

Figure 28. Concluded

(b) Landing Flaps.

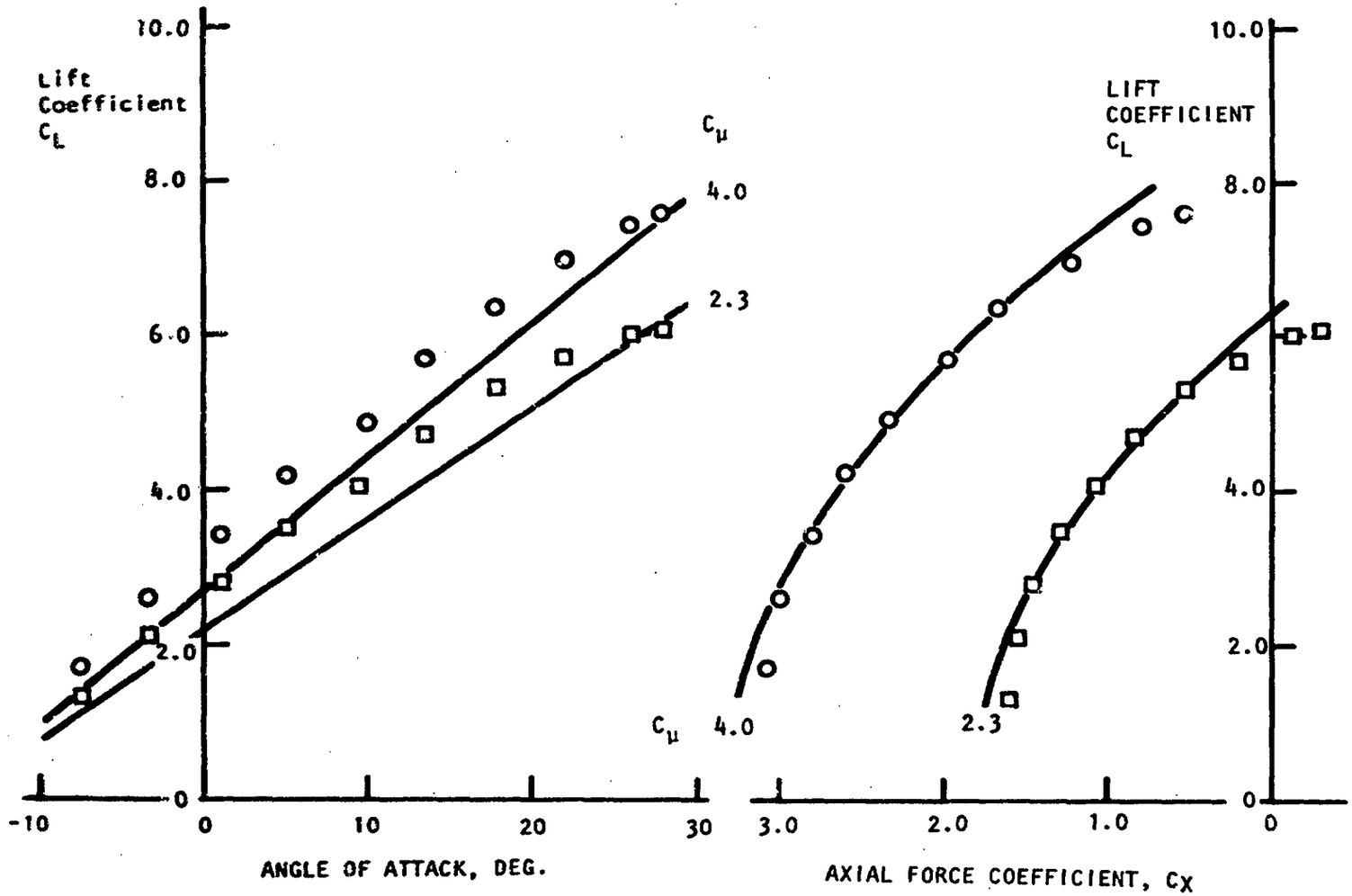

Figure 29. Lift and Axial Force Comparisons, Large Scale EBF

(a) Take-off Flaps

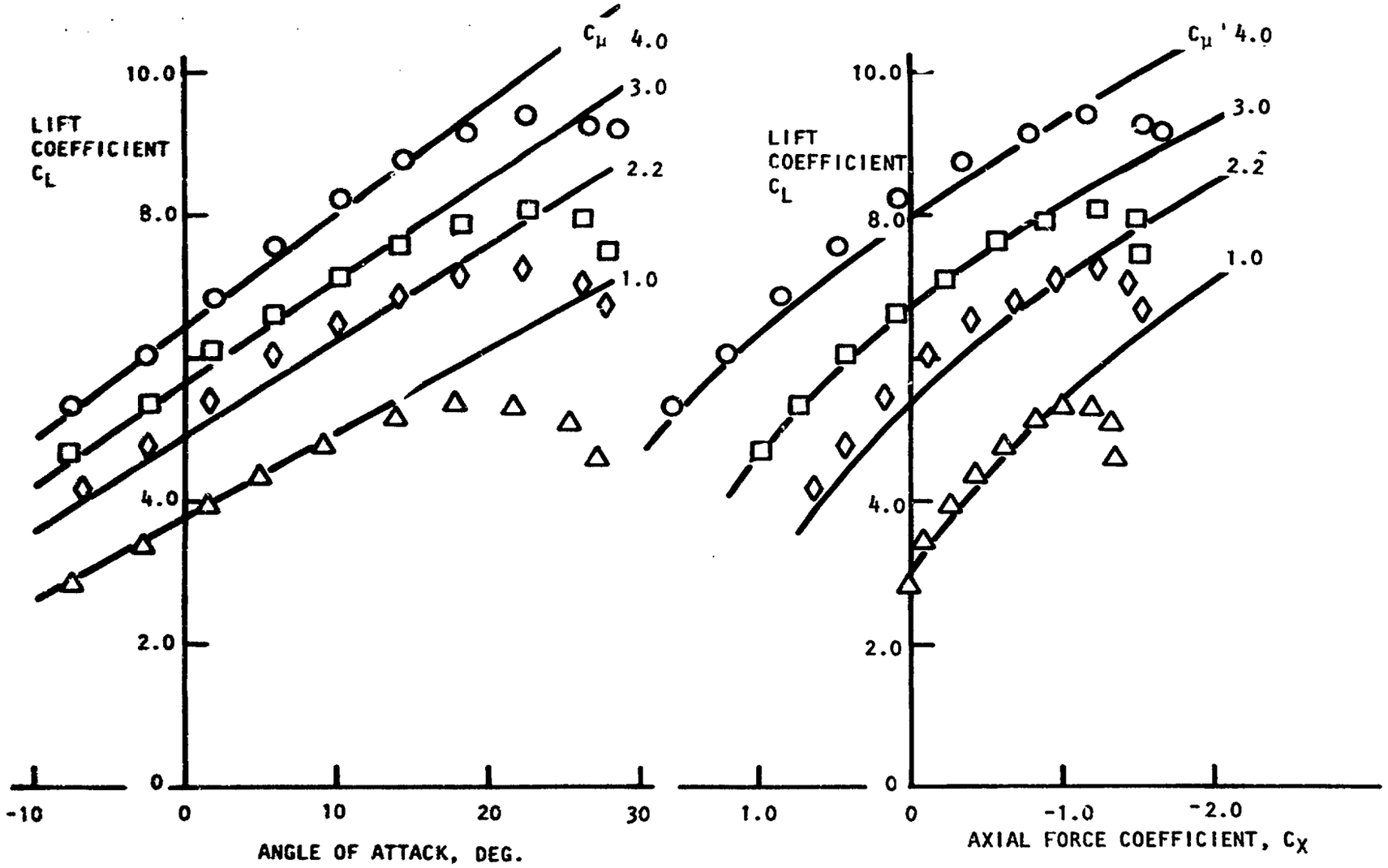

Figure 29. Concluded

(b) Landing Flaps

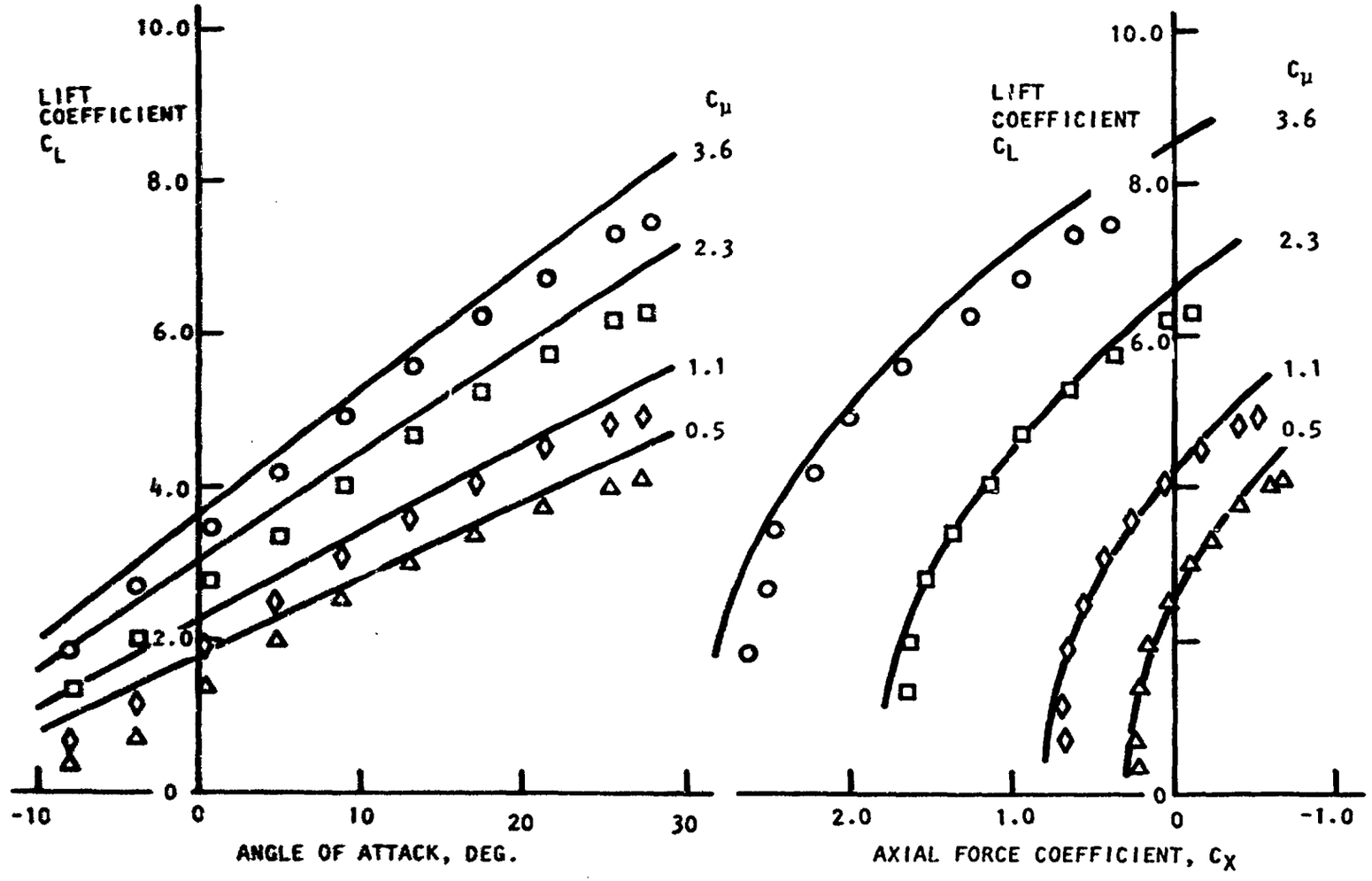

Figure 30. Lift and Axial Force Comparisons, Large Scale USB

(a) Take-off Flaps

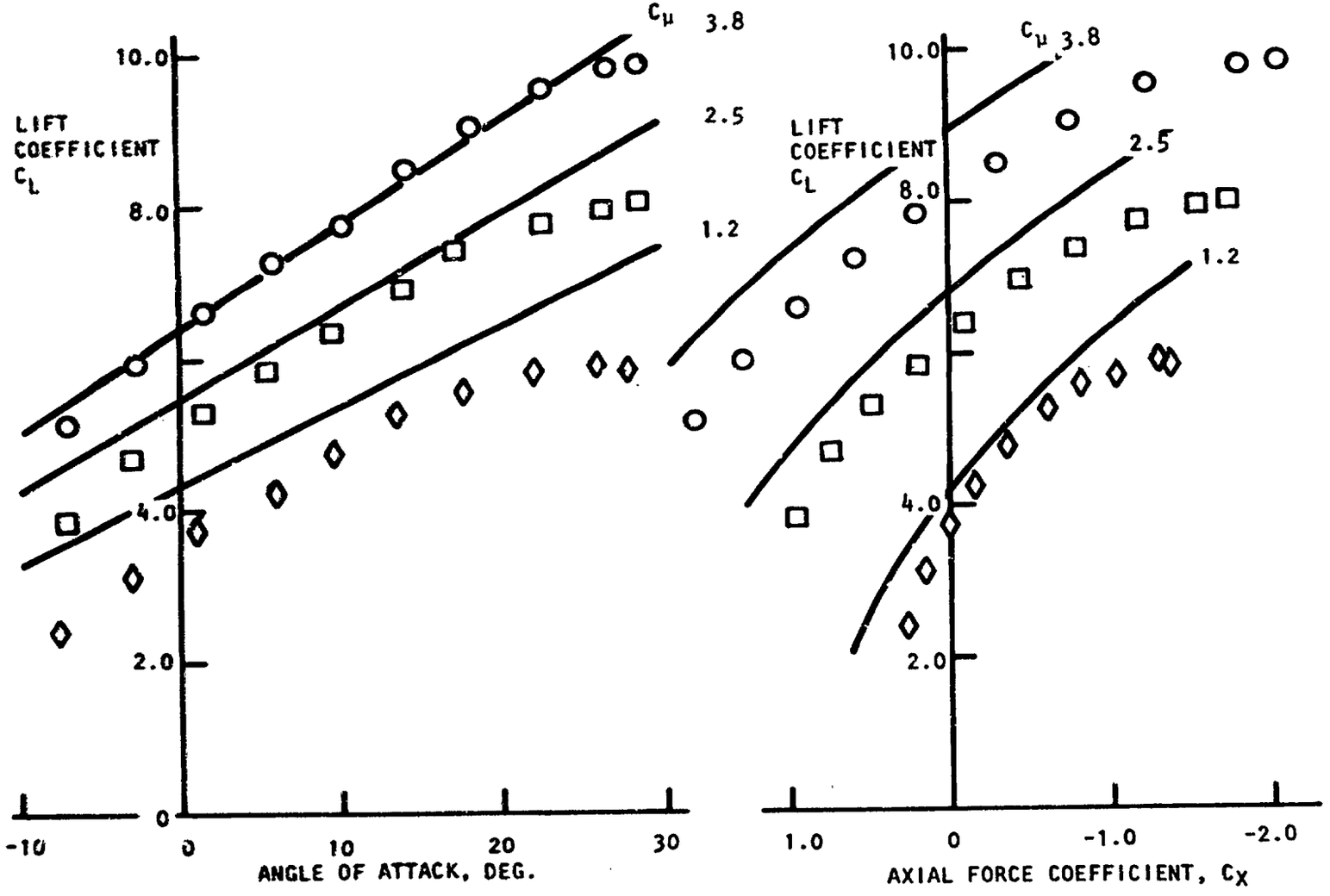

Figure 30. Concluded

(b) Landing Flaps

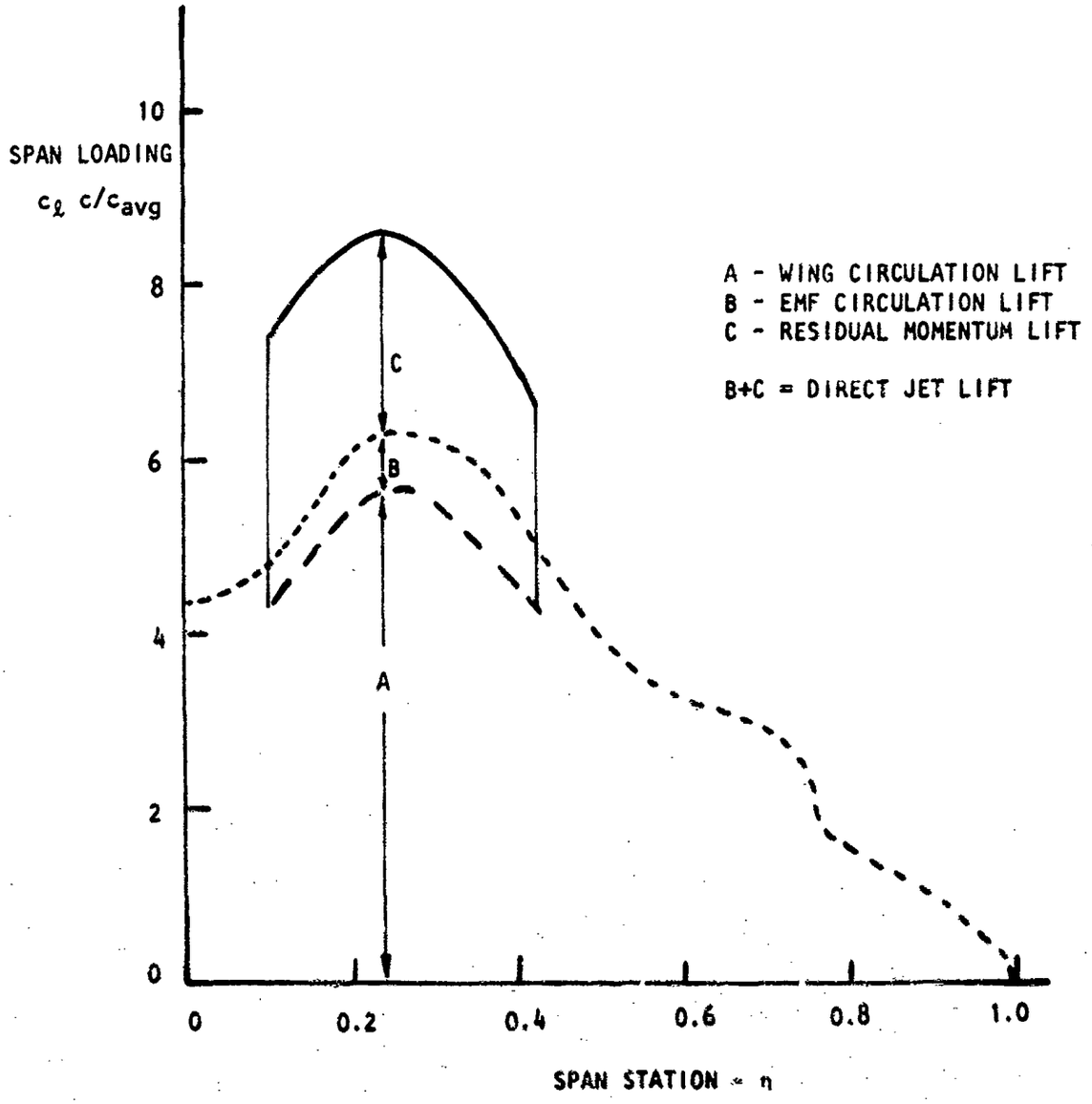

Figure 31. Calculated Span Loading, Large Scale USB Model, Landing Flaps, C_μ = 1.2, α = 5°

Flap Deflections - Degrees			Angle of Attack α, Degrees	Wing Momentum Coefficient C_μ
Main δ_f	Aileron δ_{ail}	Auxiliary (Control) δ_{f_a}		
30	30	0	4	0.51
			12	0.51
			4	1.01
	Same		12	1.02
			4	1.52
			12	1.53
60	30	0	4	1.05
	Same		12	1.05
60	30	20	4	0.52
			12	0.52
	Same		4	1.05
			12	1.05
			4	1.58
			12	1.58
60	30	40	4	1.03
	Same		12	1.03
All runs tail on, 5% aileron blowing, 95% on inboard flap.				

TABLE I SUMMARY OF SIDESLIP TEST RUNS, LARGE SCALE NASA-AMES 18F MODEL

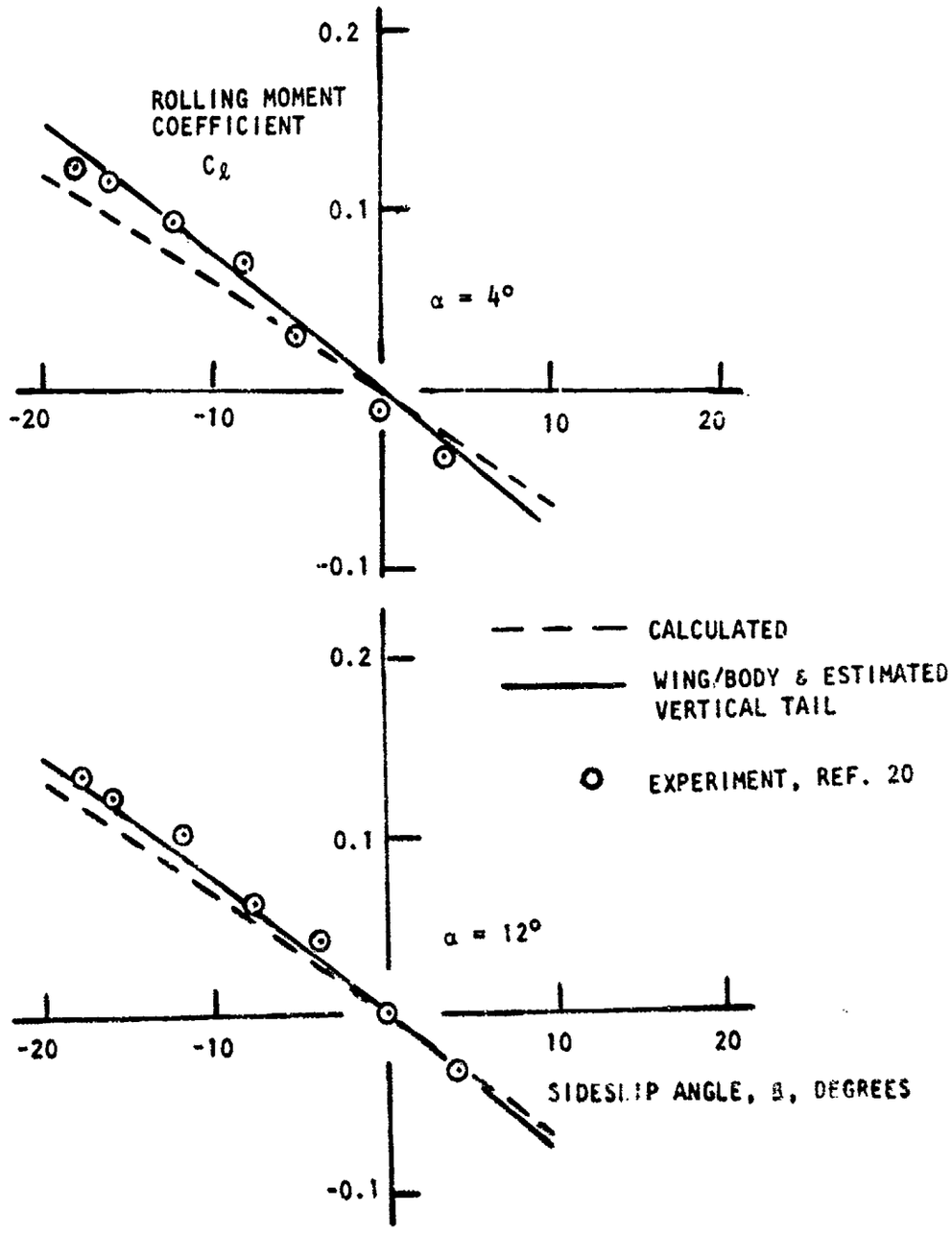

Figure 32. Rolling Moment Comparisons, Large Scale IBF, AR = 8, $\Lambda_{c/4}$ = 27.5 λ = 0.3, Part Span Jet Flap Blowing, 5% Aileron Blowing

(a) C_μ = 0.51, δ_f = 30°, δ_{ail} = 30°, δf_a = 0°

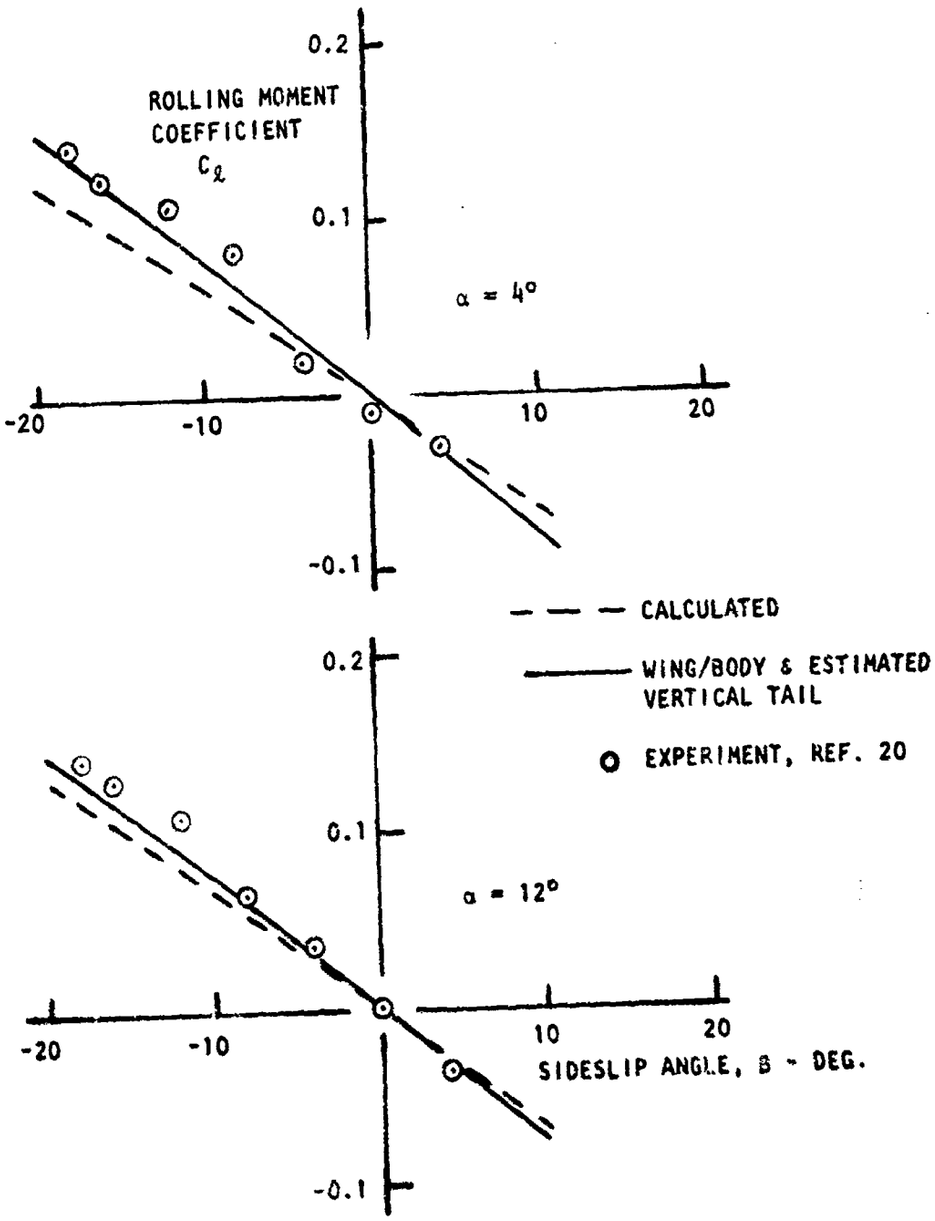

Figure 32. Continued

(b) $C_{\mu} = 1.01$, $\delta_f = 30$, $\delta_{ail} = 30$, $\delta_{f_a} = 0$

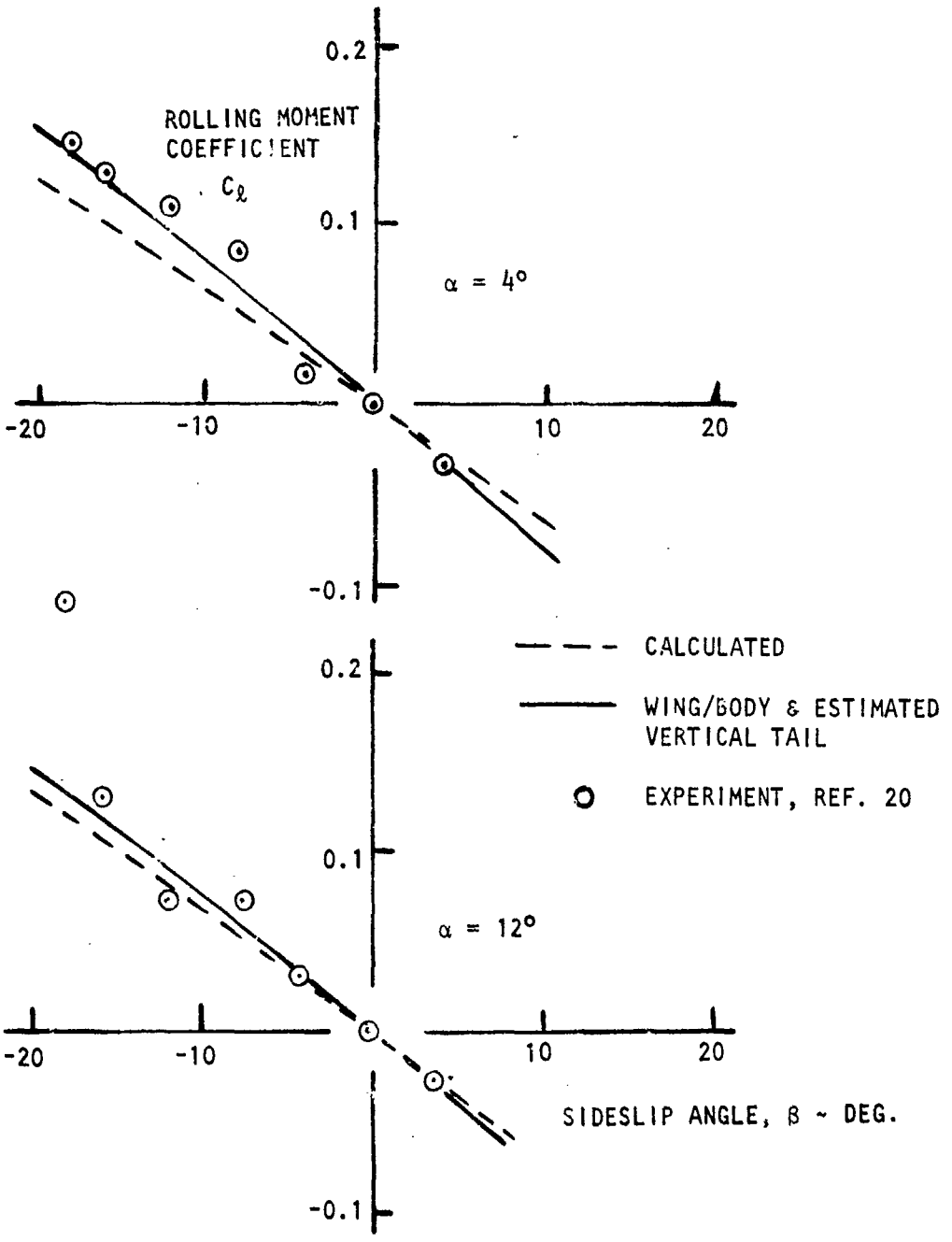

Figure 32. Continued

(c) $C_\mu = 1.52$, $\delta_f = 30°$, $\delta_{all} = 30°$, $\delta_{fa} = 0°$

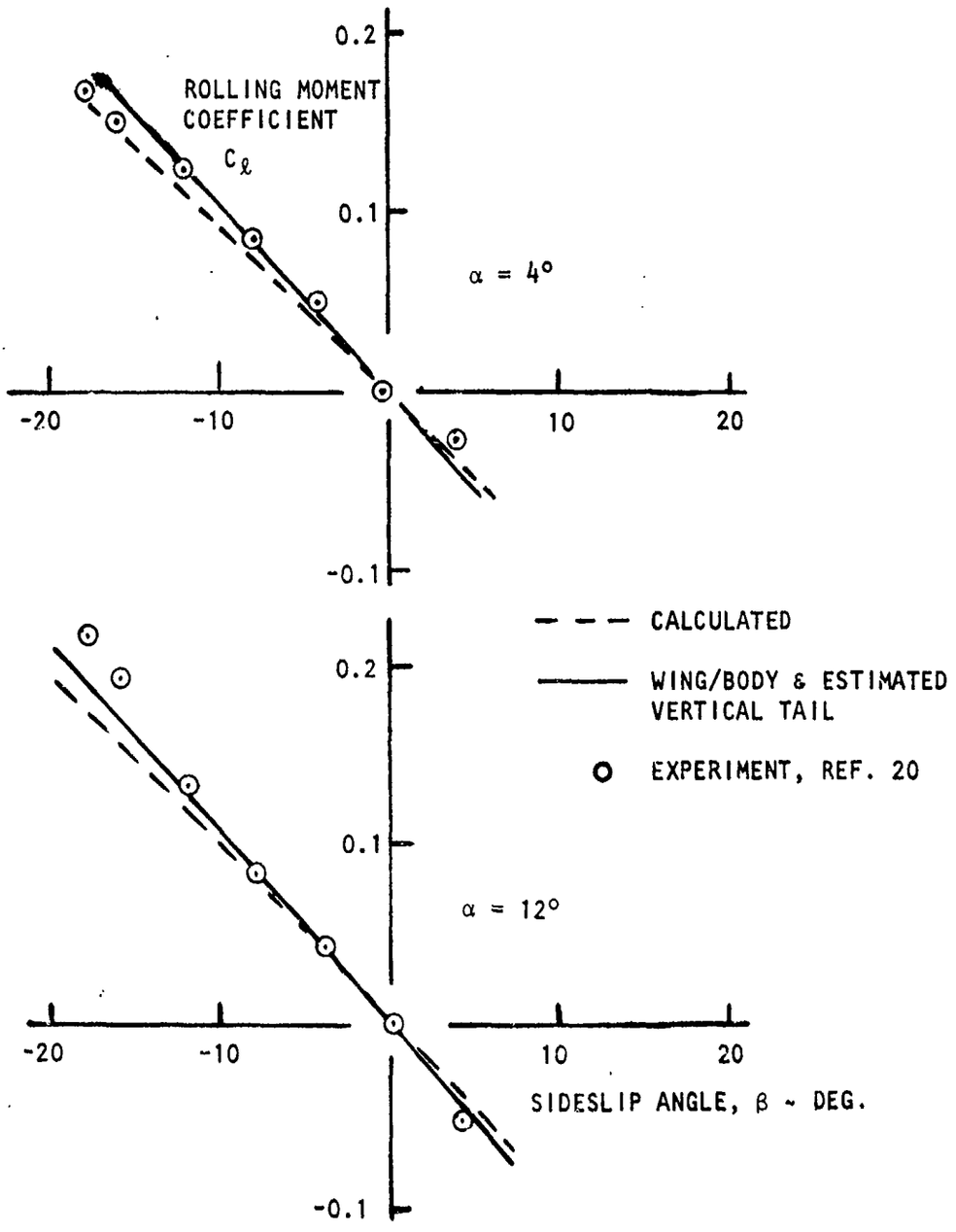

Figure 32. Continued

(d) $C_\mu = 1.05$, $\delta_f = 60°$, $\delta_{all} = 30°$, $\delta f_a = 0°$

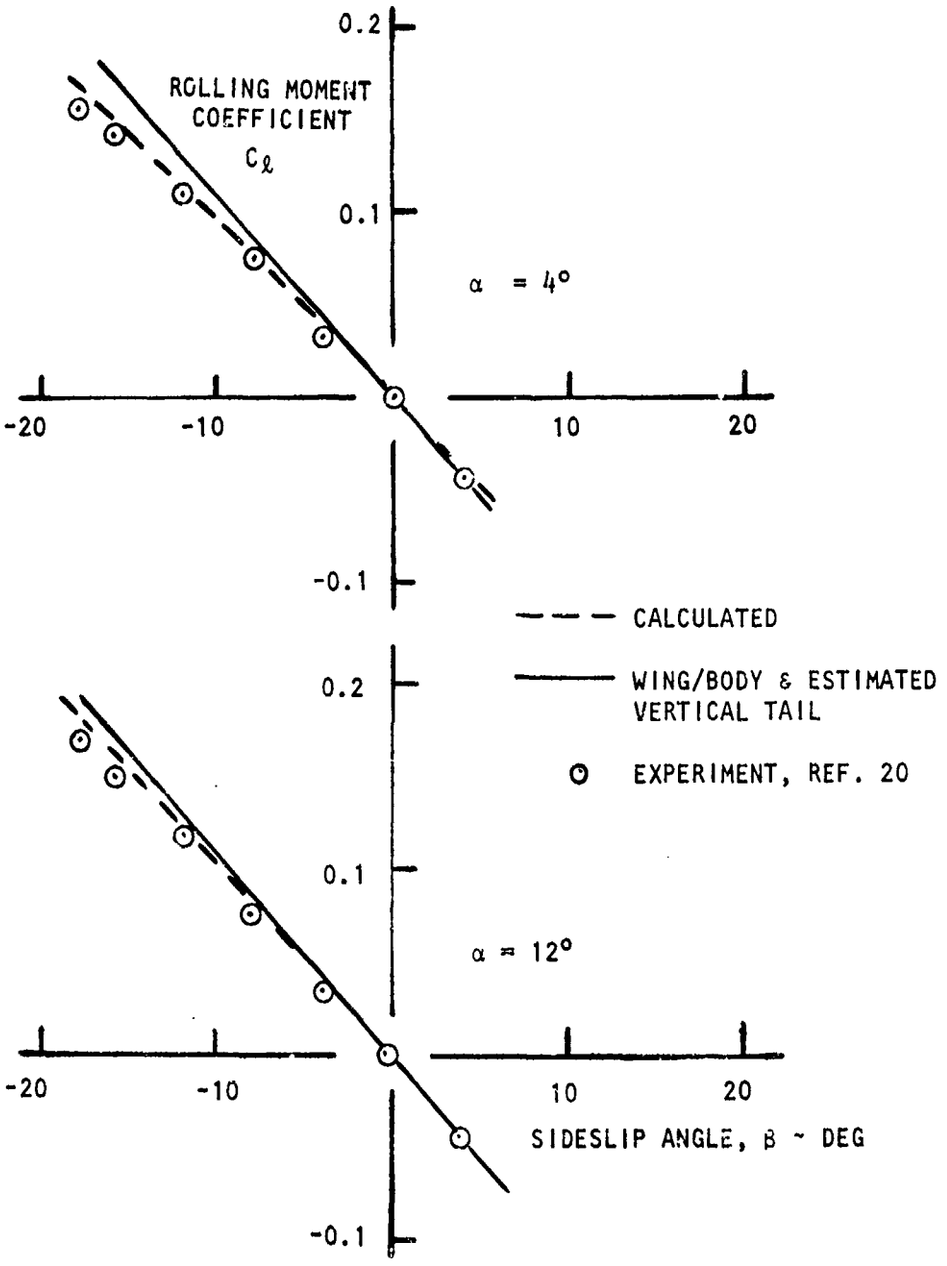

Figure 32. Continued

(e) $C_\mu = 0.52$, $\delta_f = 60°$, $\delta_{all} = 30°$, $\delta_{f_u} = 20°$

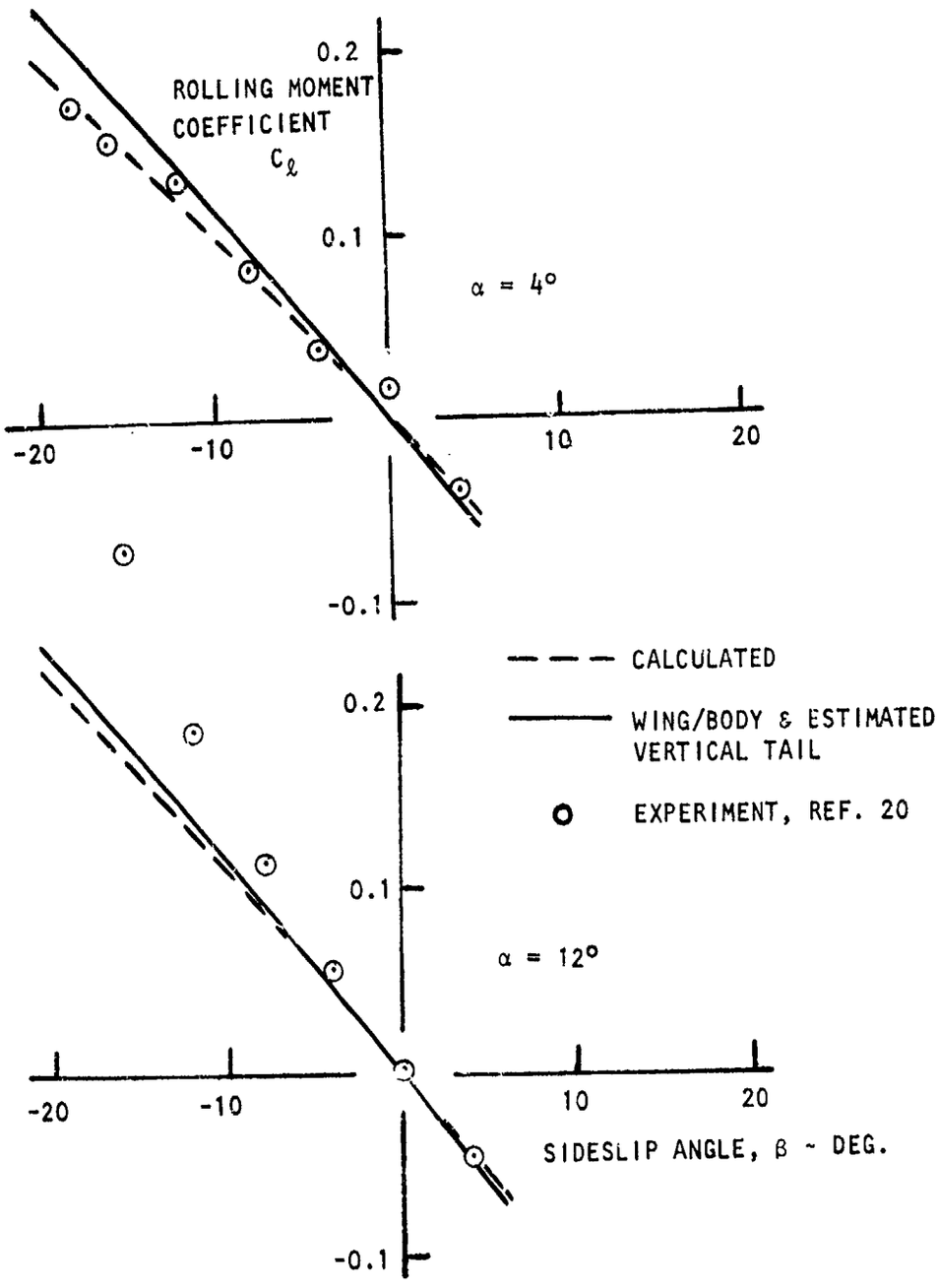

Figure 32. Continued

(f) $C_\mu = 1.05$, $\delta_f = 60°$, $\delta_{all} = 30°$, $\delta_{f_u} = 20°$

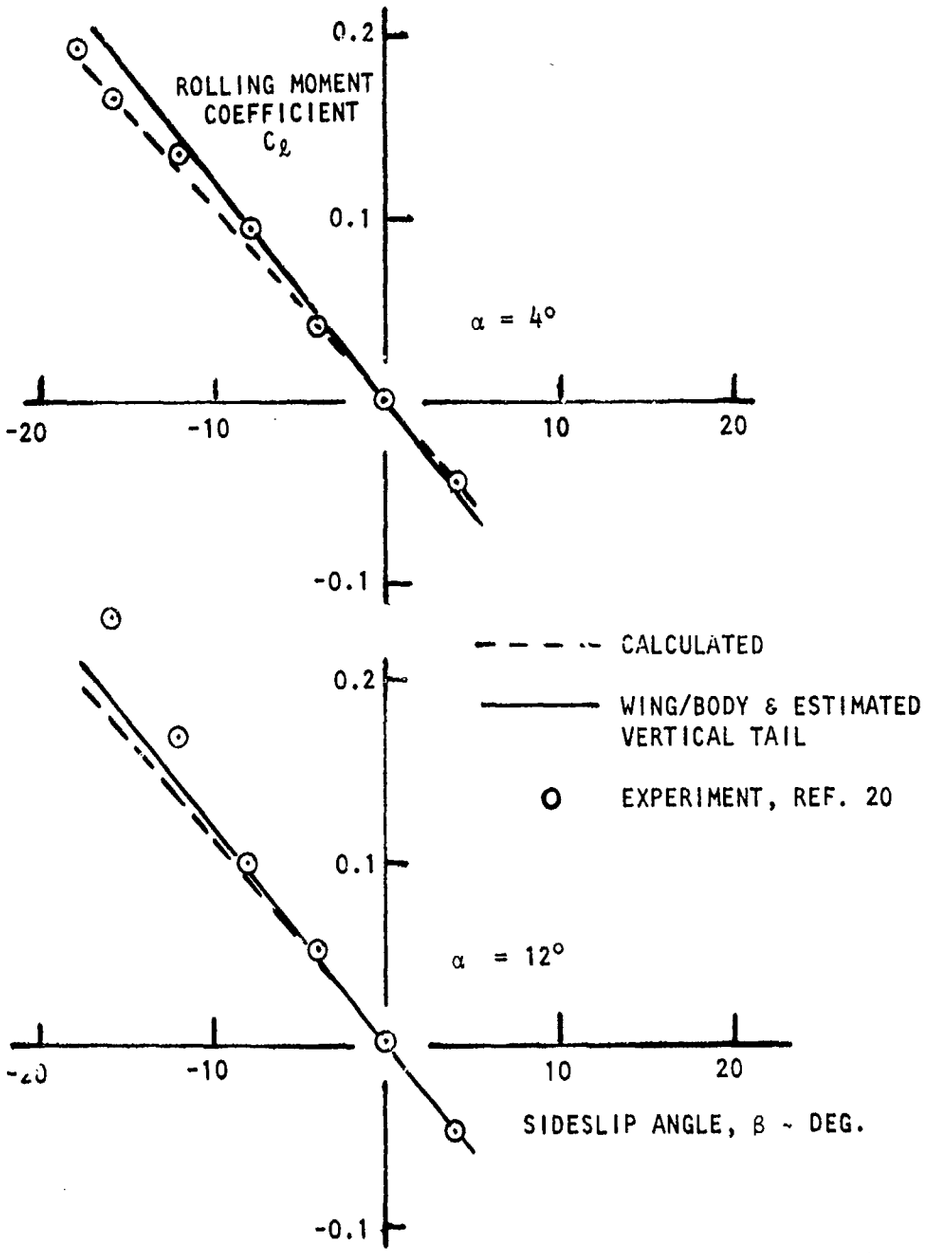

Figure 32. Continued

(g) $C_\mu = 1.58$, $\delta_f = 60°$, $\delta_{ail} = 30°$, $\delta_{f_a} = 20°$

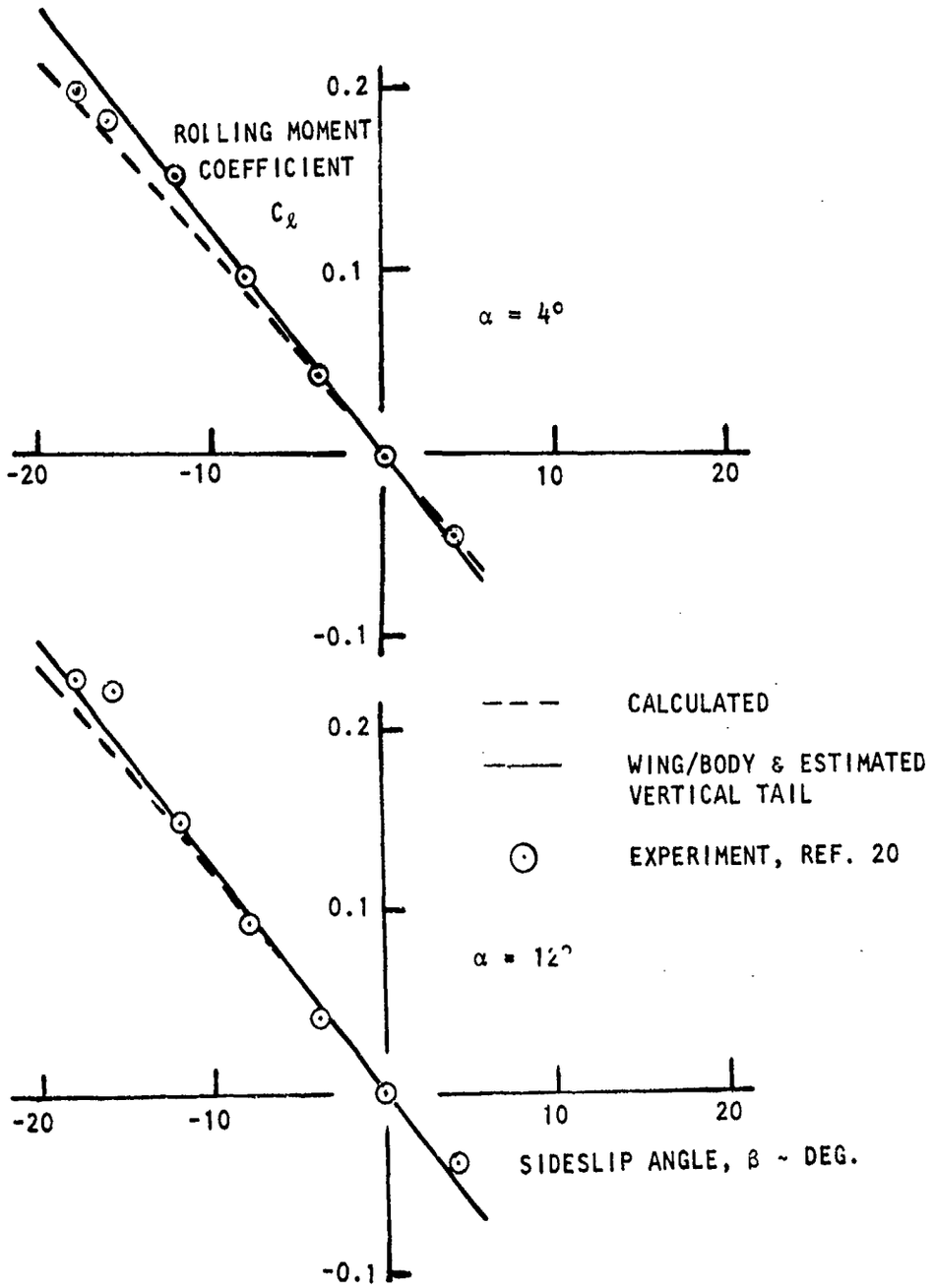

Figure 32. Concluded

(h) $C_\mu = 1.03$, $\delta_f = 60°$, $\delta_{ail} = 30°$, $\delta f_u = 40°$

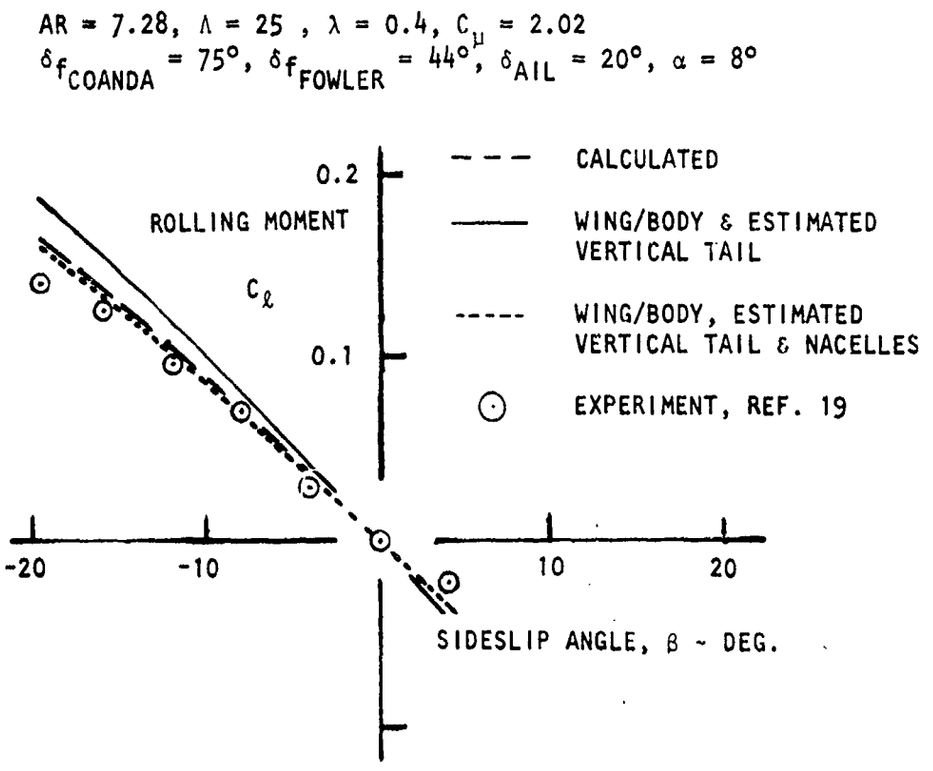

Figure 33. Rolling Moment Comparison, Large Scale USB

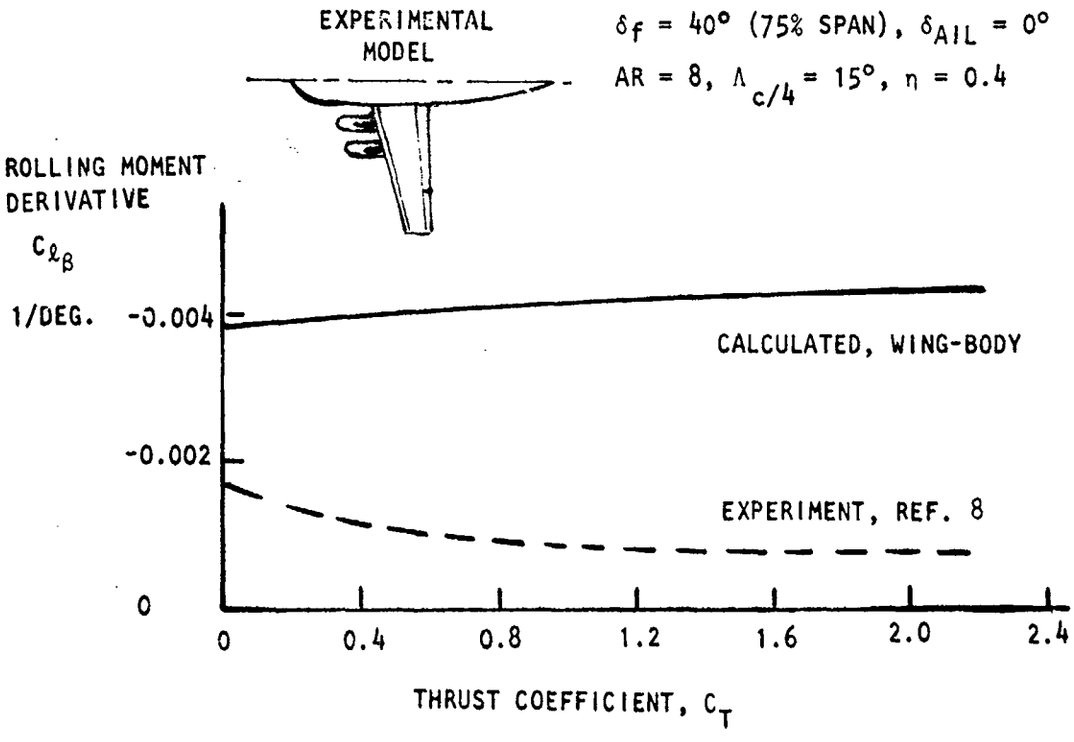

Figure 34. Rolling Moment Comparison, Small Scale IBF Model

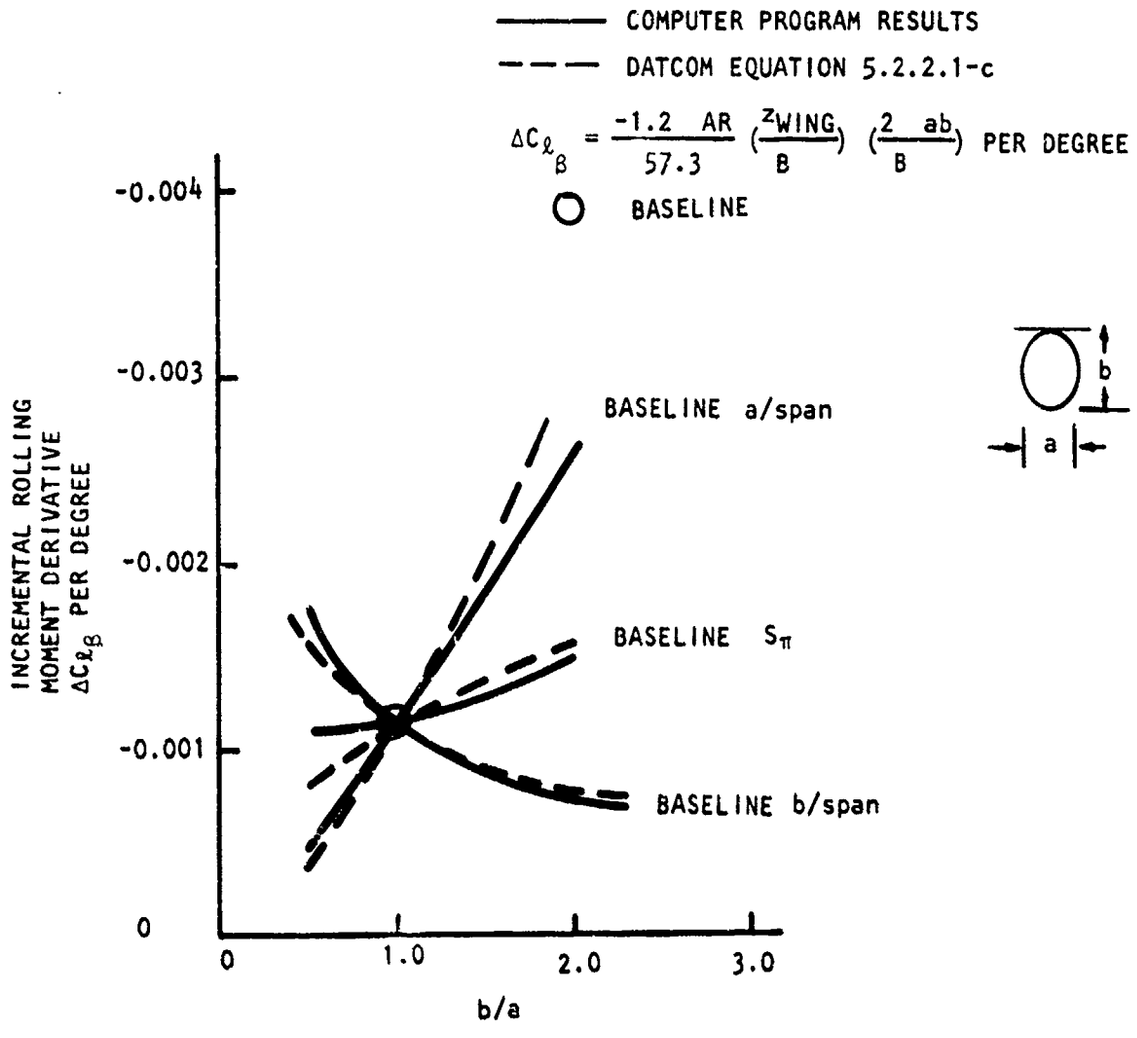

Figure 35. Effects Studies - Rolling Moment Derivative

(a) Effect of Body Shape and Size

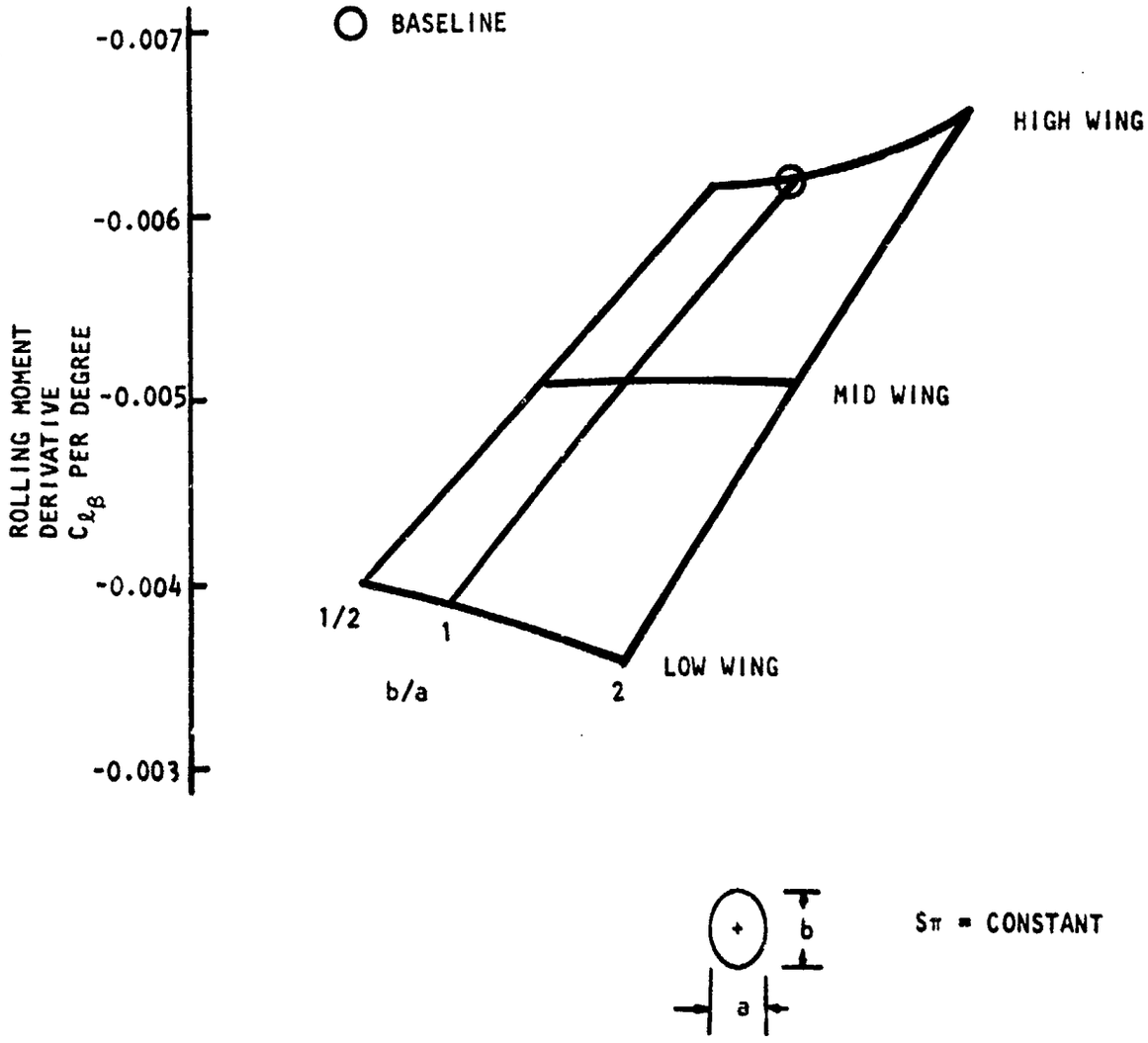

Figure 35. Continued

(b) Effect of Body Shape and Location

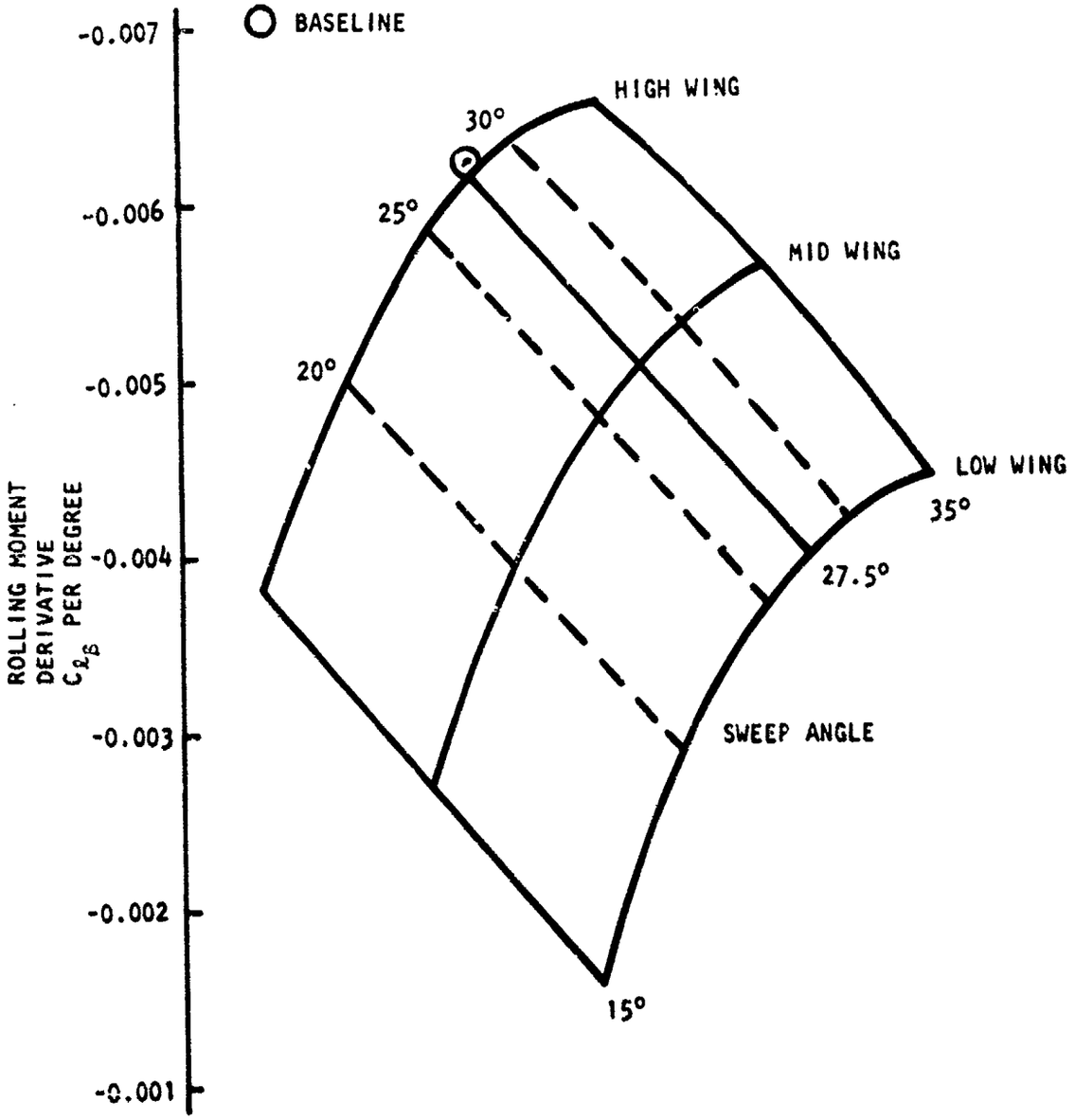

Figure 35. Continued

(c) Effect of Wing Sweep; Baseline with Elliptic Body, b/a = 0.5

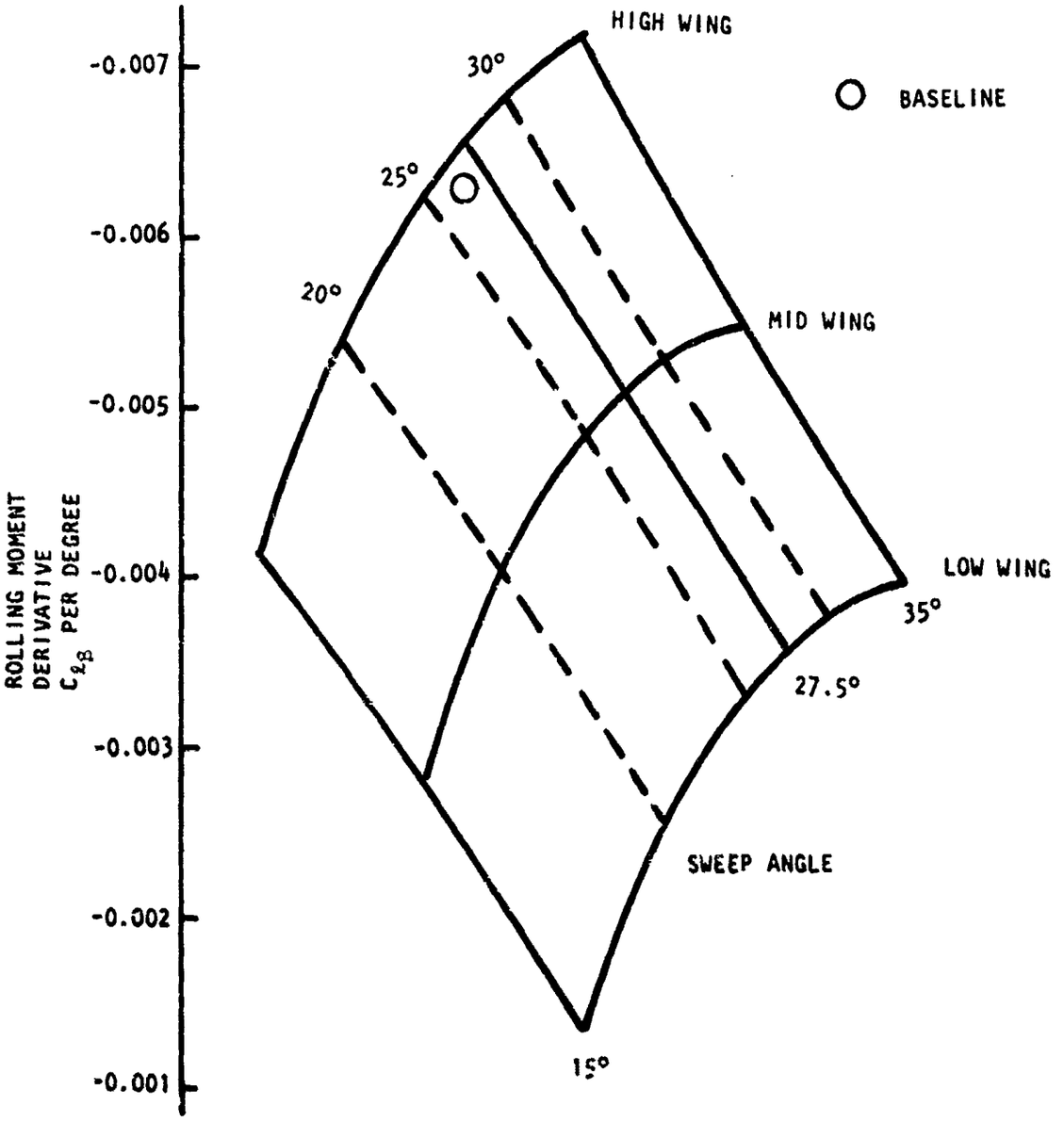

Figure 35. Continued

(d) Effect of Wing Sweep; Baseline with Elliptic Body, b/a = 2

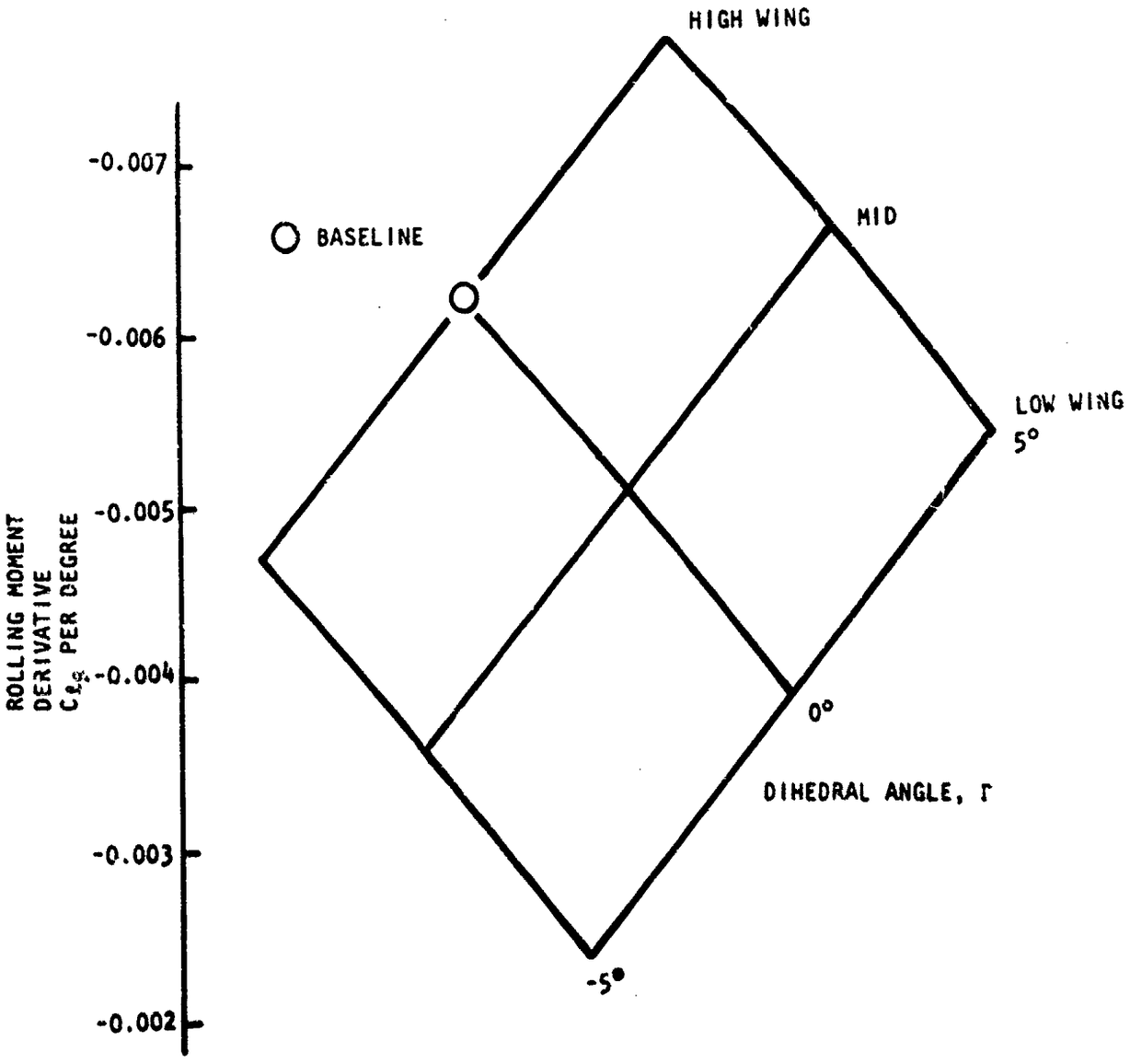

Figure 35. Continued

(e) Effect of Geometric Dihedral

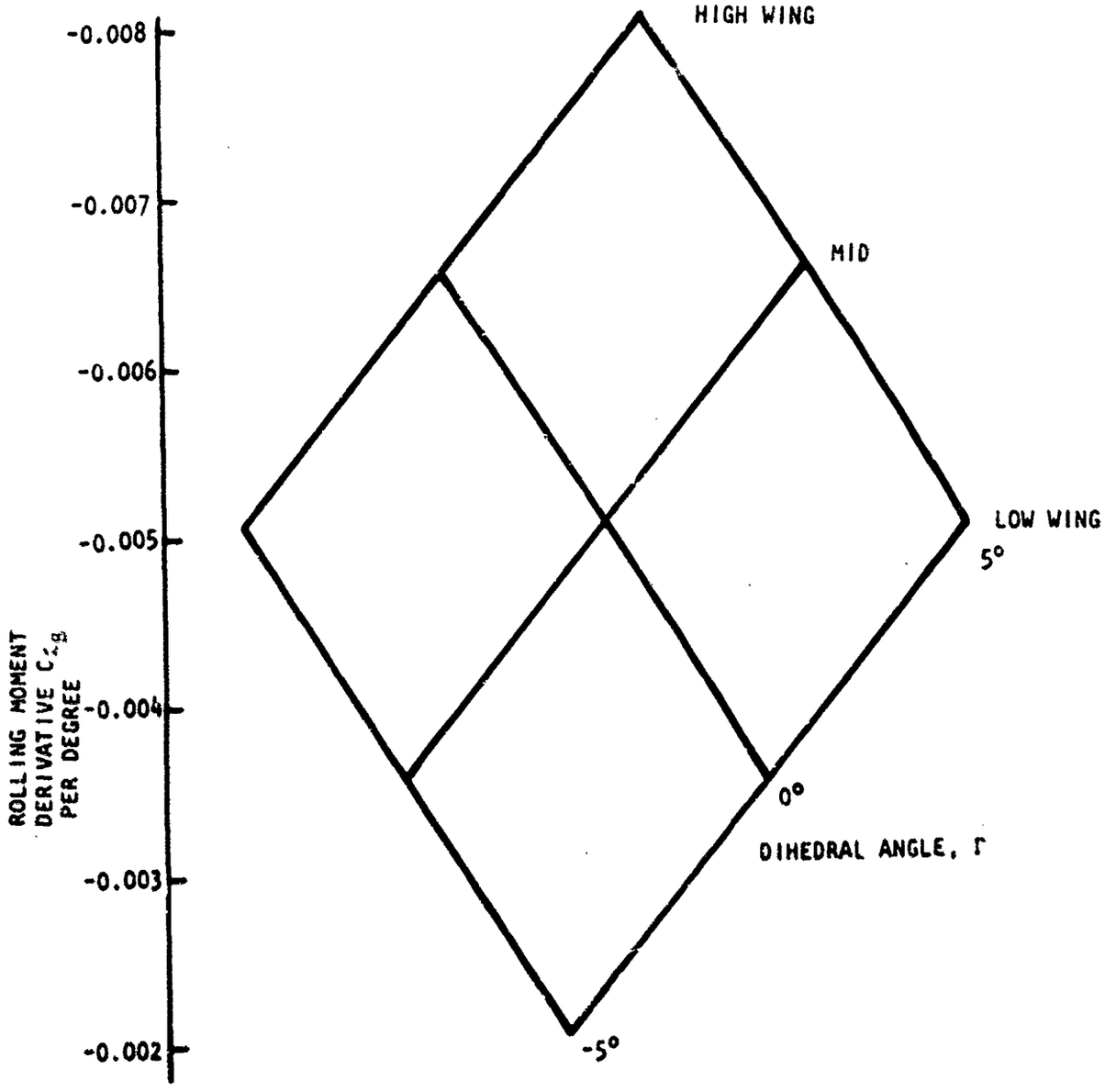

Figure 35. Continued

(f) Effect of ~~Geometric~~ Dihedral; Baseline with Elliptic Body, b/a = 2

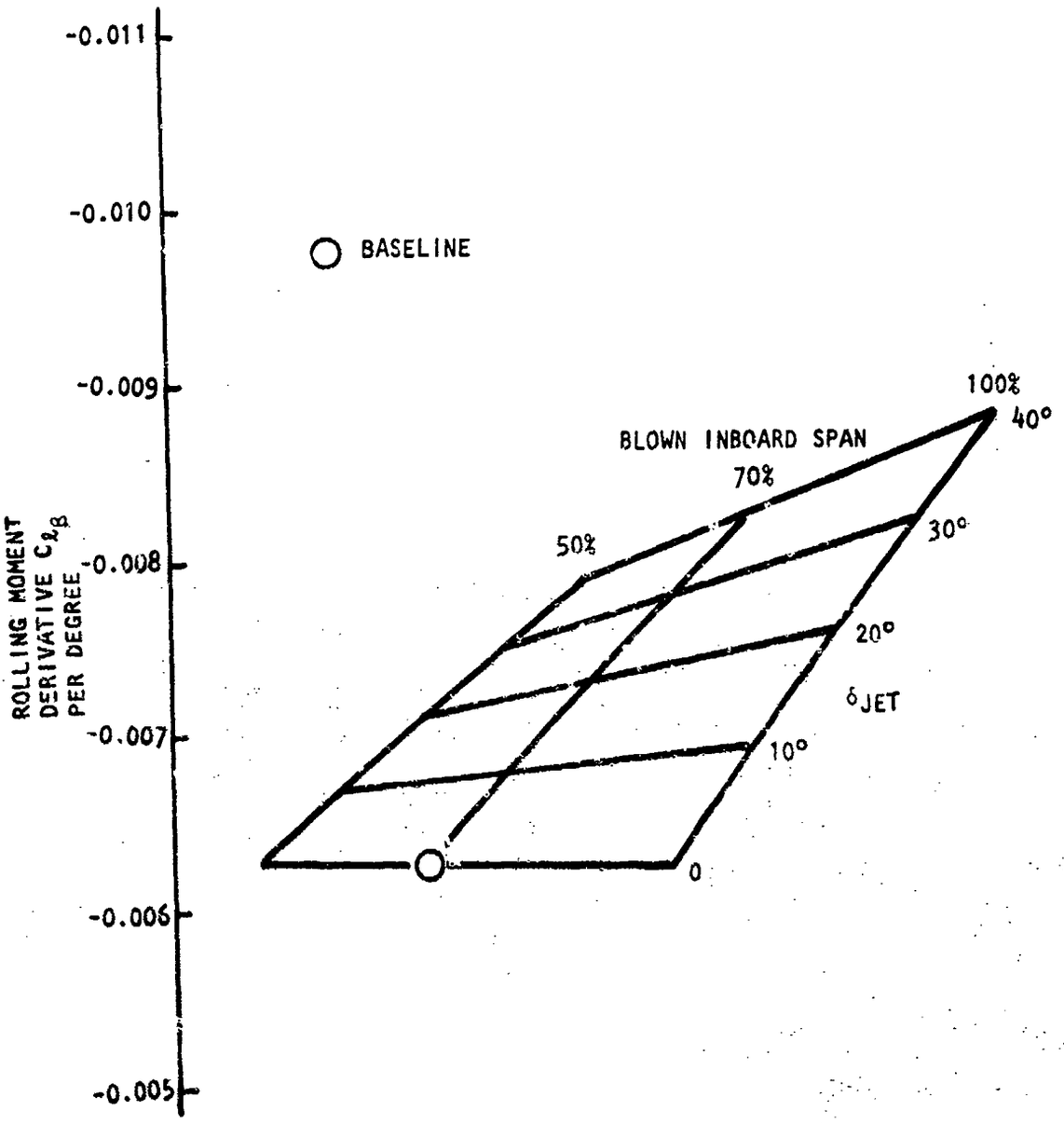

Figure 35. Continued

(g) Effect of Momentum Distribution

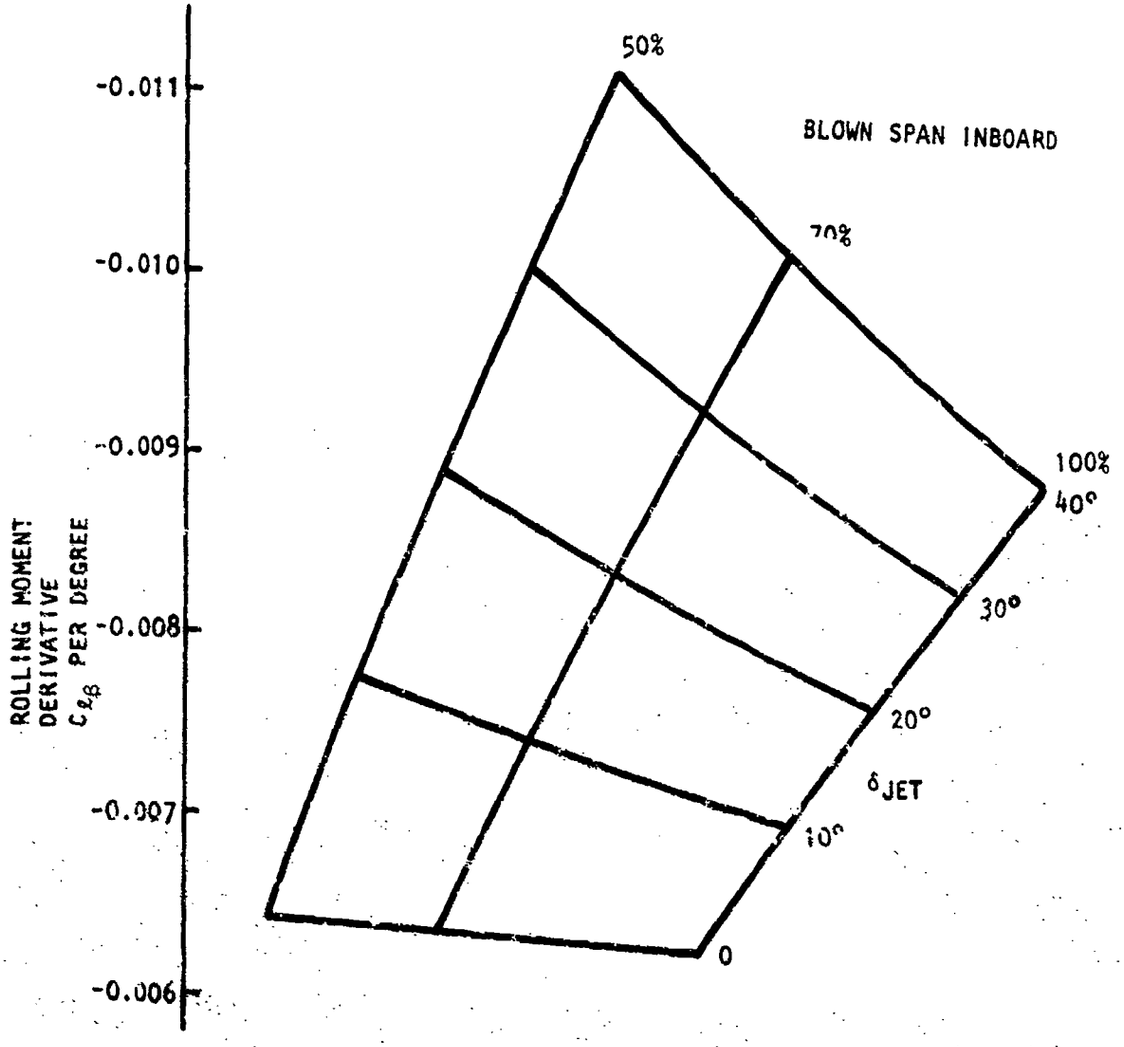

Figure 35. Continued

(h) Effect of Momentum Distribution; Baseline with No Outboard Blowing

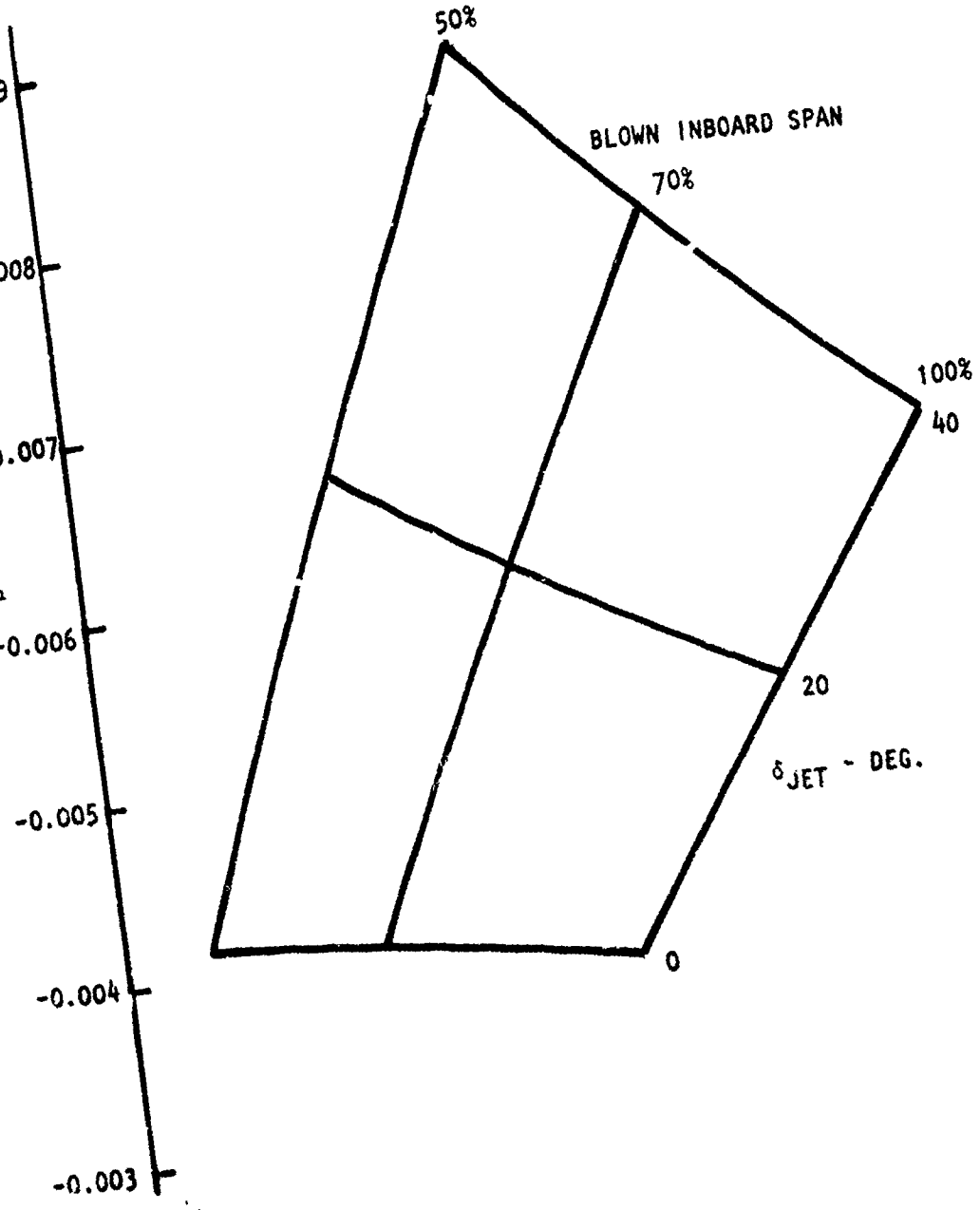

Figure 35. Continued

(l) Effect of Momentum Distribution; Baseline with Low Wing and No Outboard Blowing

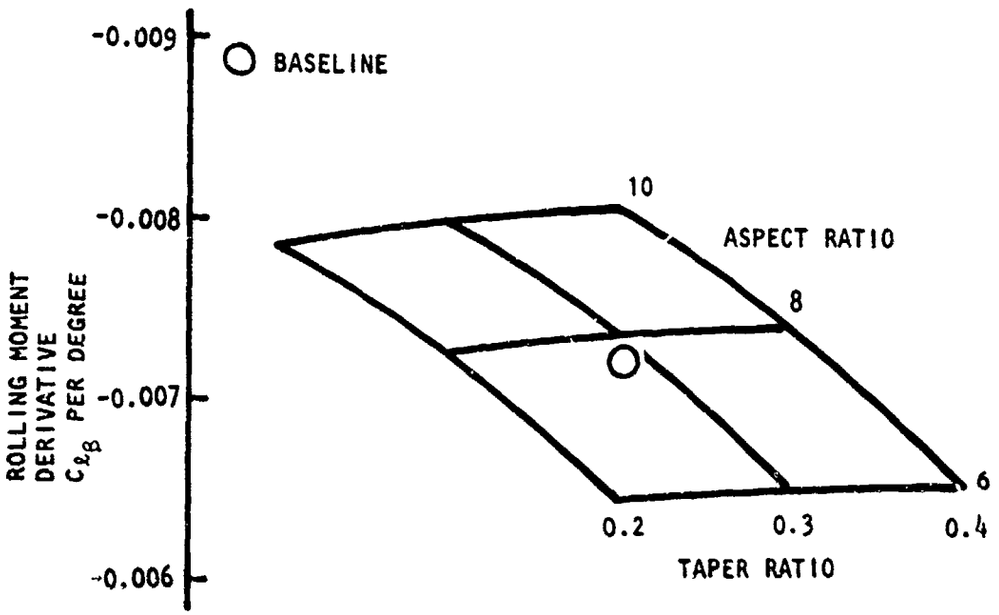

Figure 35. Concluded

(j) Effect of Planform Variations

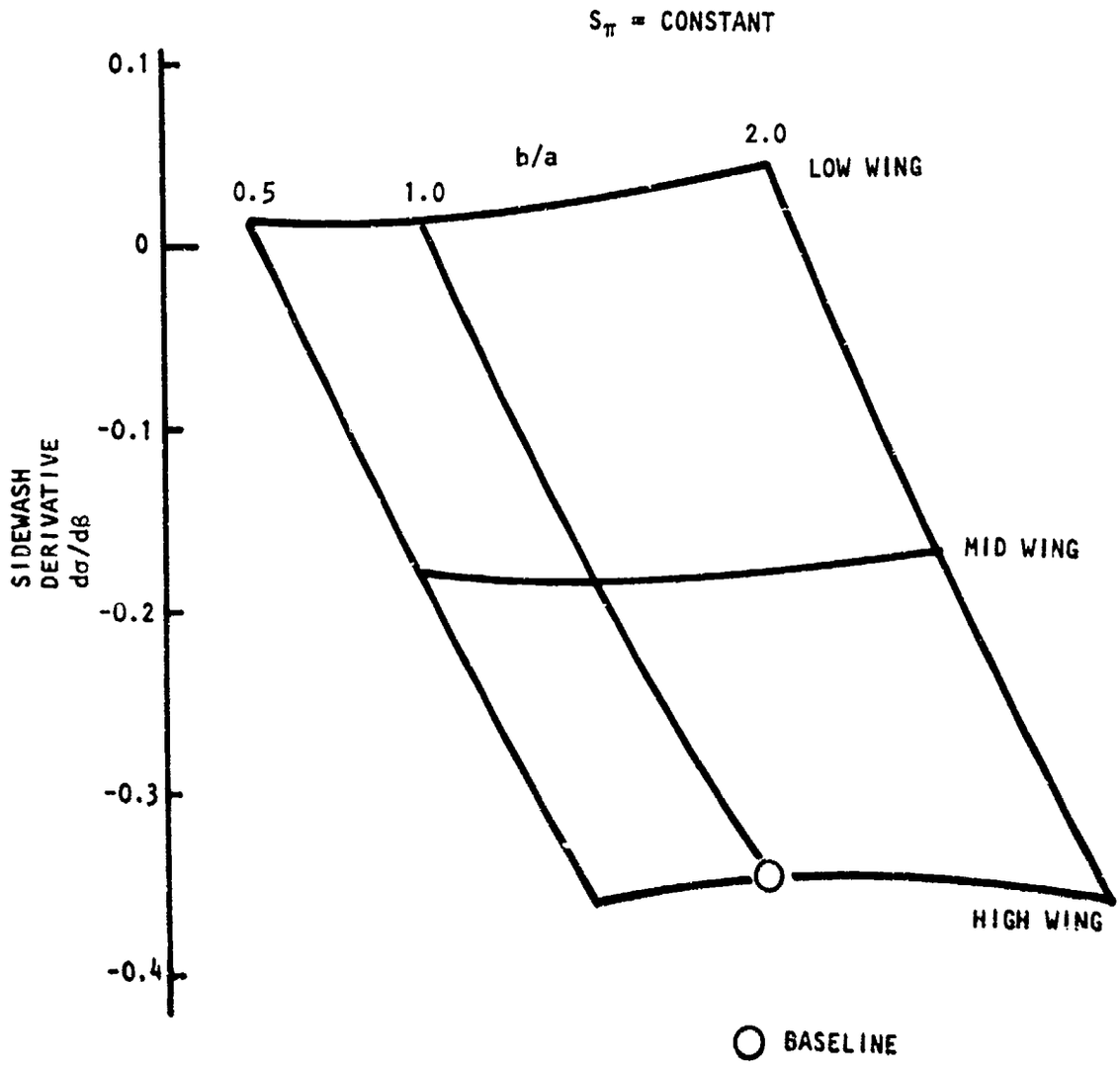

Figure 36. Effect Studies - Sidewash Derivatives

(a) Effect of Body Shape and Location

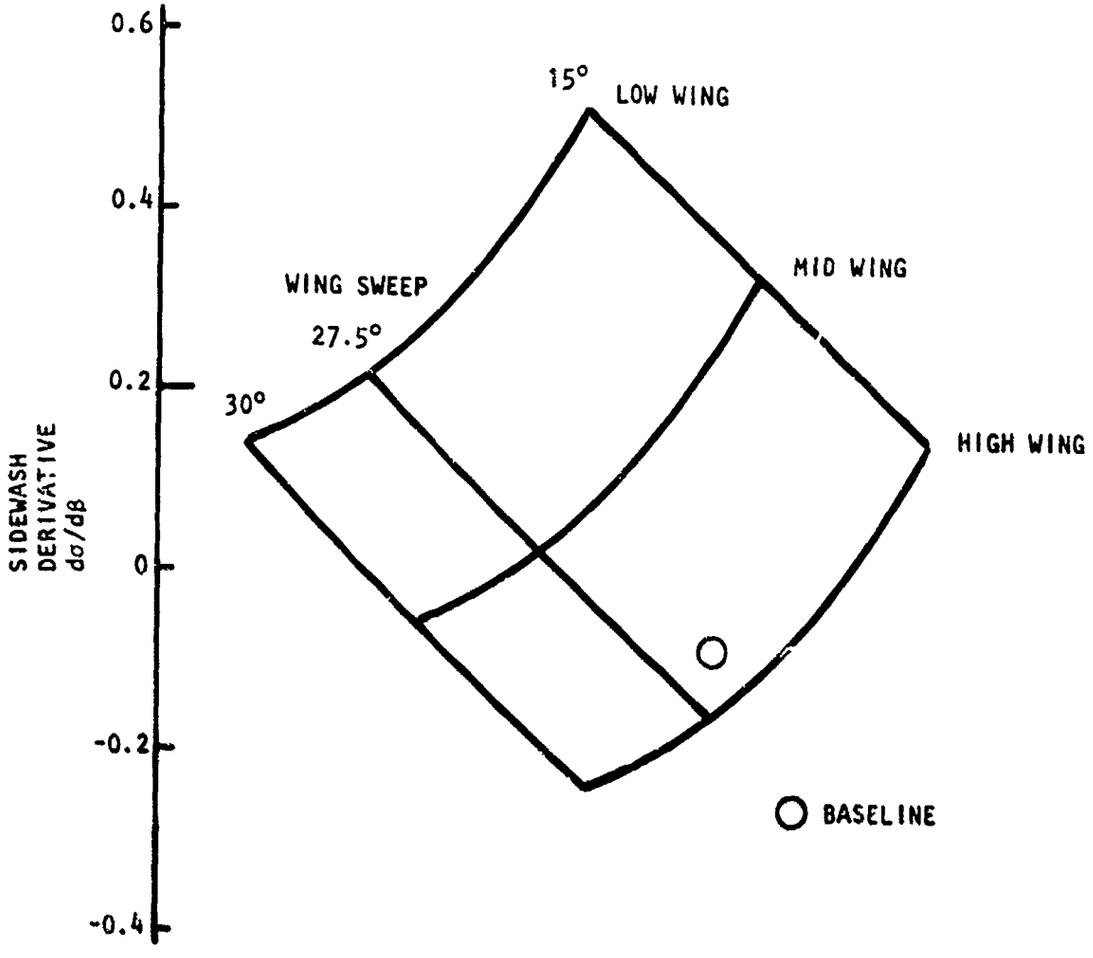

Figure 36. Continued

(b) Effect of Wing Sweep; Baseline with Elliptic Body, b/a = 0.5

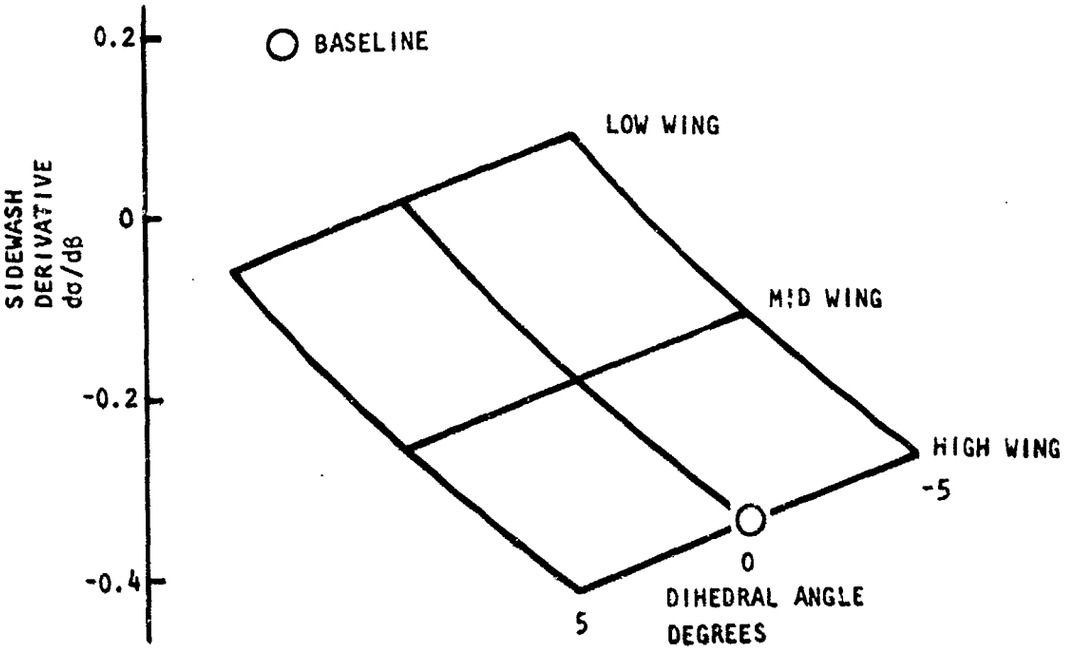

Figure 36. Continued

(c) Effect of Geometric Dihedral

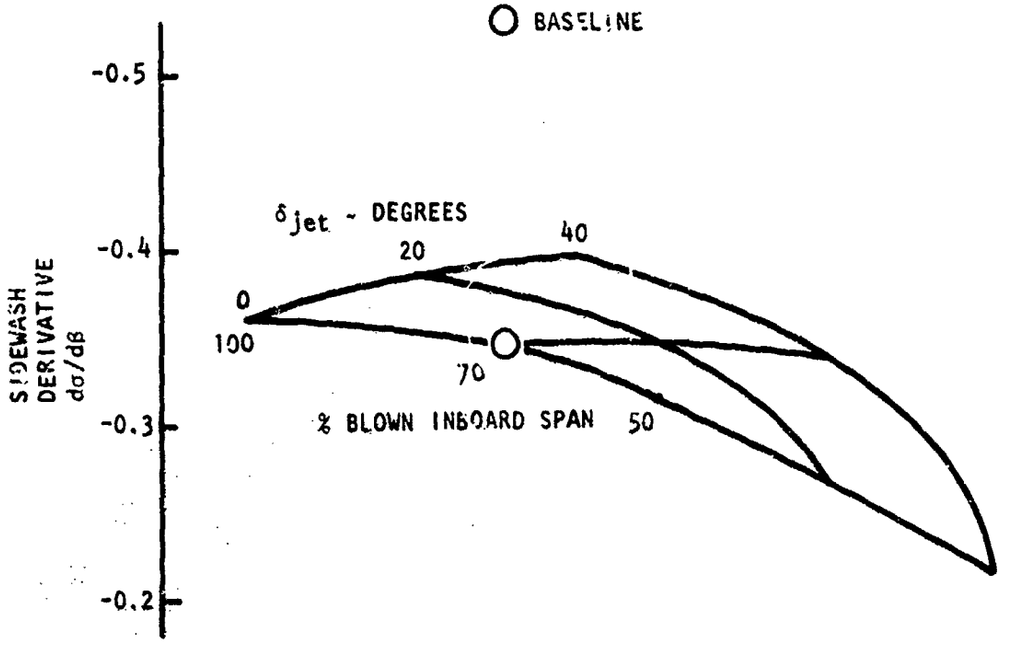

Figure 36. Continued

(d) Effect of Momentum Distribution

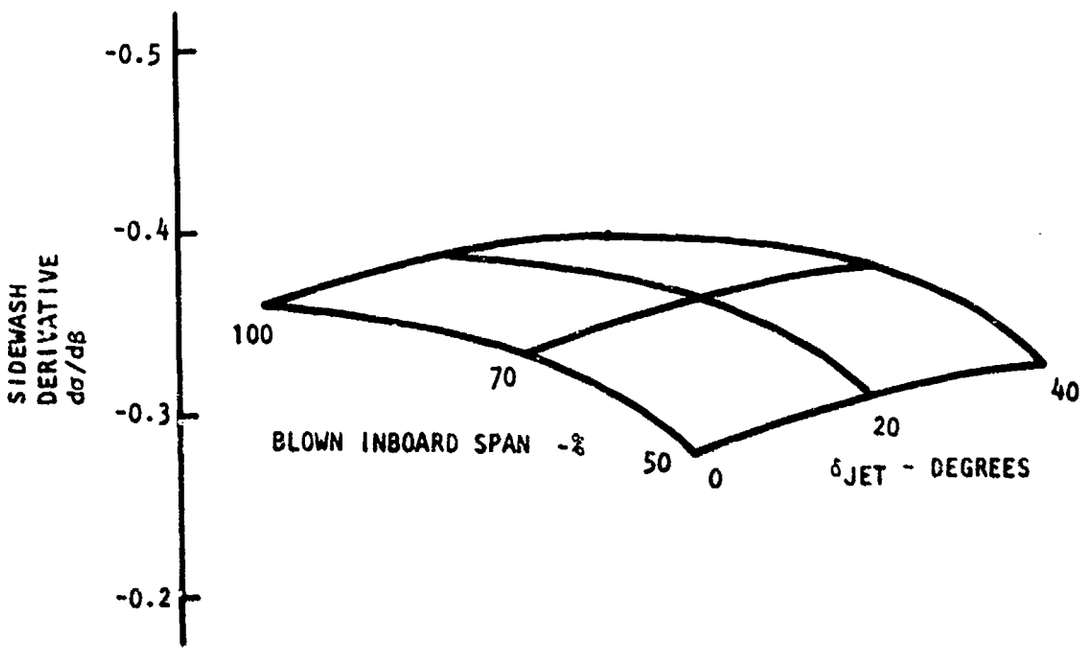

Figure 36. Continued

(e) Effect of Momentum Distribution; Baseline with No Outboard Blowing

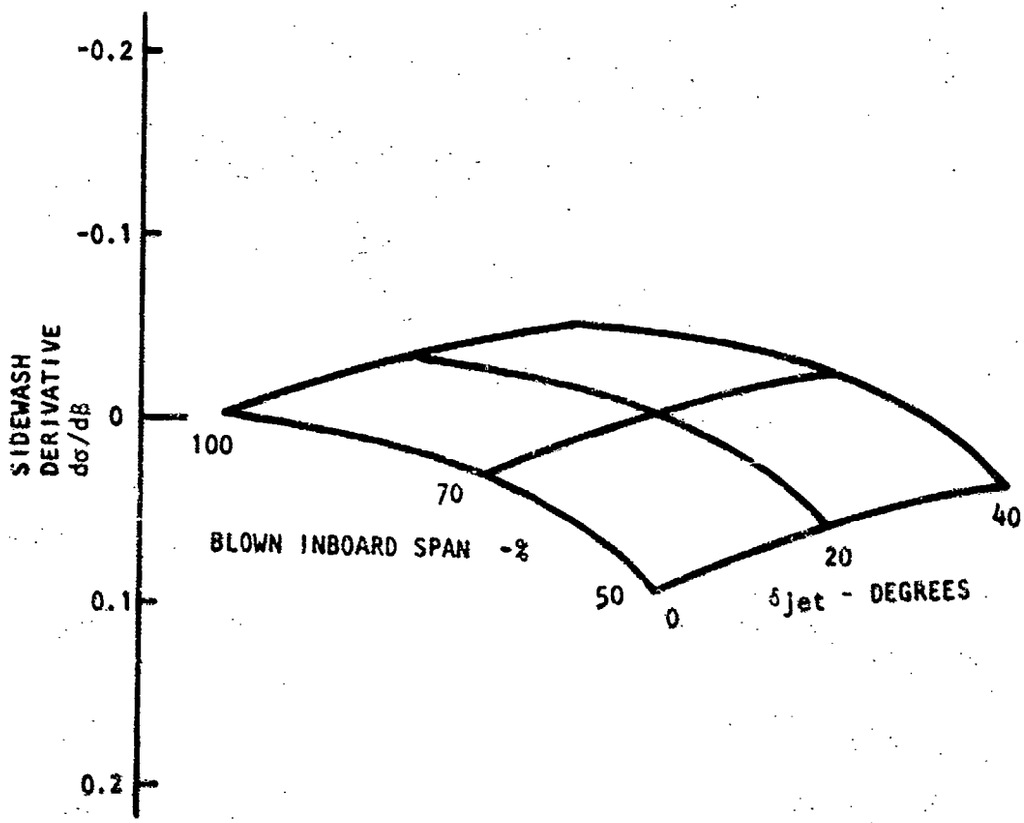

Figure 36. Continued

(F) Effect of Momentum Distribution; Baseline with Low Wing and No Outboard Blowing

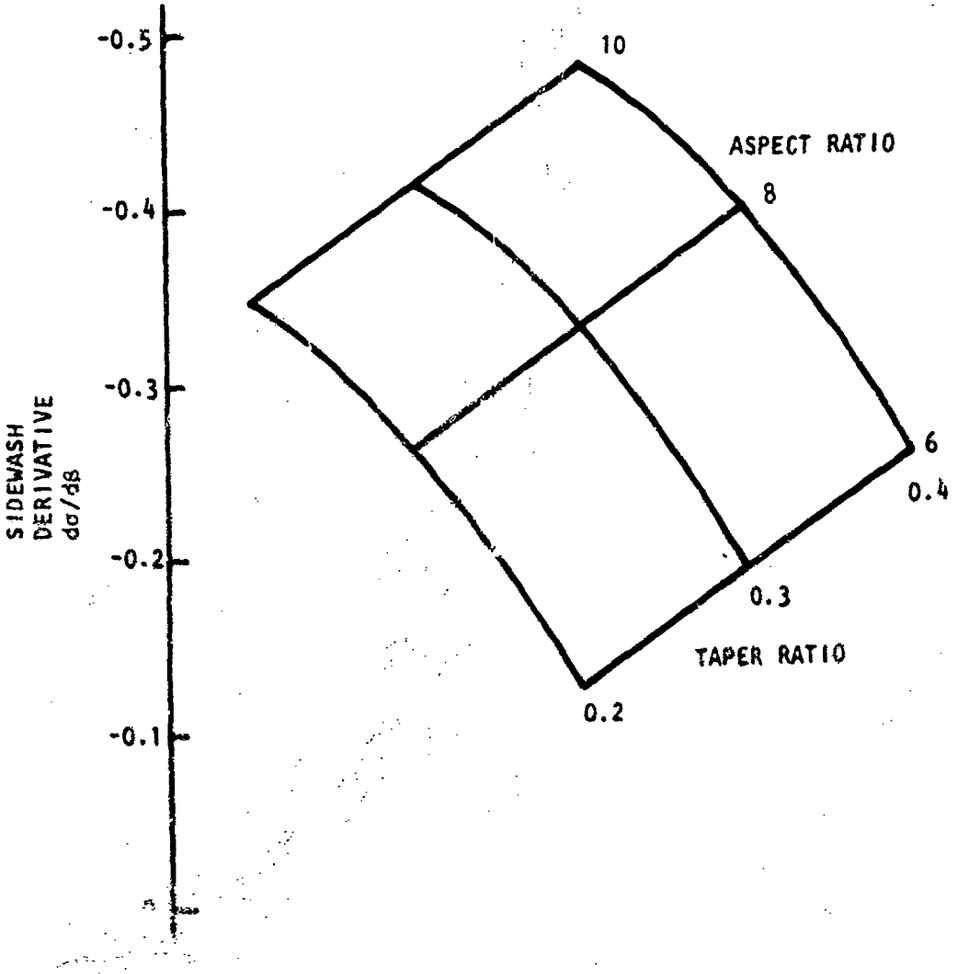

Figure 36. Concluded

(g) Effect of Planform Variations; Baseline with No Outboard Blowing

APPENDIX A

CALCULATION OF BODY-INDUCED ANGLE OF ATTACK ON THE WING

The geometries of the elliptic cross section and its circular transformation are shown in Figure A-1. The sideslip crossflow velocity $V\sin\beta$ and the (v,w) and (v',w') velocities are also noted. The case shown is for the long dimension vertical $(b/a > 1)$, for which

$$Z = \zeta - \frac{a^2}{\zeta} \tag{A.1}$$

transforms the ellipse to a circle. The complex potential in sideslip is

$$F(\zeta) = -V \sin\beta\left[\zeta + \frac{R^2}{\zeta}\right] \tag{A.2}$$

The complex velocity in the real plane is (note that $V\sin\beta$ is in negative y direction)

$$\frac{dF}{dZ} = v + iw = \frac{dF}{d\zeta}\frac{1}{\frac{dZ}{d\zeta}} = \frac{\frac{dF}{d\zeta}}{1 + \frac{a^2}{\zeta^2}} \tag{A.3}$$

From Eqs A.2 and A.3, one obtains

$$\frac{\Delta\alpha}{\beta} = \frac{w}{V\beta} = \frac{(R^2 + a^2)\,(2\xi\eta)}{(\xi^2 - \eta^2 + a^2)^2 + 4\xi^2\eta^2} \tag{A.4}$$

where

$$\frac{R}{a_1} = \frac{\frac{b_1}{a_1} + 1}{2}\cdot\left(\frac{a}{a_1}\right)^2 = \frac{\left(\frac{b_1}{a_1}\right)^2 - 1}{4} \tag{A.5}$$

and where

$$y = \xi - \frac{a^2\xi}{\xi^2 + \eta^2}, \quad z = \eta + \frac{a^2\eta}{\xi^2 + \eta^2} \qquad A.6$$

The induced angle $\Delta\alpha/\beta$ in the real plane is written in transformed coordinates (η,ξ) since a quartic solution is required to express it in real coordinates. However, the transformed coordinates (η,ξ) are quickly obtained by writing Eq A.6 as

$$\left.\begin{aligned}\left(\frac{\xi}{a_1}\right)_i &= \left(\frac{y}{a_1}\right) + \frac{\left(\frac{a}{a_1}\right)^2 \left(\frac{\xi}{a_1}\right)_{i-1}}{\left(\frac{\xi}{a_1}\right)^2_{i-1} + \left(\frac{\eta}{a_1}\right)^2_{i-1}} \\ \left(\frac{\eta}{a_1}\right)_i &= \left(\frac{z}{a_1}\right) - \frac{\left(\frac{a}{a_1}\right)^2 \left(\frac{\eta}{a_1}\right)^2_{i-1}}{\left(\frac{\xi}{a_1}\right)^2_{i-1} + \left(\frac{\eta}{a_1}\right)^2_{i-1}}\end{aligned}\right\} \qquad A.7$$

and iterating simultaneously in each step, starting with

$$\left(\frac{\xi}{a_1}\right)_o = \left(\frac{y}{a_1}\right), \quad \left(\frac{\eta}{a_1}\right)_o = \left(\frac{z}{a_1}\right)$$

The iterated results, with Eq A.4 , give the induced angle $\Delta\alpha/\beta$ as a function of (y,z) coordinates.

In pitch, the crossflow velocity is rotated 90 degrees from the sideslip case, for which the complex potential is

$$F(\zeta) = i\, V \sin\alpha_{body} \left[\zeta - \frac{R^2}{\zeta}\right]$$

With Eq A.3, but with $dF/dZ = v - iw$, this gives

$$\frac{\Delta\alpha}{\alpha_{body}} = \frac{(\xi^2 + \eta^2)^2 + (\xi^2 - \eta^2)(R^2 + a^2) + R^2a^2}{(\xi^2 - \eta^2 + a^2) + 4\xi^2\eta^2} - 1$$

where Eqs A.5, A.6, and A.7 apply.

For $b_1/a_1 < 1$, the appropriate transformation is

$$Z = \zeta + \frac{a^2}{\zeta}$$

However, since a^2 is replaced by $-a^2$, it also follows that

$$-\left(\frac{a}{a_1}\right)^2 = \frac{\left(\frac{b_1}{a_1}\right)^2 - 1}{4}$$

so that algebraic signs compensate when the preceding results are used intact.

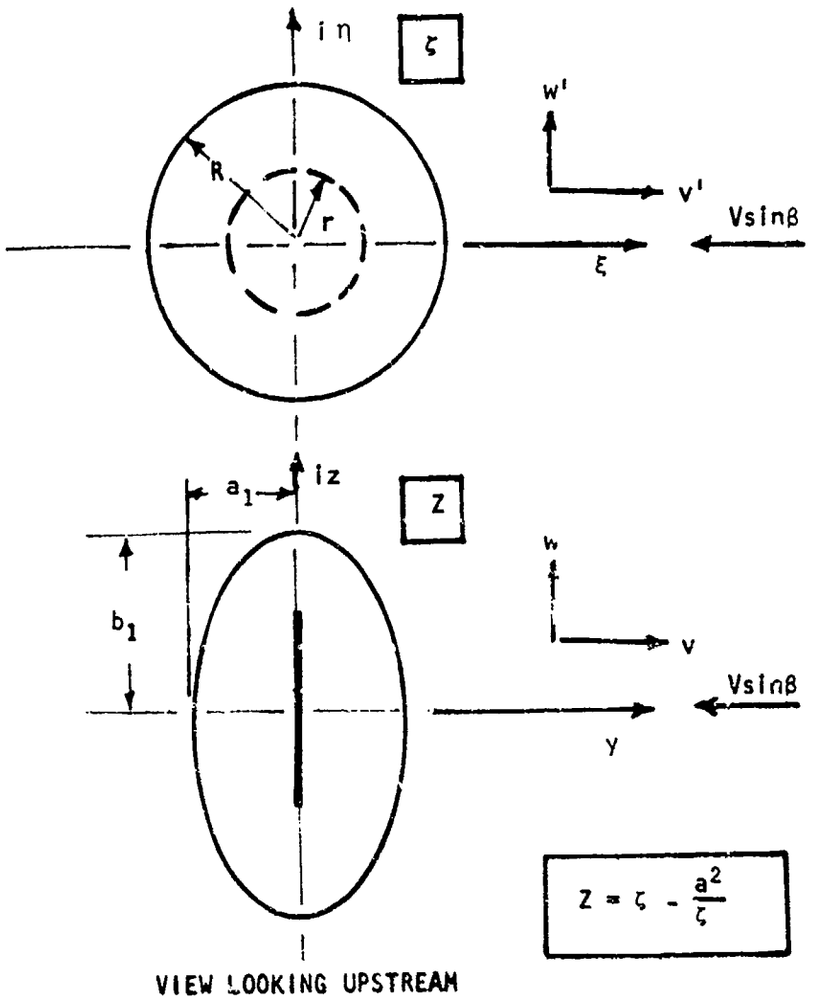

Figure A-1. Transformation of Body Cross Section for Calculation of Body Interference on Wing in Sideslip

APPENDIX B

CALCULATION OF AXIAL FORCE COEFFICIENT

The far field wake is assumed to consist of a rolled up vortex system which is coaxial with the redirected jet, deflected downward by an angle β_∞. The vortex strength on each side is denoted by Γ_o, where Γ_o is the centerline circulation around both wing and sheet, and is therefore the wake vorticity accumulated by shedding. The total jet momentum in the far field is assumed to be ηC_μ, where η is the usual "turning efficiency."

The geometry is illustrated in Figure B-1. The jet and vortex are approximated by a line vortex and jet as shown, and the two sides are separated by a distance $(\pi/4)bA_1$, where A_1 is to be determined. The vortices are in equilibrium at an angle β_∞ when the freestream crossflow velocity balances the mutually induced velocity, giving

$$\sin\beta_\infty = K \frac{\Gamma_o}{2bVA_1} \qquad B.1$$

where $K = 4/\pi^2$ for the rolled wake shown, and where $K = 2$ for a flat wake.

The vortex or circulation lift is the transverse momentum per unit length of vortex, and is given by

$$L_\Gamma = \rho V \Gamma_o \frac{\pi}{4} A_1 b \qquad B.2$$

from which

$$\frac{C_{L_\Gamma}}{\pi AR A_1^2} = \frac{\Gamma_o}{2bVA_1} \qquad B.3$$

Integration of lifting vortex loads directly gives

$$L_\Gamma = \rho V \bar{\Gamma} b \qquad B.4$$

where $\bar{\Gamma}$ is the average Γ across the span. From Eqs B.2 and B.4 it is seen that $A_1 = 4/\pi \ \bar{\Gamma}/\Gamma_o$. It is noted that $A_1 = 1$ for an elliptic vortex distribution.

The vortex "drag" force, inclined by β_∞ to the freestream, can be shown to be

$$\frac{C_{D_{vortex}}}{\pi AR} = B \left(\frac{\Gamma_o}{2bV}\right)^2 \qquad B.5$$

where B is the ratio of vortex drag to that for an elliptic vortex distribution at the same $\Gamma_o/2bV$. Substitution from Eq. C.3 allows the preceding to be written

$$\frac{C_{D_{vortex}}}{\pi AR} = \frac{B}{A_1^2}\left(\frac{C_{L_\Gamma}}{\pi AR}\right)^2 \equiv \frac{1}{e_\Gamma}\left(\frac{C_{L_\Gamma}}{\pi AR}\right)^2 \qquad B.6$$

where e_Γ is the span efficiency of the <u>total</u> vortex system.

With this in mind, the total vorticity in the wake is given by

$$\frac{\Gamma_{o_{Total}}}{2bVA_1} = \frac{C_{L_\Gamma}}{\pi AR\, A_1^2}$$

$$= \frac{C_{L_{Total}}}{\pi AR\, A_1^2} - \frac{\eta C_\mu}{\pi AR\, A_1^2}\sin\beta_\infty$$

$$= \frac{C_{L_{Total}}}{\pi AR\, A_1^2} - \frac{\eta C_\mu}{\pi AR\, A_1^2} K \frac{\Gamma_{o_{Total}}}{2bVA_1}$$

from which

$$\frac{\Gamma_{o_{Total}}}{2bVA_1} = \frac{\dfrac{C_{L_{Total}}}{\pi AR\, A_1^2}}{1 + \dfrac{KnC_\mu}{\pi AR\, A_1^2}} \qquad B.7$$

The pitch plane projection of the injected jet is denoted by ηC_μ in keeping with the usual efficiency-turning polar notation. The Trefftz plane efflux of pitch plane momentum is assumed to be ηC_μ and the lateral components are ignored. This can be done since the effective "span" of the lateral components is, in the present context, the vertical dimension or thickness of the jet. This corresponds to an extremely high value of $j_{lat}/[q\ (\text{thickness})^2]$ (analogous to very high C_μ/AR), so that substantially no bend-back and associated thrust recovery and vortex drag are expected. The axial force coefficient is written (see Figure 10)

$$\frac{C_x}{\pi AR\, A_1{}^2} = \left(\frac{\eta C_\mu}{\pi AR\, A_1{}^2} - \frac{C_{D_{vortex}}}{\pi AR\, A_1{}^2} \right) \cos\beta_\infty$$

which, for small β_∞, becomes

$$\frac{C_x}{\pi AR\, A_1{}^2} = \frac{\eta C_\mu}{\pi AR\, A_1^2} - \left[\frac{\eta C_\mu}{\pi AR A_1^2} \frac{\beta_\infty{}^2}{2} + \frac{C_{D_{vortex}}}{\pi AR\, A_1^2} \left(1 - \frac{\beta_\infty{}^2}{2}\right) \right] \qquad B.8$$

From previous relationships (see Eqs B.1, B.5, and B.6), it is seen that

$$\beta_\infty{}^2 = K^2 \left(\frac{\Gamma o}{2bVA_1}\right)^2$$

$$\frac{C_{D_{vortex}}}{\pi AR\, A_1{}^2} = \frac{1}{A_1{}^2 e_\Gamma} \left(\frac{C_{L_\Gamma}}{\pi AR}\right)^2 = \frac{A_1{}^2}{e_\Gamma} \left(\frac{\Gamma o}{2bVA_1}\right)^2$$

Substitution of these relationships, with Eq. B.7, into Eq. B.8 gives, after some manipulation,

$$C_x = \eta C_\mu - \frac{C_{L_{\Gamma o t}}{}^2}{\pi AR\, e_\Gamma} \frac{\left(1 - \frac{e_\Gamma}{A_1^2} \frac{\beta_\infty{}^2}{2} + \frac{K^2 e_\Gamma}{2A_1^2} \frac{\eta C_\mu}{\pi AR\, A_1{}^2}\right)}{\left(1 + \frac{K\eta C_\mu}{\pi AR\, A_1{}^2}\right)^2} \qquad B.9$$

Terms of order β and $C_\mu/\pi AR$ are usually small compared to unity. By neglecting their squares and products and accounting for profile and ram drag the axial force expression B.9 becomes

$$C_x = \eta C_\mu - C_{D_{RAM}} - C_{D_p} - \frac{C_{L_{Tot}}^2}{\pi AR\, e_\Gamma} \frac{1}{\left[1 + \frac{2K\eta C_\mu}{\pi AR\, A_1^2}\left(1 - \frac{K}{4}\frac{e_\Gamma}{A_1^2}\right)\right]} \qquad \text{B.10}$$

In two dimensional flow ($AR\, e_\Gamma \to \infty$), the axial force expression B.10 corresponds to a 100 percent recovery of the effective gross thrust ηC_μ, which is reduced by ram and profile drags. Accordingly, the last term is a total drag due to the three dimensionality of the flow, and is therefore properly considered as induced drag. The induced drag consists of the induced drag in the normal sense (extended to include the effects of jet sheet vortex system) plus a loss of thrust recovery resulting from failure of the jet efflux momentum to ultimately align itself with the freestream direction.

It will be observed that the induced drag at $C_\mu = 0$ corresponds to the usual expression

$$C_{D_i} = C_L^2/\pi AR\, e_\Gamma \qquad \text{B.11}$$

The span efficiency, e_Γ, is of course associated with the spanwise distribution of circulation lift over the combined wing and vortex sheet. However, an additional distribution factor A_1 is associated with the C_μ term. The presence of two parameters e_Γ and A_1 in the induced drag expression (in contrast to the usual single parameter e_Γ) is explained as follows.

The classic expression for induced drag, Equation B.11, is based on a small wake inclination β. When rigorously developed from Trefftz plane considerations, this result is in fact *independent* of the wake angle, β, parameter. This is true for the induced drag of vortex systems associated with either a wing or a wing plus jet sheet. The additional induced drag, which is the three dimensional loss of thrust recovery, is

$$\Delta C_{D_i} = \eta C_\mu \frac{\beta^2}{2}$$

It is directly dependent upon β, where β is partially defined by the term A_1 (Eq. B.1). It is noted that A_1 is the spanwise distance between "centroids" of the left and right hand trailing vortex systems, normalized on the corresponding distance for an elliptic bound vortex distribution. In the literature it is generally referred to as the "centroid of impulse".

Equation B.10 was developed on the assumption of a fully rolled wake for which $K = 4/\pi^2$. However, if the wake is taken to be flat, $K = 2$, in which case Eq. B.10 is still valid. For a flat wake and elliptic loading ($A_1 = 1$, $e_\Gamma = 1$), Eq. B.10 reduces to the Maskell-Spence equation. As long as

$$\frac{C_\mu}{\pi AR\, A_1^2} << 1$$

the axial force is relatively insensitive to K. For large C_μ, with the blowing concentrated over a portion of the span, this is not true, so a realistic value of K must be used. It is believed that $K = 4/\pi^2$, for the rolled up wake, is most representative and is the basis for all axial force calculations presented in the main text.

Utilization of Eq. B.10 requires that A_1 and e_Γ be calculated. It is emphasized that these are distributional quantities associated with the *total* vortex system. Some approximation is therefore necessary.

The span load distributions calculated by the method presented in the main body of the report consist of a vortex loading on the wing and EMF plus a residual lift term, corresponding to $K = 1$, for which the conversion of jet momentum to sheet vortex loading is incomplete. The appropriate vortex distribution for calculation of A_1 and e_Γ is therefore somewhere between the vortex lifts and total lift distributions as presently calculated, and illustrated in Figures (10a) and (10b) in the main text.

The differences in A_1 and e_Γ evaluated for these extremes are typically small; both quantities are therefore based on the vortex lift distribution with $K = 1$.

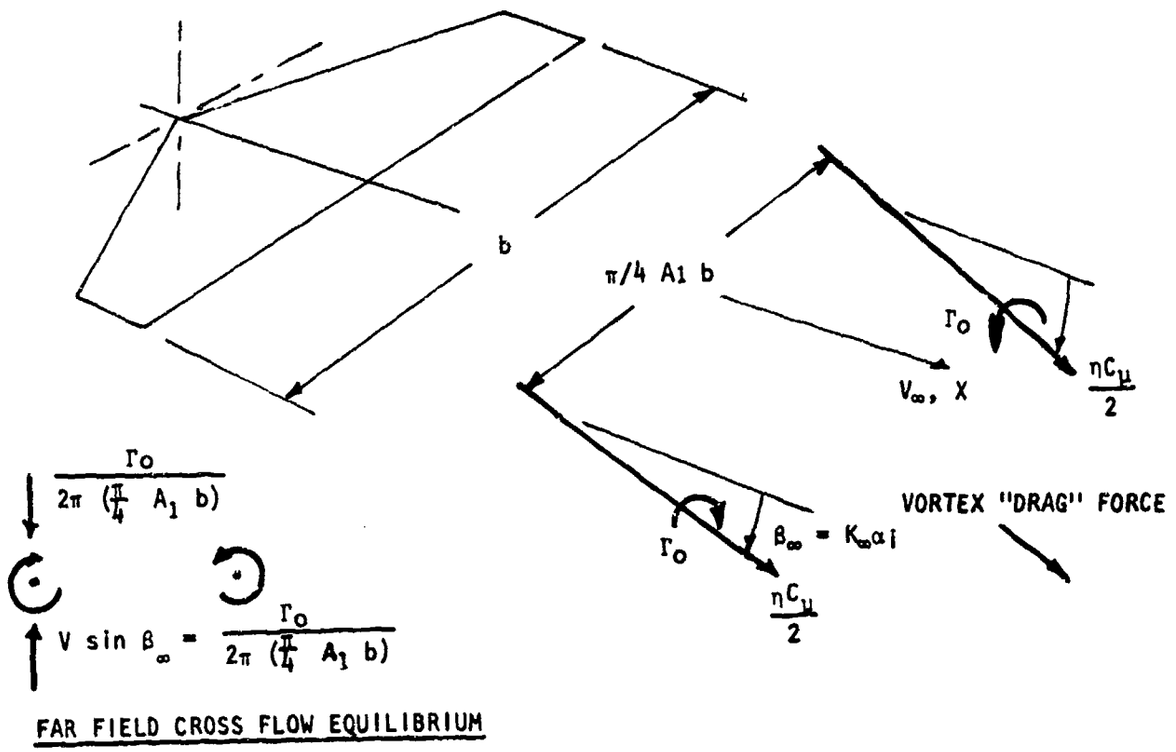

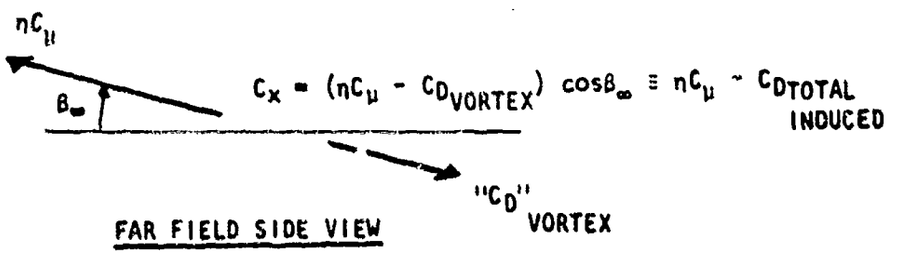

Figure C-1. Far Field Concept for Axial Force Calculation

APPENDIX C

COMPUTER PROGRAM INPUT, OUTPUT, AND EXAMPLE PROBLEM

1. INPUT FORMAT AND SPECIAL INSTRUCTIONS

a. Basic Input

The total number of input cards varies according to both the number of points used to describe the planform and the number of field points at which flow angularity is to be calculated. Card 1 is a title card containing 70 columns of free-form alphameric data which is printed out as the output heading.

The remaining card input is numerical data. The majority of these inputs are in a floating point format of seven, 10-column fields per card (7F10.0) and are indicated by "Field 1", "Field 2", etc., in the following instructions. The remaining input is in integer form (2I2) and is indicated in the following instructions by "Columns 1 and 2", etc. All integer input is "right justified", and must be located as far as possible to the right-hand side of the allocated columns.

The input for each card follows. In certain places reference is made to Note 1, Note2, etc., which follow the card description.

Card 1: Title (70 column alphameric input).

Card 2:

Columns 1 & 2; NY, number of span stations at which section properties will be input (right justified). This is for one wing panel only, and will include the theoretical wing root and tip. $2 \leq NY \leq 20$.

The following block of cards contains section characteristics for the NY number of points specified in Card 2. Two cards are required for each point. Cards 3 and 4 are for the wing centerline. Subsequent cards are input in order of spanwise location, ending with the wing tip. The locations of the input points, while arbitrary, should be chosen to include those span stations at which section characteristics change rapidly or are discontinuous. At such locations, properties should be input both just inboard and just outboard of discontinuities in geometry and/or at blowing levels. Section properties at non-input locations are obtained by linear interpolation. All inputs used are for mechanical flaps extended but rotated back into the wing plane and are in a streamwise reference system.

Card 3: Input the following for wing centerline:

Field 1 dimensional value of y coordinate

2 dimensional cnord, all flaps extended

3 section incidence with respect to the fuselage reference (in degrees)

4 section zero lift angle of attack, in degrees (see Note 1)

5 main flap chord: wing chord ratio (all flaps extended)

6 section momentum coefficient (see Note 2)

7 main flap deflection, degrees, positive trailing edge down

Card 4: Field 1 δ_j, jet momentum injection angle, degrees, positive downward from flap

2 ε, jet skew angle (see Note 2)

3 $C_{\ell o}$, section lift coefficient, unflaped, at zero angle of attack

4 leading edge flap chord: wing chord ratio

5 leading edge flap deflection, degrees, positive nose down

Card 5
Card 6: } Same as for Cards 3 and 4 but for second point of definition.

Card 7
Card 8: } Repeat preceding input for third point of definition.

Card 2(NY)+1
Card 2(NY)+2 } Repeat preceding input for wing tip.

Card 2(NY)+3:

Field 1 body width or diameter, dimensional

2 wing height above body center, dimensional

3 body height for elliptic bodies, dimensional, input blank or zero for circular body

Card 2(NY)+4

Field 1 drag coefficient; total of configuration profile drag plus ram drag. (Used in final axial force calculation) Based on reference area.

2 turning efficiency, η, projection of resultant efflux momentum into pitch plane and normalized on input total.

3 increment of semispan at which loading will be output, i.e., 0.05, 0.10, etc.

4 EOKPCT, permissible percent RMS error in calculated effective angle of attack for all control points (see Note 1), suggested value is 2.0 percent.

Card 2(NY)+5:

Columns 1 & 2; NC, number of control points per semispan used in calculation procedure. (Right justified). This number will include a centerline control point and a tip control point. $4 \leq NC \leq 16$. Total used in sideslip calculation is 2(NC)-1. (see Note 3)

Columns 3 & 4; NPTS, Number of field points where sidewash and downwash is desired (Right justified). $0 \leq NPTS \leq 20$, blank or zero if none required.

Card 2(NY)+6: Location of first sidewash/downwash field points, dimensional, optional if blank or zero input in Columns 3-4 of previous card. All locations relative to wing apex.

Field 1 x (positive towards aft fuselage)

2 y (positive out R.H. wing)

3 z (positive up)

Card 2(NY)+7: x,y,z location of second field point.

Card 2(NY)+5+NPTS Location of last field point.

Card 2(NY)+6+NPTS

Field 1 wing span, dimensional

2 aspect ratio (based on span and desired reference area)

3 wing sweep (degrees)

4 dihedral (degrees)

5 flap hinge line sweep (degrees)

Card 2(NY)+7+NPTS

Field 1 ALPHAB, angle of attack of the fuselage reference line, degrees

2 sideslip angle, degrees, positive far incident wind from pilot's right

3 FACTOR, convergence factor. Normally leave blank, otherwise see Note 1.

b. Special Notes.

(1) Note 1: Input Parameters to Aid in Program Convergence. For most normal caseruns, the three input parameters which deal with convergence are input as zero or blank.

Cards 3, 4, ...2(NY)+2, Field 4

Section angle of attack for zero lift (flapped and powered). This input parameter is used only for setting up an initial point for the convergence procedure. Normally, zero values for this parameter are sufficiently close for convergence. For cases where convergence is not obtained (output ESTAR>>EOK), a more accurate estimate of this parameter may be required. Variations of this parameter is the most effective means of solving convergence problems.

Card 2(NY)+4, Field 4: permissible error, EOKPCT

If left blank or input as zero, the program internally sets the value at 1% of the input angle of attack of the fuselage reference line, EOK = (1.)(.01)(ALPHAB). For many cases a larger permissible error may yield equally valid results thus requiring less iterations and computer time.

Card 2(NY)+7+NPTS, Field 3: FACTOR, convergence factor.

> Normally left blank or zero, whereby the computer internally sets FACTOR to 0.4. If the first attempt at convergence fails, the computer changes FACTOR to 0.8 and starts over. If convergence is not obtained on the second time (final output of ESTAR>EOK), the case may be rerun with another input value for FACTOR. Recommended range is greater than 0.2 but less than 2.0. Note: Do not set FACTOR equal to 1.0.

The n^{th} term of the n^{th} guess is multiplied by FACTOR. Do not set FACTOR equal to 1.0 since a singular matrix results.

(2) Note 2: Momentum Coefficient. It is important that the trailing edge momentum vector be properly defined, since (a) its projection into the simple sweep plane is required for iterative determination of EMF size and total circulation and (b) its projection into the pitch plane is required for calculation of residual lift and for calculation of axial force coefficient. The momentum coefficient given in Card 3, Field 6, is the magnitude of the local momentum efflux vector c_μ per unit of physical span (y direction) which leaves the trailing edge, normalized on freestream dynamic pressure and freestream chord. This is the total per unit of span regardless of the direction of the efflux. The jet skew angle ε of Card 4, Field 2 is the angle between the local efflux vector and the simple sweep plane.

The input angles ε, δ_f, δ_j, Λ_{HL} and $\Lambda_{c/4}$ are sufficient for the required resolution. For IBF systems the efflux from slot blowing is substantially in the normal plane; for such cases one should input ε as zero. In this case the pitch plane projection or "turning efficiency" η is a fallout quantity (scrubbing losses are assumed to be accounted for in the input c_μ).

For cases other than the IBF the skew angle ε is a spanwise variable which is generally not well known. The required assumptions concerning efflux spreading are left to the user's experience, his available flow visualization and static force data, and his knowledge of wind-on interactions with static spreading and turning. In general, the input ε and c_μ should, when integrated over the span, be consistent with the input "turning efficiency" η.

(3) Note 3: Spanwise Control Points; Number and Location. The spanwise location of the control points are specified for each number of control points chosen. These are tabulated for quick reference in Table C-1 for four through sixteen control points.

Most powered high lift systems are characterized by sharp breaks in flap chord, flap deflection and momentum distribution. Control point locations should be chosen, wherever possible, to give a more or less balanced recognition to the various segments between these breaks. Best results have been obtained when major segments of the span have approximately the same number of control points. It is also desirable to avoid having control points

located too near sharp breaks. In certain cases it may be desirable to run more than one number of control points and examine the resulting span load distribution.

2. OUTPUT FORMAT

Line 1

TITLE as input

Lines 2 & 3

ALPHA	-	Reference angle of attack, degrees.
BETA	-	Sideslip angle, degrees.
Sweep	-	Sweep angle of the wing one-quarter chord - degrees.
AR	-	Wing aspect ratio.
Span	-	Wing span, dimensional as input.

Lines 4 & 5

CL	-	Wing lift coefficient in the presence of the body.
CL(CIRC)	-	Wing circulation lift coefficient.
CDP	-	Wing/body profile drag coefficient, as input.
CX	-	Wing axial force coefficient.
ETA	-	Turning efficiency, η, projection of resultant efflux momentum into pitch plane and normalized on input total.
CMU	-	Blowing coefficient, C_μ.
CR(ROLL)	-	Wing rolling moment coefficient.

Table 1

ETA	-	Wing station as fraction of semispan.
GAMA/V	-	Wing section circulation non-dimensionalized on freestream velocity

CL*C/CAVG - Wing load distribution parameter (section lift per unit span non-dimensionalized on average wing chord)

ALPHA E - Section effective angle of attack, degrees.

Table 2

X POINT, Y POINT, Z POINT - x, y, z coordinates of downwash, sidewash points, as input.

EPSILON - Downwash angle, degrees.

SIGMA - Sidewash angle, degrees.

3. SAMPLE CASE INPUT & OUTPUT

An initial set of control cards are required by the CDC 6600 computer at Wright-Patterson Air Force Base, Dayton, Ohio. The card deck as supplied by the contractor will compile the source program and save the object deck under the catalog name "HOLMES,CY=4". Once this is completed one must estimate the computer run time in seconds by the following approximate formula:

$$\text{TIME} \sim 7 + 10 * \text{Number of cases},$$

a case being each α,β combination. For the sample case (one α,β combination), TIME $\approx$ 17sec.

The required control cards and input data are shown in Figure C-1. The "SETCORE." card must be used to initialize the core storage to zero. The resulting output is shown in Figure C-2.

NUMBER OF CONTROL POINTS PER SEMISPAN

4	5	6	7	8	9	10
0	0	0	0	0	0	0
0.3827	0.3090	0.2588	0.2225	0.1951	0.1736	0.1564
0.7071	0.5878	0.5000	0.4339	0.3827	0.3420	0.3090
0.9239	0.8090	0.7071	0.6235	0.5556	0.5000	0.4540
	0.9511	0.8660	0.7818	0.7071	0.6428	0.5878
		0.9659	0.9010	0.8315	0.7660	0.7071
			0.9749	0.9239	0.8660	0.8090
				0.9808	0.9397	0.8910
					0.9848	0.9511
						0.9877

TABLE C-1 LOCATIONS OF CONTROL POINTS IN FRACTIONS OF SEMISPAN

(a) Four through Ten Control Points per Semispan

NUMBER OF CONTROL POINTS PER SEMISPAN					
11	12	13	14	15	16
0	0	0	0	0	0
0.1423	0.1305	0.1205	0.1120	0.1045	0.0980
0.2817	0.2588	0.2393	0.2225	0.2079	0.1951
0.4154	0.3827	0.3546	0.3303	0.3090	0.2903
0.5406	0.5000	0.4647	0.4339	0.4067	0.3827
0.6549	0.6088	0.5681	0.5320	0.5000	0.4714
0.7557	0.7071	0.6631	0.6235	0.5878	0.5556
0.8413	0.7934	0.7485	0.7071	0.6691	0.6344
0.9096	0.8660	0.8230	0.7818	0.7431	0.7071
0.9595	0.9239	0.8855	0.8467	0.8090	0.7730
0.9898	0.9659	0.9350	0.9010	0.8660	0.8315
	0.9914	0.9709	0.9439	0.9135	0.8819
		0.9927	0.9749	0.9511	0.9239
			0.9937	0.9781	0.9569
				0.9945	0.9808
					0.9952

TABLE C-1 (Concluded)

(b) Eleven through Sixteen Control Points per Semispan

```
UNIVAC(T17,CM60000)          ACCOUNT,ENGINEER,PHONE
ATTACH(LGO,HOLMES,CY=4)
SETCORE.
LGO.
7/8/9          (OVERPUNCH)
FDL/ARL CHECK CASE , AMES J/H IBF BASELINE, DEL F=30.
 4
0.0         9.405       0           0.1         .307        1.0294      28.5
 0.0 1      0.1         .338        .1228       57.0
15.0        4.796       0.0         0.0         .307        1.0294      28.5
0.00        0.0         .338        .1228       57.
15.01       4.796       0.0         0.0         .307        0.26 8      28.5
0.0         0.0         .3 8        .1228       57.0
21.4475     2.82        0.0         0.0         .307        0.2628      28.5
0.00        0.0         .338        .12 8       57.
5.833       2.91          5.833
.25         .96         0.2         2.0
09 4
26.791      3.769       9.042
24.06       0.0         9.042
24.06       0.          4.296
24.06       0.0         0.
42.895      8.0         27.5        0.0         23.0
4.0         1.0
99.
6/7/8/9/          (OVERPUNCH)
```

Figure C-1. Sample Problem Input

```
 ALPHA=          4.00
ESTAR=   .22[illegible]E+02
ESTAR=   .[illegible]43E+00
ESTAR=   .[illegible]E-02
ITTER=  [illegible]   [illegible]K=     .[illegible]   [illegible]STAR=     .00442
```

FDL/ARL CH CK CASE , [illegible] BASELINE,CEL F=30.

ALPHA	BETA	[illegible]	CF	SPAN
4.00	1.00	27.50	0.00	42.69

CL	CL(CIRC)	CDI	CX	ETA	CMU	CR(ROLL)
3.42290	3.24595	.27000	.26569	.960	1.00970	-.00625

ETA	[illegible]	CL*C/CAVG	ALPHA
-1.00000	0.00000	0.00000	-22.50776
-.80000	6.27428	2.35660	4.17395
-.60000	8.94152	3.45511	-3.65305
-.40000	10.28943	4.02911	-4.15622
-.20000	10.[illegible]	4.31[illegible]	-6.45750
0.00000	10.72532	4.41364	-9.21221
.20000	10.99319	4.41603	-6.71192
.40000	10.46535	4.10217	-4.36017
.60000	9.10130	3.52665	-3.22723
.80000	6.40344	2.38571	3.99322
1.00000	0.00000	0.00000	-22.96396

X POINT	Y POINT	Z POINT	EPSILON	SIGMA
26.74100	3.76900	9.04200	16.90110	2.16517
24.05000	0.00000	9.04200	16.89932	.03930
24.05000	0.00000	4.29600	13.22762	-.34546
24.05000	0.00000	0.00000	13.47046	.57672

Figure C-2. Sample Problem Output

APPENDIX D

COMPUTER PROGRAM LISTING

The original computer program was written in Fortran V for the Univac 1106 DEMAND System. The program listing which follows has been adapted to the CDC 6600 computer at Wright-Patterson Air Force Base.

```
      PROGRAM UNIVAC(INPUT,OUTPUT,TAPE5=INPUT,TAPE6=OUTPUT)
      COMMON NS PAN,B,ALPHAA(35),A(3 ,3 ),C(35),
     1  G(3 ),X(35, 3),ERROR(3 , 3),E(3 ),ALPHAE(3 )
     2 ,ALFAI1(35),YTAB(20),ALPZL(20)
     3 ,NY,CLAM
     5 ,CMUTAB(20),CFOCIN(20),DELFTB(20),DELJTB(20),KWAKE
     6 ,EPSTAB(20),SWE P,LAMHL,BETA,SGAMA,CLOTAB(20)
     7 ,CNOCIN(20),DELNTB(20)
      REAL IwTAB(20),Iw,LB(35,35),LAMHL
      INTEGER BM,BMP1,BMP2
      DIMENSION CTAB(20),          ALFAE1(3 ),ETAII(35),
     1 ETA(40),PHII(3 ),ALPHAI(35),GAMAOV(3 ),
     2 CLCO A(35),CDICOC(35),
     3 ALFAI(3 ),HSTAR(35,3 )
     4 ,PHII2(3 ),PHI(40),FBAR(3 , 3 ),GBAR(3 ,3 ),SUM48(3 )
     5 ,CROLL(3 ),TITLE(10)
     6 ,XPB(20),YPB(20),ZPB(20)
      READ(5,1  2) (TITLE(KK ),K =1,8 )
      READ (5,4) NY
      RAD=57.296
    4 FORMAT (3I2)
      PRINT=0.0
   10 DO 15  I=1,NY,2
      READ(5,26) YTAB(I),CTAB(I),IwTAB(I),ALPZL(I)
     + ,CFOCIN(I),CMUTAB(I),DELFTB(I),DELJTB(I)
     + ,EPSTAB(I),CLOTAB(I),CNO IN(I),DELNTB(I)
      READ(5,26) YTAB(I+1),CTAB(I+1),IwTAB(I+1),ALPZL(I+1)
     + ,CFOCIN(I+1),CMUTAB(I+1),DELFTB(I+1),DELJTB(I+1)
     + ,EPSTAB(I+1),CLOTAB(I+1),CNO IN(I+1),DELNTB(I+1)
   15 CONTINUE
   20 FORMAT (6F10.0)
   25 FORMAT (6F10.0)
   26 FORMAT(7F10.0)
      KWAKE=1
      READ (5,26) DIAB,ZWING,BMAJOR
      READ(5,26) CDOT,ETACMU,DELY,EOKPCT
      IF(EOKPCT.LE.0 0) EOKPCT=1.0
      READ (5,4)  NH,NPTS
      IF(NPTS.LE.0) GO TO 3  4
      DO 3     KP=1,NPTS
      READ(5,20) XPB(KP),YPB(KP),ZPB(KP)
3     CONTINUE
3 4 READ (5,20) B,AR,SWE P,GAMA,LAMHL
      TAPER=CTAB(NY)/CTAB(1)
      SGAM =SIN(GAMA/RAD)
      CAVG=B/AR
   30 READ (5,20) ALPHAB, ETA,FACTOR
      IF(ALPHAB.GE.9 .) GO TO 785
      IF (FACTOR) 6   ,    ,   7
5     FACTOR=0.4
6   7 CONTINUE
   40 FORMAT ('1'     )
```

```
   50  FORMAT(/,14X,'ALPHA       BETA       ',
     + 'SWEEP',
     1 7X,'AR        SPAN')
   60  FORMAT(9X,6F10.2,F8.3,7X,I1)
       PI=3.1415926S
       PGCORR=1.0
       M=2*NB-1
       NSSPAN=2
       BM=M
       MP2=M+2
       MP3=M+3
       BMP1=BM+1
       BMP2=BM+2
       MUZERO=BMP2
       M1=M+1
       NUMU=NB-1
       CLAM=COS(SWEEP/RAD)
       SLAM=SIN(SWEEP/RAD)
       TLAM=SLAM/CLAM
   65  DO 80  NU=1,M
       PHI(NU)=(PI*NU)/(M+1.)
       ETA(NU)=COS(PHI(NU))
       Y=ETA(NU)*B*0.5
       ABSY=ABS(Y)
       CALL BODY(ALPHAB,BETA,DIAB,ZWING,BMAJOR,B,Y,ALFCOB)
       C(NU)=GIRC(ABSY,YTAB,CTAB,NY,1)
       IW=GIRC(ABSY,YTAB,IWTAB,NY,1)
       ALPHA (NU)=(IW+ALPHAB+ALFCOB)/RAD
   80  CONTINUE
       ETA(MUZERO)=1.0
       ETA(BMP1)=-1.0
       PHI(MUZERO)=0.0
       PHI(BMP1)=PI
       DO 40    N=1,M
   84  DO 30    NU=1,M
   85  SUM=0.0
       DO 20    MULOOP=1,BMP2
       MU=MULOOP
       IF (NU-1)  775,84,105
    8  FBAR(N,MU)=0.0
   90  DO 10      MU1=1,M
       FBAR(N,MU)=FBAR(N,MU)+(MU1*SIN(MU1*PHI(N))*COS(MU1*PHI(MU)
     1 *(2./(M+1.))
   10  CONTINUE
  105  IF (N-1) 775,107,130
  107  TWOAM=1.+(B*PGCOR *TLAM*(ABS(ETA(NU) -ETA(MU) /C(NU)
       TWOAP=1.+(B*PGCOR*TLAM*(ABS(ETA(NU)+ETA(MU))/C(NU)
       TWOB=B*PGCOR*(ETA(NU)-ETA(MU))/C(NU)
       TWOC=B*PGCOR *(ETA(NU)+ETA(MU))/C(NU)
       DENOMP=1.+(B*(ABS(ETA(NU))+ETA(NU) *PGCOR)*TLAM)/C(NU)
       DENOMM=1.+(B*(ABS(ETA(NU) -ETA(NU))*PGCOR)*TLAM)/C(NU)
       FOURA=1.+(B*ABS(ETA(NU) *PGCOR)*TLAM)/C(NU)
       FOURB=B*PGCOR*ETA(NU)/C(NU)
       FIVEP=(SQRT(TWOAP* 2)+(TWOB**2) /DENOMP)-1.0
```

```
      FIVEM=(SQRT((TWOAM**2)+(TWOB**2) /DENOMM)-1.0
      SIX=2.0*TLAM*SQRT((FOURA** 2)+(FOURB**2))/(DENOMM*DENOMP)
      IF(ETA(MU)  1 0,120,120
  110 IF(MU-NU) 1 5,1 8,1 5
  115 THRE=1./(B*(ETA(NU)-ETA(MU))*PGCOR/C(NU))
      HSTAR(NU,MU)=THRE *FIVEP+SIX
      GO TO 130
  118 HSTAR(NU,NU)=-TLAM+SIX
      GO TO 130
  120 IF(MU-NU) 125,128,125
  125 THRE=1./(B*(ETA(NU)-ETA(MU))*PGCOR/C(NU)
      HSTAR(NU,MU)=THRE*FIVEM
      GO TO 130
  128 HSTAR(NU,NU)=TLAM
C
C      ETA BAR= ETA .GE. ZERO
C
  130 CONTINUE
      IF(MU-BM)180,180,20
  180 SUM=(-1./(2.*(BM+1)) *(FBAR(N,MU)*HSTAR(NU,MU))+SUM
  200 CONTINUE
      GBAR(NU,N)=(-1./(2.*(BM+1)))*((FBAR(N,MUZERO)*HSTAR(NU,MUZERO)
     +  +FBAR(N,BMP1)*HSTAR(NU,BMP1) /2.0)+SUM
   30 CONTINUE
   40 CONTINUE
      DO 60   NU=1,M
      DO 405 N=1,M
      LB(NU,N)=0.0
      DO 402 MU1=1,M
      LB(NU,N)=LB(NU,N)+MU1*SIN(MU1*PHI(NU))*SIN(MU1*PHI(N))/( M+1.)
     1 *SIN(PHI(NU)  *(2.)
  402 CONTINUE
  405 CONTINUE
      DO 50   N =1,M
  430 A(NU,N)=LB(NU,N)+GBAR(NU,N)*B*PGCOR/C(NU)
   50 CONTINUE
      A(NU,NP1)=A(NU,NU)-B/(C(NU)*CLAM*PI)
   60 CONTINUE
      IF (PRINT) 79  ,7980,7979
 7979 WRITE(6,6969) ( NU,N,A(NU,N),N=1,M),NU=1,M)
 6969 FORMAT(4 * A(',I1,',  ,I1,')=',F10.5)
      WRITE(6, 973) ( N,MU,FBAR(N,MU),N=1,M),MU=1,MP2)
      WRITE(6,6974) ( NU,MU,HSTAR(NU,MU),NU=1,M),MU=1,MP2)
 6973 FORMAT(4(' FBAR(',I1,',',I1,')=',F10.5))
 6974 FORMAT(4(' HSTAR(',I1,',',I1,')=',F10.5)
      WRITE(6,6979) ( NU,N,LB(NU,N),NU=1,M, N=1,M)
 6979 FORMAT(4(' LB(',I1,',',I1,')=',F8.5)
      WRITE(6,6972) ((NU,N,GBAR(NU,N),NU=1,M),N=1,M)
 6971 FORMAT(4(' B(',I1,',',I1,')=',F8.5))
 6972 FORMAT(4(' GBAR(',I1,',',I1,')=',F8.5)
 7980 CONTINUE
      EOK=ABS(EOKPCT/10 .*ALPHAB)
      IF(EOK.LT..0 5) EOK=.005
      LINE=1
```

```
      WRITE(6,7982) ALPHAB
 7982 FORMAT('1 ALPHA=',F10.2)
      CAL  GUES(N ,FACTOR,LINE)
      CALL SOLVE(NU,EOK,ITTER,ESTAR,FACTOR)
      WRITE(6,910) ITTER,EOK,ESTAR
  910 FORMAT(1X,'IT ER=',I3,'  EOK=',F10.5,'  ESTAR=',F10.5)
      DO 920 I=1,M
      DALFE=ALPHAE(I)*RAD
      CL1=2.*B*G(I)/C(I)
      DALFA=ALPHA (I)*RAD
  920 IF(PRINT.GT.0.0) WRITE(6,925) ETA(I),DALFE,CL1,DALFA
  925 FORMAT(1X,4F10.5)
      WRITE(6,40)
      WRITE(6,1 1 ) (TITLE(K K),K =1, 8)
  11  FORMAT(/,1X, 8A10)
  1 2 FORMAT(8A10)
      WRITE(6,50)
      WRITE(6,50) ALPHAB, ETA,SWELP,AR,B
 1050 CONTINUE
      SUM48T=0.
      DO 1200 NU=1,M
      SUM48(NU)=0.
      DO 1180 N=1,M
      SUM48(NU)=SUM48(NU)+LB(NU,N)*G(N)/2.0
 1180 CONTINUE
      SUM48T=SUM48T+G(NU)*SUM48(NU)*SIN(PHI(NU)
  120 CONTINUE
      CDI921=(PI*B/CAVG)/(M+1)*SUM48T
 1250 DO 130  I=1,M
      MP2MI=MP2-I
      IP1=I+1
      PHI (IP1)=PHI(I)
      PHI2(I)=PHI(I)
      ETA (IP1)=-ETA(I)
      Y=ETA(I)*B*.5
      ABSY=ABS(Y)
      CMU=GIRC(ABSY,YTAB,CMUTAB,NY,1)
      AE=AE/CLAM
      GAMAOV(IP1)=G(I)*B
      COO=0.
      ALPHAI(I)=SUM48(I)
      CL=(2.0*B*G(I)) /C(I)
      EPS=GIRC(Y,YTAB,EPSTAB,NY,1)
      RLAM=COS( SWE P-LAMHL)/RAD)/COS(LAMHL/RAD)
      DELFS=GIRC(Y,YTAB,DELFTB,NY,1)
      DELF=ATAN( AN(DELFS/RAD)*RLAM)*RAD
      DELJS=GIRC( ,YTAB,DELJTB,NY,1)
      DELJ=ATAN(TAN( DELFS+DELJS)/RAD)*RLAM)*RAD-DELF
      CUPOCU=1.0-(SIN( EPS-LAMHL)/RAD)+COS(EPS/RAD)*SIN(LAMHL/RAD)
     1  *(1.0-COS( DELF+DELJ)/RAD)  * 2
      CMUP=CUPOCU*CMU
      CL( A(IP1)=(CL+CMUP*SIN( RAKE)*(ALPHA (I)-ALPHAE(I)   *C(I)
     1  /CAVG
      CROL (IP1)=(-CL*C(I)/CAVG)*Y/B
```

```
      CDICOC IP1)=CLCOCA(IP1)*SIN(ALPHAA(I)-ALPHAE(I)
      CM=0.)
      ALFAE1(I)=ALPHAE(I)
      ALFAI(I)=ALFAI1(I)
  130 CONTINUE
      CLCOCA(MP2)=0.0
      CROLL(MP2)=0.0
      CDICOC(MP2)=0.
      GAMAOV(MP2)=0.0
      PHII(MP2)=PI
      ETAII(MP2)=1.0
      CLCOCA(1)=0.0
      CROLL(1)=0.0
      CDICOC(1)=0.0
      GAMAOV(1)=0
      ETAII(1)=-1.0
      PHII(1)=0.
C     WRITE(6,7777) (KK,PHII(KK),KK=1,BMP2)
C     WRITE(6,7778) (KKK,ETAII(KKK),KK=1,BMP2)
C     WRITE(6,7779) (KKK,CLCOCA(KK),KK=1,BMP2)
   77 FORMAT(4(' PHII(',I2,')=',F10.5))
 7778 FORMAT(4(' ETAII(',I2,')=',F10.5)
 7779 FORMAT(4(' CLCOCA(',I2,')=',F10.5)
      CMUT=0.)
      DO 1305 KU=2,NY
      KUM1=KU-1
      CMUT=CMUT+(CMUTAB(KUM1)*CTAB(KUM1)+CMUTAB(KU)*CTAB(KU) *
     1 (YTAB(KU)-YTAB(KUM1))/(B*CAVG)
 1305 CONTINUE
      CLT=QTAB(ETAII,CLCOCA,1,MP2)/2.0
      CROLLT=QTAB(ETAII,CROLL,1,MP2)/2.0
      CDIT=QTAB(ETAII,CDICOC,1,MP2)/2.0
      SUM46=0.0
      DO 1310 N=1,M
      SUM46=G(N)*SIN(PHI(N))+SUM46
 1310 CONTINUE
      CL921=(PI*B)/(CAVG*(M+1))*(SUM46)
C
C     CX  ALCULATION PER L. BARNETT
      EGAMA=CL921**2/(PI*AR*CDI921)
      A1=4.*CL921/(PI*CLCOCA(N))
      XKBAR=4./(PI*2)
      G 1=1.0-(EGAMA*XKBAR/(4.*A1**2)
      G 2=1.0+(2.*ETACMU*CMUT*XKBAR*G 1/(PI*AR*A1**2))
      G 3=CLT**2/(PI*AR*EGAMA*G 2)
      CXT=ETACMU*CMUT-CDOT-G 3
C
      WRITE(6,710)
  710 FORMAT (/,1X,'     CL       CL(CIRC)     CDP',
     1       '          CX           ETA       CMU       CR(ROLL)')
  720 WRITE(6,730) CLT, L921,CDOT,CXT,ETACMU,CMUT,CROLLT
  730 FORMAT(1X,6F10.5,F8.3,2X,2F10.5)
  740 WRITE(6,750)
```

```
  750 FORMAT (/,5X,'   ETA            GAMA/V        CL*C/CAVG',
     2 '     ALPHA E')
      OUT=0.0
      ABSBET=ABS(BETA)
      DO 7 2  I=1,20
      YW=-1.0+DELY*(I-1)
      IF(ABSBET.LE. 001) YW=0.0+DELY*(I-1)
      CHECK=1.-YW
      IF (CHECK)  775,756,75
  756 OUT=1.0
      YW=1.0
      YWPHI=0.0
      GO TO 1759
  757  IF (YW) 759,758,759
  758  YWPHI=PI/2.0
      GO TO 1759
  759  IF(YW+1) 775,1756,1758
 1756 YWPHI=PI
      GO TO 1759
 1758 YWPHI=ACOS(YW)
 1759 GAMAW=GIRC(YWPHI,PHII,GAMAOV,MP2,1)
C     WRITE(6,925),YW,YWPHI
      CLW=GIRC(YWPHI,PHII,CLCOCA,MP2,2)
      CDIW=GIRC(YWPHI,PHII,CDICOC,MP2,2)
      ALPW=GIRC(YWPHI,PHII2,ALPHAI,M,2)*RAD
      CMW=GIRC(YWPHI,PHII,CMCOC ,MP2,2)
      ALPE=GIRC(YWPHI,PHII2,ALFAE1,M,2)*RAD
      TEMP5=GIRC(YWPHI,PHII2,ALFAI,M 2)*RAD
  760 WRITE(6,7 0) YW,GAMAW,CLW,ALPE
  770 FORMAT (5X,1F10.5,3X,1F 0.5,3X,1F10.5,3X,1F10.5,3X,
     1 F10.5)
      IF  (OUT)  772,772,7 5
  772 CONTINUE
  7 5 IF(NPTS) 782,782,781
  781 CAL  FIELD(N ,NPTS,B,ALPHAB, ETA,SWE P,GAM,
     1 ,PHII,GAMAOV,XPB,YPB,ZPB,MP2)
  782 IF(N -16) 30,3 ,783
  783 STOP
      END
```

```
      SUBROUTINE GUESS(NS,FACTOR,LINE)
      COMMON NS,PAN,B,ALPHAA(3 ),A(35,3 ),C(3 ),
     1 SKIP(3 ),X(35,35),ERROR(35, 5),E(3 ),XSET(3 )
     2 ,SKIP2(35),YTAB(20),ALPZL(20)
     3 ,NY,CLAM
      DIMENSION TEMP(3 , 5),G(5 ),ERRSET(3 ),TEMALF(35)
      RAD=57.296
      PI=3.14159265
      NCP=NS
      M=2*NS -1
      IF(NS PAN.EQ.2) NCP=M
      NCP1=NCP+1
      IF (LINE-2) 40,2.5, 0
C
C     THIS PORTION COMPUTES A LINEAR SOLUTION FOR A FIRST GUESS
C
 40   DO 150 I=1,NCP
      Y=ABS( *.5*COS(PI*I/(M+1)
      ALFLO=GIPC(Y,YTAB,ALPZL,NY,1)
      TEMALF(I)=ALPHAA(I)-ALFLO/RAD
      DO 100 J=1,NCP
      IF(I-J) 50,60,50
 50   TEMP(I,J)=A(I,J)
      GO TO 100
 60   TEMP(I,I)=A(I,I)+B/(C(I)*PI*CLAM)
100   CONTINUE
150   CONTINUE
      CALL GJRV(TEMP,NCP,35 ,0.0   1,IER )
      IF(IER ) 160,170,170
160   WRITE(6,165) IER
165   FORMAT(1X,'IER =',I2,' IN INVERSION FOR LINEAR SOLUTION')
 170  CALL MATMPY(TEMP,TEMALF,G,NCP, NCP,1,35 ,5 )
      DO 20  I=1,NCP
      X(I,1)=B*G(I)/(C(I)*PI*CLAM)+ALFLO/RAD
      XSET(I)=X(I,1)
C     WRITE(6,180) I,X(I,1)
C180  FORMAT(1X,'I=',I2,'   X(I,1)=',F10.5)
 20   ERROR(1,I)=1.0
      XNCP=NCP
      ERROR(1,NCP+1)=1.0
      CALL CALC(NS ,ERR SET, (1))
      XSUM=0.0
      DO 210 I=2,NCP-1
      IM1=I-1
      ERROR(I,1)=ERRSET(IM1)
210   CONTINUE
C
C     THIS PORTION MAKES NCP MORE GUESSES BASED ON FIRST GUESS
C
 250  DO 30  J=2,NCP-1
      DO 250 I=1,NCP
      IF(J-NCP+1) 240,230,230
230   IF(I-1) 235,235,240
235   X(I,J)=FACTOR*X(I,1)
```

```
      GO TO 248
240   IF(J-I) 245,235:245
245   X(I,J)=X(I,1)
248   XSET(I)=X(I,J)



250   CONTINUE
      CALL CALC(NS',ERRSET,E(J))
      DO 260 I=2,NCPP1
      IM1=I-1
      ERROR(I,J)=ERRSET(IM1)
260   CONTINUE
300   CONTINUE
 50   RETURN
      END
```

```
      SUBROUTINE BODY(ALPHAB,BETA,DIAB,ZWING,BMAJOR,B,Y,ALFCOB)
      IF(DIAB) 50,5 ,25
   25 IF(BMAJOR) 30,30,26
   26 IF(BMAJOR-DIAB) 60,30,60
C
C     CIRCULAR BODY CALCULATIONS
C
   30 TEST=Y**2+ZWING**2-(DIAB/2.0)** 2
      IF(TEST) 50,3 ,35
   35 ETABOD=2.0*Y/B
      ANUM=(ETABOD*B/DIAB)** 2-(ZWING*2./DIAB)**2
      ADEN=( ETABOD*B/DIAB)**2-(ZWING*2./DIAB)**2)** 2
     +  +4.0*(ETABOD*(B/DIAB)*(ZWING*2.0/DIAB))**2
      BNUM=8.0*ZWING*Y/(DIAB** 2)
      BDEN=(4.0*((ZWING/DIAB)**2+(Y/DIAB)**2)** 2
      ALFCOB=(ANUM/ADEN)*ALPHAB+(BNUM/BDEN)*BETA
      GO TO 10
C
C     NO BODY, RETURN WITH ZERO ALPHA EF ECT.
C
   50 ALFCOB=0.0
      GO TO 10
C
C     EL IPTIC BODY CALCULATIONS
C       BMAJOR (VERTICAL), DIAB (HORIZONTAL)
C
   60 A1=DIAB/2.0
      B1=BMAJOR/2.0
      A2=((B1/A1)**2-1.0)/4.0
      R2=( B1/A1)+1.0)/2.0)**2
      TETA=ZWING/A1
      TPSI=Y/A1
      TEST=(Y/A1)**2+(ZWING/B1)**2-1.0
      IF(TEST) 62,63,63
   62 ALFCOB=0.
      GO TO 10
   63 IT=0
```

```
  648  DO 75 I=1,80
       IT=IT+1
       ETA=TETA
       PSI=TPSI
       TPSI=Y/A1+((A2*PSI)/( PSI)**2+(ETA)**2))
       TETA=ZWING/A1-((A2*ETA)/(PSI**2+ETA**2)
       IF(ABS(ETA-TETA)-.0 01) 65,,,,7)
   65  IF(ABS(PSI-TPSI)-.00 1) 80,80,75
   75  CONTINUE
   80  CONTINUE
C      WRITE(6,,99) IT,Y,ETA,TETA,PSI,TPSI
       ETA=TETA
       PSI=TPSI
C69)   FORMAT(1X,I4,6F10.5)
       BNUM=(R2+A2)*.*PSI*ETA
       BDEN=(PSI* 2-(ETA* 2)+A.')* 2+(4.*(PSI*2)*(ETA**2))
       ANUM1=(PSI**2+ETA**2)**2+(PSI* 2-ETA* 2)*(R2+A2)*R2*A2
       ADEN1=(PSI* 2-ETA**2+A )**2+4.*(PSI* 2)*(ETA* 2)
       ALFCOB=((ANUM1/ADEN1)-1.0)*ALPHA8+(BNUM/BDEN)*BETA
   10  RETURN
       END
```

```
      SUBROUTINE GJRV(A,N,NL,EPSIL,IERR)
C     A IS INPUT ARRAY WHICH WILL BE DESTROYED
C     N IS DIMENSION OF A
C     EPSIL IS TEST VALUE FOR PIVOT
C     IERR IS VALUE RETURNED IF PIVOT IS TOO SMALL
      DIMENSION A(1),B(128),C(128),IP(128),IQ(128)
      IERR=0
      DO 140 K=1,N
      PIVOT=0.0
C     GET LARGEST ELEMENT IN MATRIX PLACE IT IN PIVOT
      DO 120 I=K,N
      DO 2 J=K,N
      IDEX=(J-1)*NL+I
      IF(ABS(A(IDEX))-ABS(PIVOT))2,2,1
1     CONTINUE
      PIVOT=A(IDEX)
      IP(K)=I
      IQ(K)=J
2     CONTINUE
120   CONTINUE
      IF(ABS(PIVOT)-EPSIL)100,100,3
3     CONTINUE
      IF(IP(K)-K)4,5,4
4     CONTINUE
C     SWAP ROWS
      DO 6 J=1,N
      IPX=IP(K)
      IDEX=(J-1)*NL+IPX
      KDEX=(J-1)*NL+K
      Z=A(IDEX)
      A(IDEX)=A(KDEX)
      A(KDEX)=Z
5     CONTINUE
6     CONTINUE
      IF(IQ(K)-K)7,9,7
7     CONTINUE
C     SWAP COLUMNS
      DO 8 I=1,N
      IPX=IQ(K)
      IDEX=(IPX-1)*NL+I
      KDEX=(K-1)*NL+I
      Z=A(IDEX)
      A(IDEX)=A(KDEX)
      A(KDEX)=Z
8     CONTINUE
9     CONTINUE
      DO 13 J=1,N
      KDEX=(J-1)*NL+K
      JDEX=(K-1)*NL+J
      IF(J-K)11,10,11
10    CONTINUE
      B(J)=1./PIVOT
      C(J)=1.
      GO TO 12
```

```
11      CONTINUE
        B(J)=-A(KDEX)/PIVOT
        C(J)=A(JDEX)
12      CONTINUE
        A(KDEX)=0.0
        A(JDEX)=0.0
13      CONTINUE
        DO 14 I=1,N
        DO 14 J=1,N
        IDEX=(J-1)*NL+I
        A(IDEX)=A(IDEX)+C(I)*B(J)
14      CONTINUE
140     CONTINUE
        DO 20 KP=1,N
        K=N+1-KP
        IF(IP(K)-K)15,17,15
15      CONTINUE
        DO 16 I=1,N
        IPX=IP(K)
        IDEX=(IPX-1)*NL+I
        KDEX=(K-1)*NL+I
        Z=A(IDEX)
        A(IDEX)=A(KDEX)
        A(KDEX)=Z
16      CONTINUE
17      CONTINUE
        IF(ID(K)-K)18,20,18
18      CONTINUE
        DO 19 J=1,N
        IPX=ID(K)
        IDEX=(J-1)*NL+IPX
        KDEX=(J-1)*NL+K
        Z=A(IDEX)
        A(IDEX)=A(KDEX)
        A(KDEX)=Z
19      CONTINUE
20      CONTINUE
        GO TO 21
100     CONTINUE
        IERR=-1
21      CONTINUE
        RETURN
        END
```

```
      FUNCTION CIRC(ARG,X,Y,NX,IC)
C     AITKIN INTERPOLATION
C     ARG=INDEPENDENT ARGUMENT
C     X=INDEPENDENT TABLE
C     Y=DEPENDENT TABLE
C     NX=NUMBER VALUES X TABLE
C     IC=1 FIRST ORDER INTERPOLATION
C     IC=2 SECOND ORDER INTERPOLATION
      DIMENSION X(1),Y(1),XX(4),YY(4),DD(3),FF(3)
      IEND=NX-IC+1
      IF(X(1)-X(2))10,20,20
C     ASCENDING ORDER
 10   DO 15 I=1,IEND
      IF(X(I)-ARG)15,30,30
 15   CONTINUE
 18   I=NX-IC
      IEX=0
      GO TO 45
 20   DO 25 I=1,IEND
      IF(X(I)-ARG)30,30,25
 25   CONTINUE
      GO TO 18
 30   IF(IC-1)35,35,40
 35   IF(I-1)36,36,37
 36   I=1
      GO TO 45
 37   I=I-IC
      GO TO 45
 40   IF(I-2)41,41,42
 41   IEX=0
      GO TO 35
 42   IEX=1
      GO TO 37
 45   DO 50 I=1,4
      XX(I)=X(I3)-ARG
      YY(I)=Y(I3)
 50   I3=I3+1
      DO 60 I=1,3
 60   DD(I)=XX(I+1)-YY(I)
      DO 70 I=1,2
 70   FF(I)=DD(I)*DD(I+1)
      DO 80 I=1,3
      DD(I)=(YY(I)*XX(I+1)-YY(I+1)*XX(I))/DD(I)
      IF(IC-1)100,100,80
 80   CONTINUE
      DO 90 I=1,2
 90   DD(I)=(XX(I+2)*DD(I)-YY(I)*DD(I+1))/FF(I)
      IF(IEX)100,100,95
 95   DD(1)=(DD(1)+DD(2))/2.
100   SIRC=DD(1)
      RETURN
      END
```

```
      SUBROUTINE MATMPY(PRE,POST,PROD, I,J,K, MPR,MPC,MPO)
      DIMENSION PRE(1),  POST(1),  PROD(1)
      DOUBLE PRECISION DUMMY
C     PRE--- PRE-MULTIPLIER
C     POST-- POST-MULTIPLIER
C     PROD-- PRODUCT MATRIX
C     I    -- NUMBER OF ROWS IN PRE  (NUMBER OF ROWS IN PROD)
C     J    -- NUMBER OF COLS IN PRE  (NUMBER OF ROWS IN POST)
C     K    -- NUMBER OF COLS IN POST  (NUMBER OF COLS IN POST)
C     MPR -- ROW DIMENSION OF PRE  (FIRST SUBSCRIPT)
C     MPC -- ROW DIMENSION OF POST  (FIRST SUBSCRIPT)
C     MPO -- ROW DIMENSION OF PROD  (FIRST SUBSCRIPT)
      DO 10 L=1,K
      LPART=MPO*L-MPO
      LPORT=MPC*(L-1)
COMPUTE PRODUCT BY COLUMNS FROM SUMMATION OF PRODUCTS
C     OF ROW-PRE AND COLUMN-POST ELEMENTS.
      DO 10 M=1,I
      JPART=LPORT
      IPART=M
      LPART=LPART+1
      DUMMY=0.0D0
      DO 9  N=1,J
      JPART=JPART+1
      DUMMY       =PRE(IPART)*POST(JPART)+DUMMY
 9    IPART=IPART+MPR
 10   PROD(LPART)=DUMMY
      RETURN
      END
```

```
C GTAB     INTEGRATION ROUTINE.
C CALLING SEQUENCE
C      ANS=GTAB(X,FX,I,J)
C X IS A TABLE OF VALUES OF THE ARGUMENT, FX IS THE TABLE OF VALUES
C OF THE FUNCTION. FX(I) = F(X(I)). THE INTEGRATION IS FROM X(I)
C TO X(J).
C A PARABOLA IS FITTED TO THE POINTS (BY THREES). THE AREAS RESULTING
C ARE SUMMED.
C
      FUNCTIONGTAB(X,FX,I,J)
      DIMENSIONX(1),FX(1)
      SUM=0.
      M=J-I-1
      IF(M)5,4,2
 2    L=J-2
      DO3K=I,L,2
      T1=FX(K+1)-FX(K)
      T2=X(K+1)-X(K)
      T3=X(K+2)-X(K)
      T4=X(K+2)-X(K+1)
      A1=T1/T2
      A2=(FX(K+2)-FX(K)-A1*T3)/(T3*T4)
      C2=(A1-A2*(X(K)+X(K+1)))/2.
      C3=FX(K)-A1*X(K)+A2*X(K)*X(K+1)
      XO2=X(K)**2
      X22=X(K+2)**2
      XO3=XO2*X(K)
      X23=X22*X(K+2)
 3    SUM=SUM+(A2*(X23-XO3)/3.+C2*(X22-XO2)+C3*(X(K+2)-X(K)))
      IF(MOD(M,2)) 3,4,5
 4    SUM=SUM+((X(J)-X(J-1))*(FX(J)+FX(J-1))/2.)
 5    GTAB=SUM
      RETURN
      END
```

```
      SUBROUTINE SOLVE(NS,EOK,ITTER,ESTAR,FACTOR)
      COMMON NSPAN,B ,SKIP(1 8),X(3 ,33),ERROR(3 ,3 ),E( ,3),XSTAR(3 )
      DIMENSION ERRSTR(3 ),B(3 ,3 ),UNITY(3 ,3 ),DXSTAR(3 ),DERRST(3 )
      ITTER=1
      NTRY=1
      NCP=NS
      M=2*NS -1
      IF(NSPAN.EQ.2) NCP=M
      NCPP1=NCP+1
      RAD=57.296
5     CONTINUE
      DO 150 J=1,NCPP1
      DO 10  K=1,NCPP1
      B(J,K)=ERROR (J,K)
10    CONTINUE
150   CONTINUE
      CALL GJRV(B,NCP 1,3 ,.0    1,IER)
      IF(IER ) 160,170,160
160   WRITE(6,165) IER
165   FORMAT(1X,'IER =',I4,'FROM GJRV MATRIX INVERSION')
      IF(IT ER-10 ) 950,164,164
 164  DO 60 I=1,NCP
60    WRITE(6, 1) (X(I,J),J=1,NCPP1)
61    FORMAT(1X,'X(I,J)',10E1 .4)
      WRITE(6, 2) (E(I),I=1,NCP 1)
62    FORMAT(1X,'E(I)',10E  .4)
      DO 70 I=1,NCPP1
70    WRITE(6,71) (ER OR(I,J),J=1,NCPP1)
71    FORMAT(1X,'ERROR(I,J)',10E .4)
      CAL  MATMPY(ER OR,B,UNITY,NCP 1,NCPP1,NCP 1,3 ,3 ,3 )
      DO 16  I=1,NCP 1
16    WRITE(6,167) (UNITY(I,J),J=1,NCP 1)
167   FORMAT(1X,'UNITY(I,J)',10E  .4)
      DO 168 I=1,NCP 1
168   WRITE(6,169) (B I,J),J=1,NCP 1)
169   FORMAT(1X,'BINV(I,J)',10E1 .4)
      GO TO 950
170   DO 30  II=1,NCP
      SUM=0.
      DO 20  JJ=1,NCPP1
      SUM=SUM+X(II,JJ)*B(JJ,1)
20    CONTINUE
      XSTAR(II)=SUM
      DXSTAR(II)=XSTAR(II)*RAD
30    CONTINUE
320   FORMAT(1X,'XSTAR',10E .4)
      CAL  CALL(NS ,ERRSTR,ESTAR)
      DO 325 I=1,NCP
      DERRST(I)=ERRSTR(I)*RAD
 325  CONTINUE
3 0   FORMAT(1X,'ERRST',10E1 .4)
      WRITE(6,391) ESTAR
390   FORMAT(1X,'ESTAR=',E14.7,/ )
```

```
391    FORMA (1X,'ESTAR=',E14.7)
       IF(ESTAR-EOK) 400,4  ,5
400    GO TO 1000
500    EMAX=E(1)
       NEXCH=1
       DO 70  K=2,NCPP1
       IF(EMAX-E(K)) 600,7  ,70
60     NEXCH=K
       EMAX=E(K)
700    CONTINUE
       EMIN=E(1)
       NMIN=1
       DO 725 K=2,NCPP1
       IF (EMIN-E(K)  725,725,71
 715   EMIN=E(K)
       NMIN=K
 725   CONTINUE
       IF(EMAX-ESTAR) 750,760,80
750    WRITE(6,75 ) ESTAR,EMAX
75     FORMAT(1X,'ESTAR=',F8.4,' IS GREATER THAN EMAX=',F8.4)
       GO TO 950
760    WRITE(6,765) EMAX
765    FORMAT(1X,'ESTAR IS EQUAL TO EMAX=',F8.4)
       GO TO 950
80     DO 850 II=1,NCP
       X(II,NEXCH)=XSTAR(I )
850    CONTINUE
       DO 90  JJ=2,NCPP1
       J M1=J -1
       ER OR(JJ,NEXCH)=ERRSTR(JJM1)
90     CONTINUE
       E(NEXCH)=ESTAR
       IT ER=ITTER+1
       GO TO 50
 950   WRITE(6,960) E(NMIN),EOK
 960   FORMAT(' MIN RMS ER O =',F10.5,'    EOK=',F10.5)
 962   K  =2
       IF(NTRY.EQ.2) KRR=1
       IF (K  ) 962,962,968
 967   FORMAT(1I1)
 968   GO TO ( 980,969, [illegible] ,962, [illegible] ) ,K
C
C      K  =2   WE  ILL CAL  GUES  AGAIN USING  THE  MIN CASE
C
 96    DO 971 I =1,NCP
       I P1=I +1
       X(I +1)=X(I ,NMIN)
       ER OR(I P1,  )=ER OR(I P1,NMIN)
 971   CONTINUE
       E(1)=E(NMIN)
       FACTOR=0.8
       NTRY=2
       CAL  GUES INS ,FACTOR,2)
       GO TO 50
```

```
C
C       KKK=1     WE WANT TO PRINT OUT MIN ERROR SOLUTION.
C
  980 DO 982 II=1,NCP
      XSTAR(II)=X(II,NMIN)
  982 CONTINUE
      CALL CALC (NSS,ERRSTR,ESTAR)
      GO TO 10
C
C       KKK=3  PRINTOUT MIN X AND ERROR SOLUTION.
C
  990 DO 994 II=1,NCP
      IIP1=II+1
      DXSTAR(II)=X(II,NMIN)*RAD
      DERRST(II)=ERROR(IIP1,NMIN)*RAD
  994 CONTINUE
      WRITE(6,320) (DXSTAR(I),I=1,NCP)
      WRITE(6,330) (DERRST(I),I=1,NCP)
      WRITE(6,390) E(NMIN)
      GO TO 902
C
C       KKK=4 CHANGE ONE OF THE MIN X VALUES.
C
 1000 WRITE (6,1010)
 1010 FORMAT(' TYPE (I2,F10.) NO. AND NEW VALUE FOR X.')
      READ(5,1015) IN,XNEW
      IF (IN-NCP) 1017,1017,1020
 1015 FORMAT(I2,F10.)
 1017 X(IN,NMIN)=XNEW/RAD
      DO 1120 I=1,NCP
      XSTAR(II)=X(I,NMIN)
 1120 CONTINUE
      CALL CALL (NSS,ERRSTR,ESTAR)
      E(NMIN)=ESTAR
      DO 1125 II=1,NCP
      IIP1=II+1
      ERROR(IIP1,NMIN)=ERRST(II)
      DXSTAR(II)=XSTAR(I )*RAD
      DERRST(II)=ERRST(I )*RAD
 1125 CONTINUE
      WRITE(6,320) (DXSTAR(I),I=1,NCP)
      WRITE(6,330) (DERRST(I),I=1,NCP)
      WRITE(6,390) E(NMIN)
      GO TO 902
 1020 RETURN
      END
```

```
      SUBROUTINE CAL (NS ,ER SET,RMSER )
      COMMON NS ,PAN,B,ALPHAA(35),A(3 ,3 ),C(35),
     1 G(3 ),X(3 ,3 ),ERROR(35, 5),E(35),XSET(3 )
     2 ,ALPHAI(35),YTAB(20),
     3 ALPZL(20),NY,CLAM
     5 ,CMUTAB(20),CFOCIN(20),DELFTB(20),DELJTB(20),KWAKE
     6 ,EPSTAB(20),LAM,LAMHL,BETA,SGAM ,CLOTAB(20)
     7 ,CNOCIN(20),DELNTB(20)
      DIMENSION ER SET(35)
      REAL LAM,LAMHL
      PI=3.14 5926
      RAD=57.296
      SBETA=SIN(BETA/RAD)
      NCP=NS
      M=2*NS -1
      IF(NS PAN.EQ.2) NCP=M
      THETA=(LAM-BETA)/RAD
      FLIP=1.0
      DO 10  I=1,NCP
      Y=ABS(0*.5*COS(PI*I/(M+1)
      IF(I.GT.NS ) THETA=(LAM+BETA)/RAD
      IF(I.GT.NS ) FLIP=-1.0
      IF(I.EQ.NS ) THETA=LAM/RAD
      IF(I.EQ.NS ) FLIP=0.
      CTHETA=COS(THETA)
      EPS=GIRC(Y, YTAB,EPSTAB,NY,1)/RAD
      CMU=GIRC(Y, YTAB,CMUTAB,NY 1)*COS(EPS)/(CTHETA* 2)
      PLAM=COS( LAM-LAMHL)/RAD)/COS(LAMHL/RAD)
      CFOC=GIRC(Y,YTAB,CFOCIN,NY,1)
      CNOC=GIRC(Y, YTAB,CNOCIN,NY,1)
      DELFS=GIRC(Y, YTAB,DELFTB,NY,1)
      DELF=ATAN(TAN(DELFS/RAD)*PLAM)*RAD
      DELN=GIRC(Y,YTAB,DELNTB,NY,1)
      DELN=AT N(TAN(DELN/RAD)/CLAM)*RAD
      DELJS=GIRC(Y,YTAB,DELJTB,NY,1)
      DELJ=AT N(TAN( DELFS+DELJS)/RAD)*PLAM)*RAD- FLP
      CLO=GIRC(Y, YTAB,CLOTAB,NY,1)
      AE=( XSET(I)*RAD+FLIP*BETA+SGAM )/CTHETA)
      ALPI=( ALPHA (I)+FLIP*BETA+SGAM )/CTHETA)-AE
      CAL  MACKET(KWAKE,CFOC,DELF,CNOC,DELN,AE,ALPI,CMU,DELJ,
     ! DELALF,COEF)
C
C       CL IS CIRCULATION LIFT ONLY
C
    7) CL=CLO+2.0*PI*( 1./CO P)*AE/(180+ ELALF)
      G(I)=CL*(CTHETA* 2)*C(I)*0.5/3
 1)   CONTINUE
      CAL  MATMPY(A,G ALPHAI,NCP,NCP,1,3 ,  , )
      DO 20  I=1,NCP
      ER SET(I )=(XSET(I)-ALPHA (I))+ALPHAI(I ) *57.296
 2)   CONTINUE
      SUM=0.0
      DO 30  I=1,NCP
```

```
300   SUM=SUM+ERRSET(II)* 2
      XNCP=NCP
      RMSERR=(SQRT(SUM/XNCP))*RAD
400   RETURN
      END
```

```
      SUBROUTINE HACKET(KWAKE,CFOC,DELF,CNOC,DELN,ALPE,ALPI,CMU,DELJ,
     1 DELALF,COCP)
C     EQUIVALENT JET-FLAP PROGRAM USING CLOSED FORM SOLUTION
C      OF JACOBS EQUATION.
C     INPUT*
C     CF IS PHYSICAL T.E. FLAP CHORD (POSITIVE)
C     DELF IS T.E.FLAP ANGLE, W.R.T  CHORD, DEGREES NOSE DOWN
C     ALPE IS EFFECTIVE INCIDENCE RELATIVE TO CHORDLINE C
C     CMU IS FLAP BLOWING MOMENTUM COEFFICIENT, BASED ON
C     PHYSICAL CHORD C
C     DELJ IS ANGLE BETWEEN FLAP CHORD AND JET
      DIMENSION A(4),PSI1(4),F(4)
      ALFDEL(X)=2.0/3.14159*(SQRT(X*(1.0-X)) +ASIN(SQRT(X)
      PI=3.14159
      RAD=PI/180.
      IF(CMU) 250,2,3
    2 CO P=1.0
      CFPOCP=CFOC
      GO TO 20
    3 IF(CFOC) 250,4,5
    4 CFOC=0.  1
    5 PI2=PI*PI
      PI3=PI2*PI
      IT=0
      PSI1(1)=0.
      XP=PI/2.0
      PSI1(3)=PI
      XDELF=RAD*DELF
      XDELN=RAD*DELN
      XDELJ=RAD*DELJ
      XALPE=RAD*ALPE
      ETA=1.-CFOC
      ETAN=CNOC
    1 XALPI=RAD*ALPI
   12 PSI1(2)=XP
      SINXP=SIN(XP)
C     WRITE(6,69 ) IT,XP,(PSI1(K),K =1,3)
C69   FORMAT(I4, (2X,F10.5)
      COSXP=COS(XP)
      IT=IT+1
      T=ETA*(1.+COSXP)-1.
      PZ=ACOS(T)
      TI=ETAN*(1.+COSXP)-1.
      PN=ACOS(TI)
      F(1)=-(XDELN-XALPE)
      A(1)=PI
      F(2)=XDELN
      A(2)=PN
      F(3)=XDELF
      A(3)=PZ
      CHECK=F(1)+A(1)*(XP-SINXP)
      DO 110 N=2,3
      ASP=SIN(0.5*(A(N)*XP)
```

```
      ASM=SIN(0.5*(A(N)-XP))
      CHECK=CHECK+F(N)*(A(N)*XP+XP*SIN(A(N))-A(N)*SINXP
     $+2.*ASM*ASP*ALOG(ASM/ASP))
  10  CONTINUE
      CHECK=CHECK+XDELJ*XP*XP
      ANSI=CHECK/(1.0+COSXP)
      ANSJ=0.25*PI*CMU*(SIN(XDELF+XDELJ+XALPE)
     +  -SIN((KWAKE-1.)*XALPI))
      RES=ABS(ANSI)-ABS(ANSJ)
      TOL=.01
      IF(ABS(RES)-TOL)100,100,15
  15  IF(RES) 40,100,30
  30  XP=(PSI1(1)+PSI1(2))/2.0
      PSI1(3)=PSI1(2)
      GO TO 50
  40  XP=(PSI1(2)+PSI1(3))/2.0
      PSI1(1)=PSI1(2)
  50  CONTINUE
      IF((IT-50))12,12,98
  98  WRITE(6,10  ) RES,TOL,ALPE,XP
 100  FORMAT('  SOLUTION FOR EQUIV. JET FLAP HAS AN ERR=',F8.5,
     1 ' TOL=',F7.5,' XSTAR=',F10.5,' PSI1=',F10.5)
 100  CONTINUE
      COCP=(1.0+COSXP)/2.0
      CFPOCP=(1.0-T)/2.0
      CNPOCP=(1.0-T1)/2.0
      EMFOCP=(1.0-COSXP)/2.0
 200  ADF=ALFDEL(CFPOCP)
      ADEMF=ALFDEL(EMFOCP)
      ADN=ALFDEL(CNPOCP)
      DELALF=(1.0/COCP)*(ADN-1.0)*XDELN+ADF*XDELF+ADEMF*XDELJ)
 250  RETURN
      END
```

```
      SUBROUTINE FIELD(NH,NPTS,B,ALPHAB,BETAS,SWEEP,GAMA,
     1 PHII,GAMAOV,XPB,YPB,ZPB,MP2)
C     PROGRAM FOR ESTIMATION OF THE VORTEX-INDUCED SUBSONIC-FLOW FIELD
C     BENEATH SWEPT AND UNSWEPT WINGS.
C     REFERENCE NACA REPORT 1327 BY WILLIAM J. ALFORD, JR.
C     PROGRAM BY A. E. HOLMES OF DEPT 72-74*****FEB. 1967*
C      UPDATED ON JAN 15 1971
C      UPDATED FOR SUBROUTINE FOR JET FLAP HIGH LIFT PROGRAM
C     23 OCTOBER 1973. AEH
C     CHANGED TO HANDLE ASYMMETRICAL LOADINGS 25 OCT 73. AEH
C      VELOCITIES INSIDE CIRCLE OF RADIUS S ARE ZEROED OUT.  29 OCT 73
C      LAST UPDATE 27 NOV 73.
      DIMENSION XP(20), YP(20), ZP(20), X(50), Y(50),
     1 Z(50),GAMOV2(50)
     2 ,PHII(33),GAMAOV(3 ),XPB(20),YPB(20),ZPB(20)
      PI=3.14159
      RAD=180./PI
      TGAM=SIN(GAMA/RAD)/COS(GAMA/RAD)
      TLAM=SIN(SWEEP/RAD)/COS(SWEEP/RAD)
      NVORTS=50
      VORSPA=B/50.
      S=VORSPA/2.0
      BETA=1.0
      DO 40 J=1,NVORTS
      Y(J)=S-(B/2.0)+(VORSPA*(J-1))
      ABSY=ABS(Y(J))
      YWPHI=ACOS(2.0*Y(J)/B)
      GAMOV2(J)=GIRC(YWPHI,PHII,GAMAOV,MP2,2)
      X(J)=ABSY*TLAM
      Z(J)=0.0
 5959 FORMAT( )
  40  CONTINUE
      SALF=SIN(ALPHAB/RAD)
      CALF=COS(ALPHAB/RAD)
      SBETA=SIN(BETAS /RAD)
      CBETA=COS(BETAS /RAD)
      DO 50 I=1,NPTS
      YP(I)=XPB(I)*SBETA+YPB(I)*CBETA
      XP(I)=ZPB(I)*SALF+(XPB(I)*CBETA-YPB(I)*SBETA)*CALF
      ZP(I)=ZPB(I)*CALF-XPB(I)*SALF
  50  CONTINUE
      WRITE  (6,11 )
   1  FORMAT (/  ,5X,'  X POINT    Y POINT    Z POINT ',
     1 '  EPSILON    SIGMA',/)
      DO 20  I=1,NPTS
      SUMGFW=0
      SUMGFV=0
      SUMGFU=0
      DO 10   J=1,NVORTS
      DELX=(XP(I)-X(J))/BETA
      DELYR=YP(I)-Y(J)
      DELZ=ZP(I)-Z(J)
      S=VORSPA/2.0
```

```
      DNSQ=SQRT((DELX/S)**2+(DELZ/S)**2)
      DNSQMR=SQRT((DNSQ**2)+((DELYR/S)-1)* 2)
      SNDELR=((DELYR/S)-1)/DNSQMR
      CSDELR=DNSQ/DNSQMR
      DNSQPR=SQRT((DNSQ* 2)+((DELYR/S)+1)**2)
      SNBETR=((DELYR/S)+1)/DNSQPR
      CSBETR=DNSQ/DNSQPR
      SNGAMA=(DELX/S)/DNSQ
      CSGAMA=(DELZ/S)/DNSQ
      IF(DNSQ.LT.1.0) GO TO 62
      FWRPL=(SNGAMA/DNSQ)*(SNBETR-SNDELR)
      GO TO 64
   62 FWRPL=0.0
   64 IF((DNSQPR.LT.1.0).OR.(DNSQMR.LT.1.0)  GO TO 78
      FWRPL=FWRPL-
     1 ( (DELYR/S)-1)/( DELZ/S)* 2+( DELYR/S)-1)* 2))*(1+SNGAMA*
     3 CSDELR)+((DELYR/S)+1)/((DELZ/S)**2+
     4((DELYR/S)+1)**2))*(1+SNGAMA*CSBETR)
      FVRPL=((DELZ/S)/( DELZ/S)* 2+( DELYR/S)+1)* 2)  *(1+SNGAMA
     2 *CSBETR)-((DELZ/S)/( DELZ/S)* 2+
     3 ((DELYR/S)-1)**2))*(1+SNGAMA*CSDELR)
      GO TO 80
   78 FVRPL=0.
   80 IF(DNSQ.LT.1.0) GO TO 8
      FURPL=(CSGAMA/DNSQ)*(SNBETR-SNDELR)
      GO TO 90
    8 FURPL=0.0
   90 SUMGFW=SUMGFW+(GAMOV2(J)*FWRPL)
      SUMGFV=SUMGFV+(GAMOV2(J)*FVRPL)
      SUMGFU=SUMGFU+(GAMOV2(J)*FURPL)
  100 CONTINUE
      WAOV=SUMGFW/(4*PI*S)
      VAOV=SUMGFV/(4*PI*S)
      UAOV=SUMGFU/(4*PI*S)
      EPSLON=(ATAN(WAOV/(1+UAOV)  )*57.3
      SIGMA=-(ATAN(VAOV/(1+UAOV)  )*57.3
      QLOO=(1+UAOV)**2+(VAOV)**2+WAOV**2
      WRITE (6,1 0)  XPB(I), YPB(I), ZPB(I), EPSLON, SIGMA
  110 FORMAT (5X,9F10.5)
   20 CONTINUE
      RETURN
      END
```

REFERENCES

1. Spence, D. A., "The Lift of a Thin Aerofoil with Jet Augmented Flap", Aeronautical Quarterly, Vol. 9, 1958.

2. Malavard, L., "Application of the Rheoelectric Analogy for the Jet Flap Wing of Finite Span", Boundary Layer and Flow Control, editor: G. V. Lachman, Pergammon Press, New York, 1967.

3. Maskell, E. C., and Spence, D. A., "A Theory of the Jet Flap in Three Dimensions", Royal Aircraft Establishment, Report No. Aero 2612, September 1958.

4. Das, A.,"Trag fluchentheorie fur Tragflugel mit Strahlkappen," Jahrbuch der Wissenchaftlichen Gesellschaft fur Luftfahrt, pp. 112-113, 1960.

5. Lopez, M. L. and Shen, C. C., "Recent Developments in Jet Flap Theory and its Application to STOL Aerodynamic Analysis, AIAA Paper No. 71-578, June 1971.

6. Lissaman, P. B. S., Analysis of High Aspect Ratio Jet Flap Wings of Arbitrary Geometry, AIAA Paper No. 73-125

7. Hackett, J. E., and Lyman, V., The Jet Flap in Three Dimensions: Theory and Experiment, AIAA Paper No. 73-653, July 1973.

8. Davenport, Franklyn J., "A Lifting Line Analysis Method for Jet-Flapped Wings", STOL Tactical Aircraft Investigation, Air Force Flight Dynamics Laboratory, Technical Report AFFDL-TR-73-19, Volume II, Part II, June 1973.

9. Jacobs, W. F., and Paterson, J. H., The Jet-Flapped Wing in Two- and Three-Dimensional Flow, IAS Preprint No. 791, January 1958.

10. von Karman, Th., and Burgers, J. M., Aerodynamic Theory, Vol. II, Section E, editor in chief: Durand, W. F., Julius Springer, Berlin, 1935.

11. DeYoung, John, and Harper, Charles W., "Theoretical Symmetric Span Loading at Subsonic Speeds for Wings Having Arbitrary Plan Form", NACA Technical Report 921,1948.

12. Williams, J. and Alexander, A. J., Aeronautical Quarterly 8, 1957.

13. Das, J., "Trag fluchentheorie Fur Tragflugel Mit Strahlklappen" Jahrbach der WGL, 1960.

14. Malavard, L. and Lepage, L. "Principes Et Resultats De Calculs D'ailas a Jet Par Analogies Rheoelectriques", La Recherche Aeronautic No. 77, Julliet-Aout, 1960.

REFERENCES (Cont'd)

15. Monk, John A., Lee, Jerry L., and Palmer, J. Patrick, "Analysis of Wind Tunnel Data: Vectored Thrust/Mechanical Flaps and Internally Blown Jet Flaps", STOL Tactical Aircraft Investigation, Vol. IV, Air Force Flight Dynamics Laboratory Technical Report AFFDL-TR-73-19, Dayton, May 1973.

16. Unpublished Data for Large Scale IBF Model, Test 415, NASA Ames Research Center, 1972.

17. Falarski, M. D., and Koenig, D. G., "Aerodynamic Characteristics of a Large-Scale Model with a Swept Wing and Augmented Jet Flap", NASA Report No. TMX-62,029, July 1971.

18. Unpublished Data for Large Scale EBF Model, Test 409, NASA Ames Research Center, 1972.

19. Unpublished Data for Large Scale USB Model, Test 426, NASA Ames Research Center, 1973.

20. Unpublished Data for Large Scale IBF Model, Test 418, NASA Ames Research Center, 1973.

21. USAF Stability and Control DATCOM, Air Force Project Engineer: D. E. Hoak, Flight Control Division, Air Force Flight Dynamics Laboratory, Wright-Patterson Air Force Base, Ohio, Oct. 1960, Revised June 1969.